Doctoral theses at NTNU, 2013:299

Bartosz Kus

Oil-free turbocompressors for CO_2 as working fluid

Doctoral Thesis

Bartosz Kus

NTNU – Trondheim
Norwegian University of
Science and Technology

Faculty of Engineering Science & Technology
Department of Energy and Process Engineering

Doctoral theses at NTNU, 2013:299

NTNU

NTNU – Trondheim
Norwegian University of
Science and Technology

ISBN 978-82-471-4731-3 (printed version)
ISBN 978-82-471-4732-0 (electronic version)
ISSN 1503-8181

Bartosz Kus

Oil-free turbocompressors for CO_2 as working fluid

Thesis for the degree of Philosophiae Doctor

Trondheim, November 2013

Faculty of Engineering Science & Technology
Department of Energy and Process Engineering

NTNU – Trondheim
Norwegian University of
Science and Technology

NTNU
Norwegian University of Science and Technology

Thesis for the degree of Philosophiae Doctor

Faculty of Engineering Science & Technology
Department of Energy and Process Engineering

ISBN 978-82-471-4731-3 (printed version)
ISBN 978-82-471-4732-0 (electronic version)
ISSN 1503-8181

Doctoral theses at NTNU, 2013:299

Printed by Skipnes Kommunikasjon as

Abstract

Compressing equipment can be found in almost every area of our industrialized society. Compressors drive our fridges, air conditioning systems and enable turbine engines to propel the aircrafts we use when going for holidays or a business trip. Without compressors an operation of virtually any conventional power plant providing electricity to our houses would not be possible. The compressor technology can therefore be regarded as a mature area of engineering with a vast theoretical and operational experience.

It may happen however that a traditional approach to certain new problems will not suffice, and alternative ways must be searched for. Such open-mindedness was required when the idea of introducing an oil-free compressor for a CO_2 commercial refrigeration system was born. Initially, hermetic radial turbomachinery was identified as a potential candidate for this task. However, it turned out that rather special properties of carbon dioxide, compared to other common refrigerants, will result in challenges uncommon in turbomachinery found in other applications. While the initial technology choice still seemed feasible, high density of the CO_2 at relevant operating conditions and significant rotational speeds required for a relatively small machine were indicating excessive levels of windage losses generated by the spinning rotor of the compressor.

It was decided to build a 1D tool for prediction of efficiencies for a wide range of machines based on a radial turbocompressor principle, but designed for CO_2 applications with different operating pressures and capacities. The predictions of the tool were compared against numerical and experimental data. Good match was found. The 1D study revealed that high compression efficiencies, exceeding 70 %, are possible for the oil-free radial compressor concept in a relatively wide range of capacities provided that the inlet pressure is low, around 1 MPa, and that the pressure ratio is moderate, below 3. Potential for good efficiency is expected to deteriorate rapidly with increasing operational pressures due to windage losses. There is no obvious strategy for improvement of overall compressor efficiency when smaller capacities and close to supercritical pressures are in the focus. The major fraction of undesirable rotational losses is generated by the electrical motor. It can be reduced either by installing longer more slender motor or by reduction of rotational speeds. Efficiency improvement reached with application of a longer motor is shown to be of limited impact and is expected to be challenging from the rotordynamics point of view. Alternatively, multi-stage multi-shaft machine can be designed, but economic viability of such a strategy remains questionable.

Reduction of the compressor speed is not straightforward either, especially at low volumetric flows when low speeds would be detrimental to the impeller and diffuser efficiency. A non-standard approach introducing partially admitted radial machine was therefore proposed. A numerical analysis of a partially admitted compressor stage with a 16 cm impeller rotating at 13000 rpm is carried out.

Transient 2D simulations indicate more than 80% efficiency of the wheel at the total pressure ratio of around 1.4. To estimate the final stage efficiency, 3D effects such as the end-wall losses, the radial leakage, and the diffuser performance must be taken into account. A transient 3D analysis of the complete stage of the novel compressor has not been completed due to its time consuming nature. 3D simulations performed for various diffuser configurations indicate however that around 75% overall stage efficiencies might be possible. It would require further optimization of both blade and diffuser shapes. Comparison of non-stage losses, for both centrifugal and partial admission concepts, allow presuming that the novel machine could be superior in terms of the overall performance provided that comparable systems are characterized by close to supercritical mean operating pressures and capacities typical for commercial scale applications. To verify the initial insights of the present work, further research, including laboratory testing, is needed.

Acknowledgments

Any creative process consists of several steps. The same applies to the road a PhD candidate must follow. First an idea is born. It is not always clear where it comes from. Maybe it is a mere result of previous experiences leading to a crystalized and conscious decision to start acting. Sometimes I think however that things just happen, as they are supposed to happen. I am only sure that once the idea is crystalized a catalyzer is needed, to encourage the next step in the process. In my case that catalyzer was my parents. For them it was clear. I should pursue my PhD education. Their clear opinion helped me to make an important decision in my life. And I do not regret it. At this point I would like to thank them for the encouragement and tireless support throughout the entire process.

Dear Parents,
I dedicate this thesis to you.

If I think about encouragements one more person should be mentioned. I want to thank Mona Mølnvik for enabling my coming back to Norway and smooth transition from my job duties to PhD activities.

The implementation of an idea to create something new and interesting, successfully or not, would not be possible without open-mindedness of my supervisors: Petter Nekså and Trygve Magne Eikevik. I want to thank you for taking a risk and allowing me to explore not entirely conventional concepts. Fortunately your positive approach was accompanied by a critical insight which, I believe, helped to keep my work within reasonable boundaries.

My final thanks must go to all the 5th floor colleagues for their positive attitude and creating friendly and open working atmosphere.

Contents

ABSTRACT ..... **I**

ACKNOWLEDGMENTS ..... **III**

CONTENTS ..... **IV**

LIST OF PAPERS ..... **VI**

LIST OF FIGURES ..... **VII**

LIST OF TABLES ..... **IX**

NOMENCLATURE ..... **X**

1 INTRODUCTION **1**

1.1 Background 1

1.2 Previous experience 3

1.3 Objectives of the study 6

1.4 Structure of the thesis 7

1.5 Extended summary of the original work 7

2 THEORETICAL BACKGROUND **12**

2.1 CO_2 as a working fluid 12

2.2 CO_2 machinery 18

2.2.1 Reciprocating and rotary compressors 21

2.2.2 Turbocompressors 28

2.2.3 Industrial scale CO_2 turbomachinery 32

2.2.4 Small and medium size CO_2 turbomachinery 37

2.3 Windage in CO_2 machines 40

2.4 Seals and bearing concepts for oil-free operation 42

2.5 Oil free bearing technology for commercial applications....48

2.6 Partial admission turbines....52

2.7 Design and analytical methods....58
2.7.1 Aerodynamic design procedures....58
2.7.2 Introduction to the applied CFD method....59

3 SUMMARY OF PAPERS....65

3.1 Paper I....65

3.2 Paper II....66

3.3 Paper III....67

3.4 Paper IV....68

4 CONCLUSIONS....69

5 SUGGESTIONS FOR FURTHER WORK....72

6 BIBLIOGRAPHY....74

PAPER I

PAPER II

PAPER III

PAPER IV

List of papers

This thesis is based on 4 papers, listed below. The Papers I, II, III, IV are referred to in the text by Roman numerals.

Paper I. Kus, B., & Nekså, P. (2013). Development Of One-Dimensional Model For Initial Design And Evaluation Of Oil-Free CO_2 Turbo-Compressor. *International Journal of Refrigeration. Available online. In press.*

Paper II. Kus, B., & Nekså, P. (2013). Oil Free Turbo-Compressors For CO_2 Refrigeration Applications. *International Journal of Refrigeration. Volume 36, Issue 5, August 2013, Pages 1576–1583*

Paper III. Kus, B., & Nekså, P. (2013). Novel partial admission radial compressor for CO_2 applications. *International Journal of Refrigeration. Available online. In press.*

Paper IV. Kus, B., & Nekså, P. (2013). Numerical study of diffuser systems for a novel partial admission compressor using CO2 as refrigerant. *Submitted to International Journal of Refrigeration.*

List of figures

Figure 1. Working-fluid-based thermodynamic cycles in the global energy structure 2
Figure 2. One of the first radial turbines using gas foil bearings. Source: DellaCorte and Bruckner (2010) 3
Figure 3. Turbocor commercial oil-free HVAC compressor for HFC refrigerants. Image courtesy of Danfoss Turbocor Compressors Inc. 4
Figure 4. Echogen's 10 MWe SCO_2 power turbine compared to a 10MWe steam turbine. Source: Persichilli et al. (2012) 5
Figure 5. T-s diagram showing the transcritical CO_2 cycle used for water heating. Source: Nekså (2002) 13
Figure 6. Volumetric refrigeration capacity for selected refrigerants 14
Figure 7. T-s diagram of T-CO_2 Rankine cycle with HT heat. Source: Kim et al. (2012) 16
Figure 8. Layout and T-s diagram for SCO_2recompression Brayton cycle 17
Figure 9. An example of a Cordier diagram (Ns- Ds chart) derived for pumps. Source: Balje (1981) 20
Figure 10. Isentropic efficiency of a small oil-free CO_2 piston compressor at varying pressure ratio for a suction pressure of 35 bar [Baumann and Conzett (2002)] 22
Figure 11. Overall isentropic efficiency of various oil-lubricated rotary and reciprocating compressors. Source: Christen et al. (2006) 23
Figure 12. Obrist/Sintef semi hermetic piston compressor 24
Figure 13. Isentropic efficiency of the new generation of semi hermetic CO_2 piston compressor 25
Figure 14. An impact of speed and operating pressure on the isentropic efficiency of a new generation of semi hermetic CO_2 piston compressor. Source: Hafner et al (2013) 26
Figure 15. Schematic view of the balanced rotor compressor-expander. Source: Stosic et al. (2002) 27
Figure 16. Velocity triangles in radial and axial turbo-compressors 29
Figure 17. Radial compressor stage 31
Figure 18. A typical centrifugal compressor characteristic 32
Figure 19. The assembly of the 5.2 MW CCS compressor. Photo courtesy of Dresser-Rand 33
Figure 20. The schematic representation of integrally-geared turbo-compressor… 34
Figure 21. Supersonic flight inlet and supersonic compressor principle. Source: Lawlor and Baldwin (2005) 35
Figure 22. Supersonic compressor stage rotor. Source: Lawlor and Baldwin (2005) 36

Figure 23. Comparison of the performance of the flight inlet systems with conventional industrial compressor efficiencies. Source: Lawlor and Baldwin (2005) 37
Figure 24. A depiction of a small impulse-type axial CO_2 turbine. Source: Hays and Brasz (2004) 38
Figure 25. The working principle of a radial outflow impulse turbine. Source: Tøndell (2005) 39
Figure 26. Depiction of assumptions for calculation of windage of a rotating cylinder 40
Figure 27. Comparison of windage estimates based on measured data (magenta) with the Vrancik model (yellow). Source: Wright et al. (2010) 42
Figure 28. Tandem style dry gas seal 43
Figure 29. Industrial turbo-compressor equipped with dry gas seals 44
Figure 30. Cross/section of a labyrinth seal 45
Figure 31. An example of a hermetic oil-free compressor configuration 45
Figure 32. Overview of the potential technology choices for oil-free CO_2 compression systems 47
Figure 33. Principle of actively controlled magnetic bearing 49
Figure 34. Hydrodynamic pressure generation 50
Figure 35. Cross section view of simple radial foil bearing 51
Figure 36. Typical velocity triangle and blade configuration of an impulse turbine. Source: Linhardt and Silvern (1961) 55
Figure 37. Two-stage re-entry partial admission impulse turbine. Source: Linhardt and Silvern (1961) 56
Figure 38. General character of blade forces in partial admission stage. Source: Pigott (1980) 57
Figure 39. Illustrated emptying, pumping and filling processes for a partial admission stage 58
Figure 40. Time averaging of velocity 60

List of tables

Table 1. Comparison of popular refrigerants 15
Table 2. Process conditions for expander design 39

Nomenclature

Roman symbols

A	area (m^2)
C	absolute velocity (m/s)
Cd	skin friction coefficient (-)
d	infinitesimal
E	energy (J)
F	force (N)
h	enthalpy (kJ/kg)
L	length (m)
M	Mach number (-)
$\dot{m}$	mass flow (kg/s)
m	mass (kg)
q	heat flow (J/s)
r	radius (m)
Re	Reynolds number (-)
s	entropy (kJ/kgK)
t	time (s)
U	tip speed (m/s)
V	velocity (m/s)
W	relative velocity (m/s)
z	transverse dimension (m)
cl	clearance (m)
α	absolute flow angle (rad)
ω	tangential velocity (rad/s)
β	relative flow angle (rad)
Δ	finite change
τ	torque (N·m)
ν	kinematic viscosity (m^2/s)
μ	viscosity (Pa s)
ρ	density (kg/m^3)
υ	velocity (m^3/s)

Subscripts

c	critical
is	isentropic
θ	circumferential direction
x	flow direction
1	inlet

2	outlet
rel	relative

Abbreviations

GWP	Global Warming Potential
ODP	Ozone Depletion Potential
LTV	Threshold Limit Value
HVAC	Heating, Ventilation, and Air Conditioning
NASA	National Aeronautics and Space Administration
ACM	Air Cycle Machine
EIA	Energy Information Administration
IIR	International Institute of Refrigeration
APU	Auxiliary Power Unit
COP	Coefficient of performance
LT	Low temperature
HT	High temperature
ORC	Organic Rankine Cycle
PEEK	Poly Ether Ether Keton
OE	Obrist Engineering
FPSO	Floating Production, Storage and Offloading
RNG	Re-Normalisation Group
DVM	Differential Viscosity Model
SST	Shear Stress Transport

1 Introduction

1.1 Background

"Improved energy efficiency is imperative to minimize the greenhouse gas emissions and to ensure future energy security. It is also a key to continued profitability in energy consuming industry" – these words introduce us into the CREATIV project which is a research initiative answering to the constantly growing need for smart, energy efficient solutions in various areas of our industrialized life. The particular focus of the project is put on the utilization of surplus heat and efficient heating and cooling based on natural working fluids.

The potential for improvements and innovations within these two industrial areas is enormous. To realize this it suffices to mention that an incredible amount of up to 50% of the total energy input in the whole industrial sector is lost in the form of heat released to the surroundings. According to EIA (2011), the total industrial energy consumption in 2008 amounted to 210×10^{18} J. Even though it is difficult to put such a number in perspective, one should be able to imagine that even its small fraction is still a huge amount of energy, energy that potentially could be utilized for a useful purpose, instead of being lost to the surroundings. This thermal energy can be used in different ways, one of which is production of electricity through the application of more or less advanced thermodynamic cycles.

Electrical energy, in turn, regardless of its origin (fossil fuels, renewable, waste heat) is further used in other industrial, commercial or private applications, very often based on similar thermodynamic principle utilizing various working fluids (i.e. domestic fridge, building air conditioning). Such applications are widely found in refrigeration and HVAC market which, according to the IIR estimates (2010) consumes around 15% of global electricity production. Even modest improvements in this one sector alone, can result in a significant contribution to the global energy share outlook. The common denominator of various energy related processes could be the working fluid used to convey various forms of energy. It may be thermal energy trapped in the latent heat of the refrigerant, pressure energy of a compressed gas or a work performed by the fluid in a turbine or an expander, see Fig 1.

Growing environmental awareness as well as the ever increasing economic pressure of the last decades brought revival of the interest in natural working fluids. Among them, carbon dioxide, a non-toxic, non-flammable easily available gas with zero global warming potential and good thermodynamic properties, that attracted quite remarkable amount of attention. This led to development of a new class of compact components capable of withstanding the uncommonly high pressures required for its efficient application. One of the key components that had to be redesigned for efficient operation of new systems was the compressors. Nowadays,

oil-lubricated piston compressors are the benchmark technology for commercial refrigeration and HVAC applications utilizing carbon dioxide, CO_2, as a refrigerant. While the technology is proven and able to provide high pressure ratios in a single stage of compression, it does not excel in other categories. The isentropic efficiencies of the reciprocating compressors are limited due to the throttling, leakage and mechanical losses. The system is complex due to the additional oil infrastructure, and the performance of remaining vital components may be reduced due to the surface contamination with oil picked up by the gas in the compressor. Thanks to recent developments in the field of the supercritical CO_2 (SCO_2) cycles for power production, a new class of oil-free high speed turbocompressors has been brought to focus. These machines, relatively new to the commercial CO_2 refrigeration market, are believed to have a potential to reach good efficiencies, providing at the same time a simplified architecture of the system and no contamination of internal parts of the system components. On the other hand, the new technology is not without challenges, posed by the nature of the working fluid itself. This thesis makes an attempt to evaluate the feasibility of introducing a new type of efficient oil-free machinery into CO_2 applications, to identify possible challenges and to propose potential solutions.

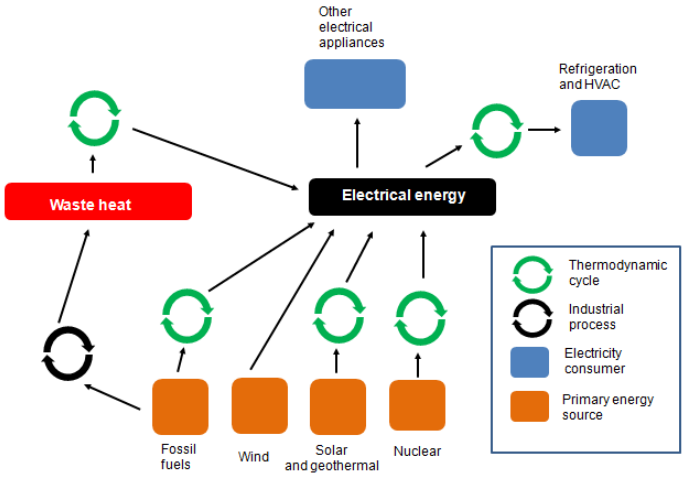

Figure 1. Working-fluid-based thermodynamic cycles in the global energy structure

1.2 Previous experience

The demand for new, efficient, environmentally sound and operationally robust compression technology is obvious as CO_2 based cycles are gaining more attention and are proposed in a growing number of applications.

While in the field of CO_2 an oil-free compression is relatively new, it has been maturing in other applications since the middle of the past century. Much of the pioneering development came from NASA where oil-free technologies had been perceived as of uniquely intrinsic and enabling value in space power conversion and aero-propulsion systems. Some of the relevant applications included air cycle machines (ACMs) used for aircraft cabin ventilation and electronic equipment cooling, cryogenic turbo-expanders and compressors, maintenance-free auxiliary power units (APUs), aircraft propulsion engines, and closed Brayton cycle turbine generators for space power [DellaCorte and Bruckner (2010)]. It is interesting to know that foil gas bearing technology that intrinsically accompanied development of oil-free machines, was originally discovered within the tape recording industry. It was found that the magnetic tape performance was degraded at ever-faster speeds as the tape began to float away and "lift off" the heads. The floating phenomenon was later named the "foil bearing problem" in reference to the flexible oil-lubricated bearings made from metal foils and studied in Europe in the 1950s. Among the very first applications of the recording tape inspired foil bearings was the 15 kW Brayton rotating unit shown in Fig 2.

Figure 2. One of the first radial turbines using gas foil bearings. Source: DellaCorte and Bruckner (2010)

Oil free turbo-machinery is also known in the refrigeration marketplace. Turbocor developed the world's first 2-stage oil-free centrifugal compressor (see fig 3) specifically designed for Heating, Ventilation and Air-Conditioning (HVAC) industry. The machine introduced in 2001 was designed for mid-size chiller applications using R134a as a refrigerant. The compressor uses magnetically

levitated bearings on a single shaft. The electrical motor of the compressor is of synchronous permanent-magnet type, operates at speeds of up to 48,000 rpm and is driven by a variable speed inverter. Reliability and commercial success of the compressor was proved, according to the manufacturer, with almost 24,000 units produced since 2003.

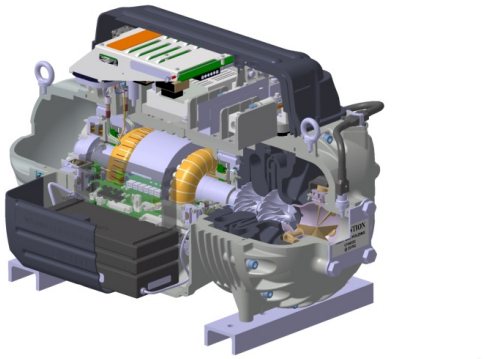

Figure 3. Turbocor commercial oil-free HVAC compressor for HFC refrigerants. Image courtesy of Danfoss Turbocor Compressors Inc.

Another variant of an oil-free compressor, in this case supported on special type of gas bearings called Herringbone Grooved Bearings was proposed by Schiffmann and Favrat (2009, 2010). The machine designed for a domestic heat pump utilizing R134a refrigerant was built and successfully tested at rotational speeds of up to 210,000 rpm, achieving pressure ratios in excess of 3.3 and efficiencies above 78%. The study proved feasibility and high efficiency potential of an oil-free concept despite usage of a very small centrifugal impeller, measuring only 20 mm in diameter.

At present, it seems that the main driving force behind development of CO_2 based oil-free machinery will come from power generation sector where potential benefits of supercritical CO_2 have gained significant attention. It is viewed that SCO_2 could be a game changer for power plant economics, efficiency and the environment. It is estimated that the cycles' efficiencies could reach between 40 and 50% depending on their complexity [Dostal (2006), (Chen (2011)]. Thanks to high density of the working fluid, footprints of one hundredth of those of traditional turbo-machinery for the same power output can be expected, see Fig 4.

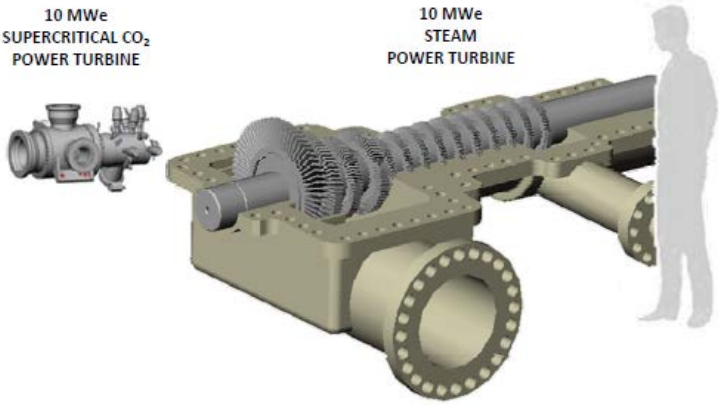

Figure 4. Echogen's 10 MWe SCO_2 power turbine compared to a 10MWe steam turbine. Source: Persichilli et al. (2012)

A great deal of emphasis on SCO_2 is placed by major American research bodies such as Sandia National Laboratories, Southwest Research Institute (SwRI) and Lawrence Berkley National Laboratory. Also major engineering companies such as Toshiba, Echogen, Dresser Rand, GE, Bechtel and Barber-Nichols are involved in making the next-generation technology viable. Unfortunately, at this stage of development only few details are made public.

The most detailed publication on the oil-free high speed CO_2 radial-compressor was released by Sandia National Laboratories [Wright et al. (2010)]. The report outlines the design of the small scale Brayton loop, describes the major components, presents models for the system and compressor performance, and describes experimental results. The compressor is designed to pump 3.5 kg/s of supercritical CO_2 at a pressure ratio of 1.8 at the design speed of 75,000 rpm and nominal power of approximately 50 kW. Measurements of parameters such as off-design compressor performance, axial loads, windage losses and seal leakage are generally in good agreement with the models. The Sandia compressor is equipped in a booster pump to reduce significant windage losses triggered by the high speed motor rotating in the high density CO_2. The reported peak compressor efficiencies are found within 65-70%. These are not necessary high values for a centrifugal type compressor, especially as the power consumption of the booster pump is not included in the calculation. The relatively small size of the compressor (diameter of the impeller is 3.7 cm) and the high pressure gradient across the labyrinth seal causes a significant portion of the compressed gas to leak from the impeller area to the motor cavity. As a result, significant energy expenditure for the booster pump must also be taken into account. The authors of the report point out that the relative pumping power will be much smaller in a large scale application, enabling use of more sophisticated seal technology.

An area where supercritical CO_2 has been around for decades is Enhanced Oil Recovery (EOR). Here the pipeline applications have traditionally been accompanied by centrifugal pumps with non-contacting dry gas seals. Recent interest in CO_2 capture and storage has brought new challenges also to this megawatt-class industry. Higher operating pressures, higher operating speeds and increased temperatures resulted in higher seal leakages and pronounced churning heat generated form viscous drag of the rotating seal components. Especially high speed applications tend to generate temperatures that are not typical in commonly used seal solutions. It is identified that such applications will require some form of additional cooling which can be remedied by proper design of the seal support system [Marquardt (2011)]. This thesis will not focus on large scale applications, but it is important to signal that although extensive industry experience may be of valuable contribution to the development of new commercial size CO_2 systems, also here challenges are present.

1.3 Objectives of the study

The main objective of the present work is to develop an efficient turbocompressor concept for CO_2 as working fluid applicable to medium capacity applications and a relatively wide range of operating pressures.

Oil-free operation is a desirable characteristic of virtually any cycle-based application. The thesis gives an overview of technologies that might be suitable for enabling oil-free compression for a wide range of CO_2 applications. A comprehensive overview of existing experiences with CO_2 machinery, as well as of the characteristics of CO_2 as a working fluid, is given. This motivates why turbocompressors are the most likely candidate for an oil-free compression technology. It is known that CO_2 has some rather uncommon properties, when compared to working fluids typically used in power generation and HVAC applications. In order to assess an impact of these properties on potential oil-free CO_2 compressor a modeling tool was needed.

A 1D mathematical model that would analytically propose a basic design of an oil-free radial turbo-compressor and predict its efficiency will be proposed. The model should take into account losses generated due to oil-free operation such as windage of radial and axial bearings and electrical motor. Attractiveness of an oil-free turbocompressor technology is expected to be dependent on the type of application, therefore efficiency of compressors designed for various capacities and operating conditions is to be assessed.

For some of the applications in focus, introduction of a typical oil-free radial compressor does not guarantee achieving reasonably high efficiency levels. In such cases alternative solutions should be sought. A novel concept of a turbocompressor, using known principles of a partial admission, but applied in radial inward flow configuration and at operating conditions not considered before, will be proposed.

The largest part of the work will be related to numerical predictions of a novel compressor aerodynamic performance, being a basis for further 1D calculations of the overall machine efficiency.

1.4 Structure of the thesis

The present thesis is divided into several parts. An extended overview of the CO_2 compressing technology is presented in Chapter 2. In that chapter various kinds of compressors together with supporting technologies, such as bearing systems, are described. While that part of the work is not necessary inventive it serves the important function to motivate why turbomachinery supported on gas foil bearings has been selected for a more in-depth analysis presented in the attached papers. The "Theoretical background" provided in Chapter 2 is supplemented by the short "Summary of the papers" given in Chapter 3. "Conclusions" and "Suggestions for further work" are presented in chapters 4 and 5, respectively. The major part of original work is comprised in the papers attached in the final part of the thesis. The description of the adopted research direction and the discussion to the obtained results is presented in the following sub-chapter called "Extended summary of the original work".

1.5 Extended summary of the original work

Modeling of turbo-machinery is an interdisciplinary undertaking that merges areas of thermodynamics, fluid dynamics, rotordynamics, material and numerical sciences. Due to the complexity of the full design procedure the scope of the present study had to be contained within reasonable boundaries.

The initial assumption for the content of this thesis was rather broad. It was founded in the need of an efficient oil-free compressor for a specific CO_2-based commercial refrigeration system. It was known that such a machine did not exist and that gave the motivation to develop one.

The matter turned out to be more complex than initially thought. The technology best suited for oil-free operation was a turbo-compressor. After initial calculations of specific speed, it was found that a two-stage hermetic radial machine could be feasible. After inclusion of various non-stage losses, it seemed that high efficiency potential of the aerodynamic stage would, to a large degree, be ruined by the rotor windage losses.

It was decided to build a tool that in a simple way would predict efficiencies of oil-free compressors designed for conditions and capacities different from the initial case. Screening through different CO_2 applications aimed at revealing whether high rotor windage was to be a general problem or an application dependent one. The method used for initial modeling was based on a rather simple 1D approach involving calculation of various losses generated in specific parts of the compressor. The accuracy of the predictions provided by the 1D model is an important aspect of this study. In the course of the present research it was unfortunately not possible to verify the model with the most reliable method of validation, namely a prototype testing. Instead cheaper and more easily available methods were used.

The part of the 1D tool predicting aerodynamic efficiency of the stage was validated with CFD simulations of 3D geometries generated based on the results from the 1D model. Again, numerical results typically also need experimental validation, but the procedures like the mesh independence study, significantly increase reliability of the method.

The simplest method of verification of 1D results is comparing non-dimensional performance coefficients of the proposed designs to these of the machines already existing and tested. Even though the non-dimensional coefficients do not include detailed information about the compressor design, such as a number and thickness of blades or their 3d curvature, they indicate realistic level of performance that can be expected, provided that a detailed design process is executed properly. As it was not the intention to give a detailed aerodynamic design of any machine, application of both validation methods seemed justifiable.

In the end, aerodynamic efficiencies predicted by the 1D model were in a good agreement with both numerical results and with the efficiency levels read from Ns (specific speed) and Φ (flow rate coefficient) charts. That led to believe that the accuracy needed for initial aerodynamic performance estimation was sufficient. Moreover, an insight into basic turbo-machinery equations and loss correlations had undeniable educational valor, vital for deeper understanding of the fundamentals underlying turbomachinery behavior.

To assess overall performance of the hermetic turbo-compressor, the 1D model was supplemented with a module calculating size of the gas bearings and the motor, and the windage caused by these components. The motor windage calculation was based on Vrancik (1968) model, validated for motors rotating in air as well as in high pressure CO_2 [Wright et al. (2010)].

The prediction of radial load was relatively simple and equivalent to calculation of the mass of the rotor. Similarly, the calculation of the journal bearing windage was based on the rule-of-thumb formula developed by Schlichting (1968) and proved sufficiently accurate for supercritical CO_2 applications by Bruckner (2009) and Howard et.al. (2007).

Much more difficult to predict with a rapid analytical model was the direction and the magnitude of the axial loads. Although fairly detailed analytical procedures exist for the prediction of axial loads for radial pumps, their direct application to high pressure CO_2 applications seems troublesome. This is due to very high absolute pressure gradients present in a radial stage of a CO_2 compressor.

Not without an impact remains a detailed 3D geometry of the impeller. The models for the axial load prediction typically require pressures and/or densities in characteristic points of the compressor to be supplied by the user. 1D aerodynamic prediction of these parameters is not always precise enough to assure reasonable thrust estimation. In effect, small variations of very big numbers lead to significant errors, giving misleading image not only of the magnitude of the force but sometimes even its direction. These challenges are confirmed by Wright et al. (2010) and Noall and Batton (2011). In Wright et al. (2010) a 1D model assuming incompressible character of supercritical CO_2 fluid is mentioned to be reasonably accurate in predicting axial load of the centrifugal machine operating in SCO_2. The more detailed presentation of that model can be found in Vernon et al. (2010). Here again an accurate matching to test data is required. Perhaps, for the time being, a numerical prediction of axial forces acting on the centrifugal compressor should be treated as a more reliable method. Such a conclusion is also supported by Shi et al. (2010). Axial thrust acting on a cryogenic liquid turbine impeller has been analyzed both analytically and numerically by Wang et al. (2011). He reports huge difference in results between both methods and attributes them to the rough approximations present in the empirical method.

During the course of the present research it became clear that if overall efficiencies of a large amount of machines were to be predicted quickly, a reasonable assumption about allowable (already balanced) axial thrust had to be made. Hopefully, based on the available data [Wright et al. (2010, Paper II, Noall and Batton (2011)] about the thrust magnitude that can be expected in a relatively small CO_2 compressor, this goal was achieved. It was also shown in loss breakdown depictions (Paper I, II and III) that relatively high load capacitates of a new generation of gas foil bearings result in acceptable levels of bearing induced losses.

CFD methods are used extensively in the present work. They were used for validation of the 1D aerodynamic model of a centrifugal stage of the CO_2 compressor as well as for the design of the stage of the novel partial admission compressor. The basics for the numerical method are presented in the thesis. Rather rich experience with numerical modeling of turbomachinery exists. There are numerous studies providing good overview of the criteria that should be followed for a reliable prediction of a compressor behavior [Denton and Dawes (1998),

Tousi and Tourani (2008), Denton (2010), Liu and Hill (2000)]. Accordingly, the following criteria were chosen for the cases simulated in the present thesis.

One of the most important aspects of the numerical simulation setup is the selection of a proper turbulence model. The main problem with turbulence models comes from the fact that their formulas are derived from special cases, experiments or simulations, and therefore they cannot be universally valid [Bradshaw (1996)].

The same limitations apply to the wall functions. In the present work k-ε models were used extensively. The standard k-ε model is the most well-known of k-ε models and its applicability has been analyzed thoroughly for many industrial problems. The model has been improved over years as its weaknesses had been identified. Galerkin et al. (2003) compared the data from the testing of a centrifugal compressor with a vaneless diffuser to the predictions obtained with different variations of the k-ε model. He observed that while k-ε RNG and k-ε RNG DVM models were most precise in the impeller efficiency and work coefficient prediction, standard k-ε model was more precise in the full stage efficiency prediction (with negligible 0.1% discrepancy).

The limitations of a standard k-ε model become more apparent in the presence of highly adverse pressure gradients. Application of a pipe diffuser to the centrifugal stage certainly introduces more severe pressure gradients acting on a fluid during the diffusion process. In such cases models different than standard k-ε model should be used.

Roberts and Steed (2004) modeled a centrifugal stage with such a diffuser using mixing-plane interface and both k-ε and SST (shear stress transport) models and compared the numerical results with the experimental rig data. It turned out that both turbulence models were able to predict the total-to-static pressure ratio characteristic well, while closer match to the test data was achieved by SST model. At 100% of the design exit-corrected flow, pressure ratio was 2.41% overpredicted by k-ε model, compared to 0.76% overprediction with the SST model. Similarly, the SST model was more precise at predicting the stage efficiency. The k-ε model overpredicted the exit-corrected flow stage efficiency by 1.99 points, while the SST model only by 0.37 points. The authors observed that the k-ε model failed to capture the stall side roll-off behavior, yielding extremely optimistic predictions near stall. It is further concluded that the poor standard k-ε model performance would be observed primarily in the pipe diffuser without severe accuracy reduction in the impeller characterized by lower adverse pressure gradients.

The better choice for pipe diffuser simulations might be a modified version of a standard k-ε model called the Realizable k-ε model, developed for problems characterized by strong adverse pressure gradients as well as separation, recirculation and strong streamline curvature. Successful application of the Realizable k-ε model was presented in the work of Simonsen and Krogstad (2004) who analyzed the flow in an axial to radial bend-diffuser configuration, typically used as a pressure recovery device in axial compressors with strict space

limitations. Realizable k-ε model was also used by Muntean et al. (2009) to analyze unsteady swirling flow in a conical diffuser with a processing vortex rope. The calculation conducted with the FLUENT code showed good match between experimentally measured and computed pressure pulsation. The fundamental frequency and higher harmonics of the vortex rope were accurately captured in the throat and up to the middle of the cone. In the last part of the cone the numerical results did not agree well with the experiments. It was concluded that to improve numerical results in the last part of the cone, more computationally expensive models should be used (like Large Eddy Simulation or Detached Eddy Simulation).

In the end, it was decided that due to the low computational cost and reasonable accuracy in many similar cases, the k-ε models were used in the present study. The standard model was used for simulations of a centrifugal stage with a vaneless diffuser and for 2D simulations of the novel partially admitted wheel. The realizable model was used for simulation of a curved duct diffuser. Due to the relative novelty of both applications, also due to the nature of the simulated fluid, the final validation of the models used can be confirmed only by an experiment, while different more computationally demanding models (such SST) should also be used for comparison.

Regarding modeling in multiple frames of reference, the Frozen Rotor interface was applied between the impeller and the vaneless diffuser of a centrifugal compressor, due to the weak intensity of coupling effects between the two domains [Liu and Hill (2000)]. The Frozen Rotor model is also considered by Tamm et al. (1999) as the most useful model for turbo-machinery providing satisfying results for both efficiency and pressure ratios around the design point of the compressor.

For the novel compressor the Sliding Mesh model was used as the more pronounced coupling effects between the compressors zones were expected due to the partial admission. Even though the simulations did not show significant differences between Frozen Rotor model and Sliding Mesh model in terms of the efficiency, the predicted flow fields differed significantly. This can be of particular importance when simulating the full stage of the compressor, where the flow profile at the inlet of the diffuser will have a considerable impact on the diffuser performance coefficients

2 Theoretical background

2.1 CO_2 as a working fluid

Refrigeration applications

Carbon dioxide as a fluid used in various thermodynamic cycles is in some aspects quite unusual compared to the most commonly used refrigerants. CO_2 has a relatively low critical temperature of 31.06 °C and a high critical pressure of 73.8 bars. For refrigeration cycles, it implies high mean operating pressures and operation in super-critical region for high heat sink temperatures. For example, at 0°C saturation temperature, the pressure of carbon dioxide is about 6 to 7 times higher than that of other commonly used refrigerants, like R404A and NH_3. From the early use of CO_2, which is the late 80s of the 19th century, this fact led to challenges as the systems components that could withstand such high pressures tended to be costly and heavy. At that time ammonia systems were preferred. An essential breakthrough for CO_2 machines was brought by Franz Windhausen in 1886. The first CO_2 ship refrigeration systems in Germany were built according to his patent. In the following decades CO_2, thanks to its harmlessness, became a popular choice for ship refrigeration. According to Bäckström (1970), in 1950 still around 60% of the global ship refrigeration and around 10% of the onshore refrigeration was operated with CO_2.The first halocarbon refrigerant R12 was first introduced in the early 1930s. The introduction of the cycles utilizing new synthetic refrigerants and characterized by good thermal efficiencies and much lower operating pressures, resulted in a decline of the interest in CO_2 systems around 1940. Factors favoring transition to the new technology included the possibility of using simpler and cheaper construction material and methods (like copper tubing), light screw or solder fittings, cheap automatic control equipment and hermetic motors [Lorentzen (1995)].

Development of the manufacturing technology in last decades of 20th century and development of novel cycle concept [Lorentzen and Pettersen (1993), Lorentzen (1995), Nekså et al. (1998)] allowed turning challenges posed by uncommon characteristics of CO_2 into advantages. Today super-critical CO_2 is used with a great success, for example in hot water heat pumps where the CO_2 temperature profile can provide a better match to the high temperature heat sink (water) than other working fluids operating at sub-critical conditions. A typical one-stage CO_2 process with internal heat exchanger is shown in the T-s diagram of Fig 5.

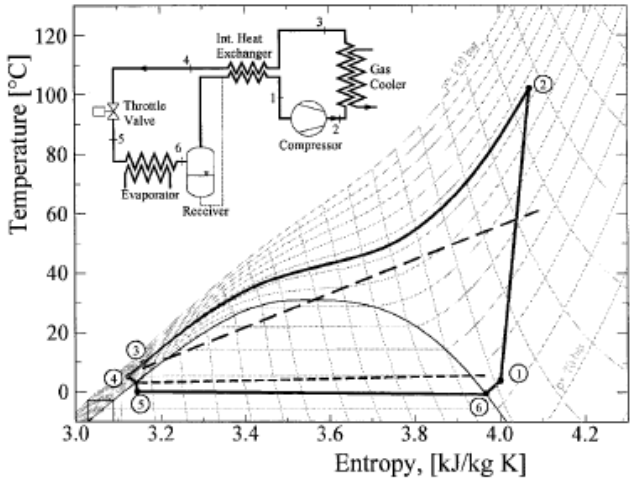

Figure 5. T-s diagram showing the transcritical CO_2 cycle used for water heating. Source: Nekså (2002)

Good temperature matching between the fluids allows avoiding so-called pinch commonly occurring when other working fluids are used inside counter flow heat exchangers. It is crucial to reducing the irreversibility of the cycle and achieving good thermal efficiency.

Comparable with other common refrigerants latent heat of evaporation of CO_2 and its much higher vapor densities at corresponding temperatures results in highest volumetric refrigerating effect of CO_2 amongst other popular refrigerants, as shown in Fig 6.

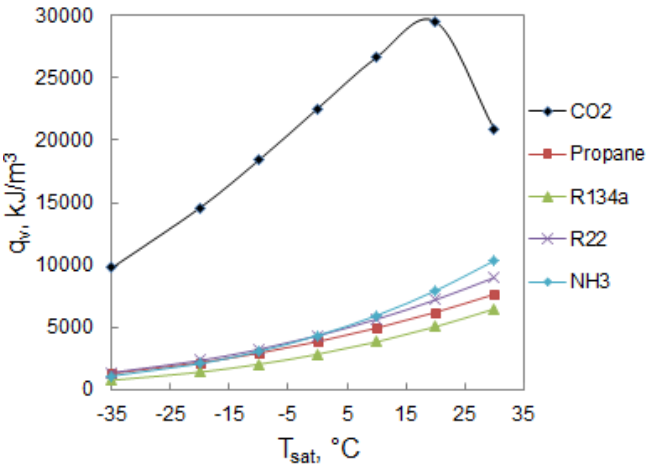

Figure 6. Volumetric refrigeration capacity for selected refrigerants

This means smaller flow rates of a refrigerant needed for a given cooling capacity. Furthermore, due to higher operating pressure, CO_2 will have lower relative pressure drop than competing refrigerants. The corresponding temperature drop will be also lower, thus making the COP of a system based on CO_2 less vulnerable to size of the piping.

When sub-critical systems are considered, low pressure drop translates directly to the low saturation temperature drop – desirable to keep the coefficient of performance (COP) of the system high. In short, high volumetric refrigerating effect, low pressure and temperature drops enable the design of more compact components of the system. This is advantageous from investment cost point of view as well as when space-saving is required, such as in mobile air conditioning. Lower amount of refrigerant in the transfer lines poses also lower threats to human life when a leakage occurs. This is important argument for usage of CO_2 regardless of whether it's a supermarket or an industrial plant. In fact, CO_2 has at least as good safety characteristics as popular halocarbons. It is non-explosive, non-flammable and relatively non-toxic. In case of an accident resulting in a large quantity loss of the refrigerant and rapid increase of CO_2 concentrations, a good ventilation system is required to reduce the risk of adverse health effects or even suffocation. It must be remembered that CO_2 is heavier than air and its vapors will tend to accumulate at the ground level or below it. In this respect CO_2 behaves similarly to the halocarbons but differently from ammonia which is lighter than air and easily vented away. Ammonia on the other hand is poisonous and burns when mixed with air. Carbon dioxide is also safe for environment. It has zero Ozone Depletion Potential (ODP) and Global Warming Potential (GWP) of 1. It is also

inexpensive and widely available as a waste product from various industrial processes. For comparison of selected refrigerants see Table 1.

Table 1. Comparison of popular refrigerants

Refrigerant symbol	Molecular mass, kg/kmol	Tc, °C	Pc, bar	ODP	GWP	TLV*
R-744 (CO_2)	44,01	31,1	70,3	0,000	1	5000
HCFC-22	86,47	96,1	49,36	0,040	1790	1000
HCFC-134a	102,03	101,1	40,6	0,000	1370	1000
R-407C	86,20	86,0	46,2	0,000	1700	1000
R-417A	106,75	86,1	46,1	0,000	2300	1000
R-410A	72,58	71,4	48,6	0,000	2100	1000
R717 (NH_3)	17,03	133,3	112,8	0,000	0	25

*The threshold limit value (TLV) or "Exposure limit", indicates the workplace exposure limits for the components of the refrigerant, typically as an 8-hour time-weighted average

Power applications

The potential of CO_2 as an efficient working fluid was noticed not only in the HVAC industry but also in the power generation sector. It is expected that application of this natural working fluid may be beneficial from a thermodynamic point of view for power cycles in fossil-, renewable- (solar thermal, biomass combustion) and advanced nuclear power plants. In case of the cycles with high temperature heat sources (nuclear power, concentrated solar, combustion) the working fluid can be used entirely in its supercritical state (supercritical cycle) or pass through both subcritical and supercritical states (transcritical cycle). It is identified that transcritical (TCO_2) Rankine cycle exhibits a large internal irreversibility in the recuperator due to the high specific heat difference between the low specific heat stream at the turbine exhaust and the high specific heat stream at the pump discharge [Hejzlar et al. (2006)]. An example of T-s diagram for TCO_2 cycle with HT (high temperature) heat source is shown in Fig 7.

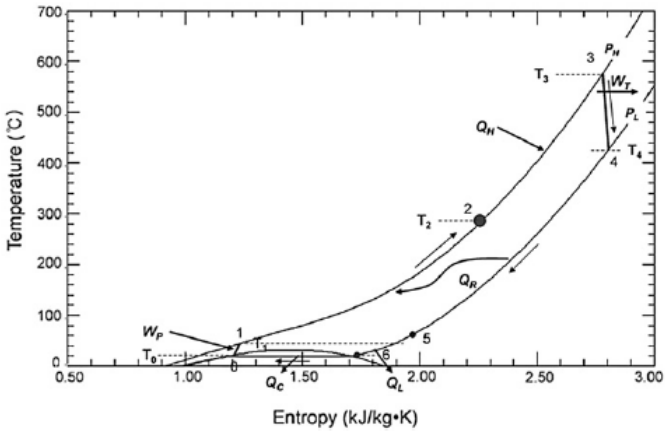

Figure 7. T-s diagram of T-CO_2 Rankine cycle with HT heat. Source: Kim et al. (2012)

The same challenge in the recuperator used in SCO_2 cycle was first revealed by Feher (1968). To address this issue a recompression cycle was proposed in which the recuperator is divided into low- and high- temperature part, each having different flow rates to cope with a large variation in the heat capacity. The schematic representation of the Brayton recompression cycle considered as one of the more promising CO_2 cycles for HT sources is shown in Fig 8.

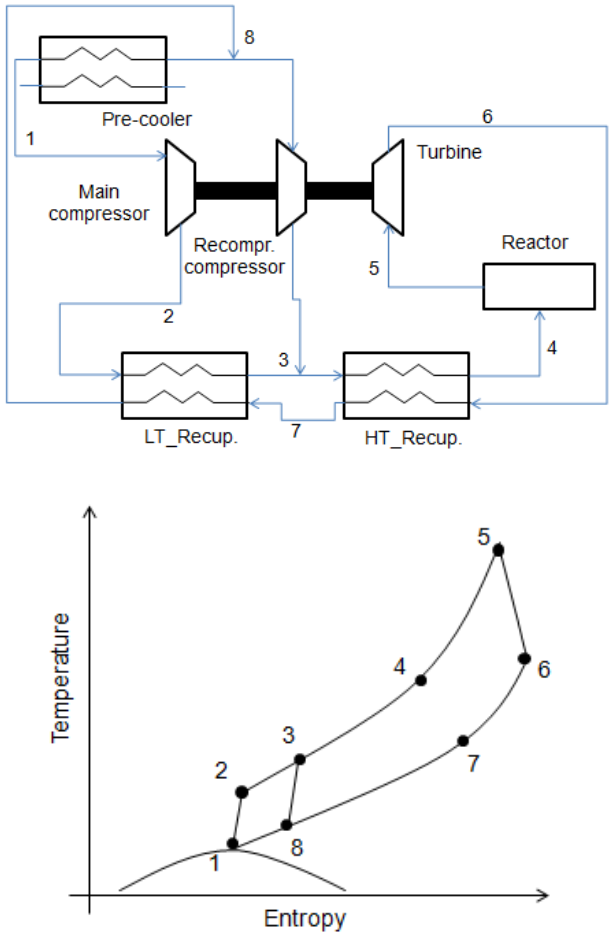

Figure 8. Layout and T-s diagram for SCO_2recompression Brayton cycle

Meanwhile, the low critical temperature of CO_2 ensures especially good temperature match to LT (low temperature) heat sources [Kim et al. (2012)]. Until recently, the most commonly investigated cycles for low-grade heat sources were Organic Rankine Cycles (ORCs) and Kalina cycle (binary fluids and fluid mixtures). The numerous drawbacks of these cycles have been pointed out. For ORC, the working fluids such as R113 and R123 are expensive, have high GWP and contribute to ozone layer depletion. Thermodynamically, the ORC cycles are disadvantaged compared to the supercritical cycles due to the possible pinching in the heat exchanger. For Kalina cycles, even though better temperature match can

be achieved, the usage of binary fluids or mixtures leads to poorer heat transfer than in case of pure fluids. One of the main drawbacks of Kalina cycle is however increased number of system components involving additional separator and intermediate heat exchangers. Moreover, ammonia-water, typically used as a working fluid pair, is considered highly toxic and corrosive.

2.2 CO_2 machinery

CO_2 has been used in different applications for decades, as a working fluid or as an agent serving various industrial purposes, such as: fire extinguishing, carbonating soft drinks and soda water, for enhanced plant growth, as technical gases, for enhanced oil recovery, in urea and methanol production, for metals production and for fumigation and removing organic compounds through its good dissolving qualities. As a result, quite significant experience with CO_2 purpose built machinery exists. This includes a significant experience with CO_2 compressing equipment. Only a few examples of CO_2 based expansion machines have been made public, and they are limited to single laboratory units.

We can distinguish between three main types of compressors: reciprocating, rotary (screw, scroll, swing) and turbo-compressors (axial and centrifugal). Examples of all of the typical compressor technologies can be found in existing CO_2 applications. Depending on the type of the application different compressor technology might be suitable. Generally, reciprocating compressors have been serving small- and medium-size, mainly stationary applications, while rotary machines have been developed for large-size stationary applications or medium stationary and mobile applications. Scroll and rolling piston compressors are examples of rotary machinery developed for smaller capacity applications, such as domestic heat pump water heaters, bottle coolers and automotive air conditioning. The main experience within CO_2 turbocomachinery comes from large industrial applications.

Several aspects must be taken into the consideration if one is to select an appropriate technology for a given application. The capacity requirement of the compressor is probably the most important parameter affecting the designer's choice. Pressure ratio achievable by different types of compressors also varies and often multistage machinery must be used. For example, typical single stage piston compressor stage will be capable of delivering higher heads than a radial stage of a turbocompressor. The off-design performance of a compressor describing its behavior under changeable operating conditions often plays an important role as well, e.g. for air source heat pumps. Sometimes, an oil-free operation must be assured. Finally, the purchase and maintenance costs cannot be ignored, as well as the running cost determined by the compressor's efficiency.

If a quick indication of an appropriate technology is needed, it is well-known practice to apply the similarity parameters developed through the technique known

as dimensional analysis. It is beyond the scope of the present work to go into details concerning derivation of the similarity parameters, but it should be stated that it is based on the assumption that machines are similar when their dynamic and geometrical similarity can be shown. A popular way of presenting machinery performance as function of the similarity is through correlation of the specific speed, N_s (1) and the specific diameter, D_s (2).

$$N_s = \frac{\omega Q^{0.5}}{\Delta h_{is}^{0.75}} \quad (1)$$

$$D_s = \frac{D\Delta h_{is}^{0.25}}{Q^{0.5}} \quad (2)$$

where: ω – *rotational speed, Q – flow rate,* Δh_{is} *– isentropic enthalpy change, D - diameter*

These two non-dimensional parameters combine several important quantities reflecting the nature of the sought machine. If these quantities, such as rotational speed, adiabatic head and capacity of the machine are known, one can get an indication of a suitable technology and its performance from the so called Cordier diagram, known also as N_s-D_s chart. An example of such a chart derived for pumping machinery is presented in Fig 9.

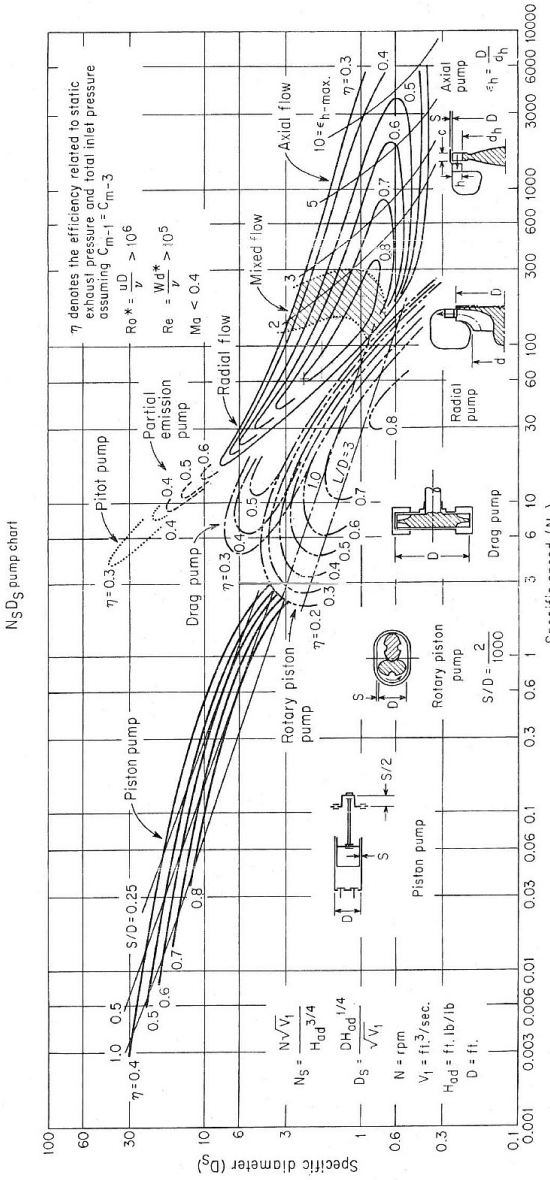

Figure 9. An example of a Cordier diagram (Ns- Ds chart) derived for pumps.
Source: Balje (1981)

The above procedure might be used as a preliminary step in defining the technology capable of fulfilling the designer's expectations. It is should be clear however that depending on a particular case, alternative strategies might be pursued.

To acquaint the reader with some more specific work done within the field of CO_2 machinery, several examples of machines operating with this natural working fluid are presented in the following chapters.

2.2.1 Reciprocating and rotary compressors

Reciprocating compressors work by the principle of reducing the volume of a trapped gas in a cyclic fashion. The most common reciprocating compressor concepts cannot work without lubrication, although examples of oil-free piston compressors, mainly for special purpose larger capacity compressors, are known. They usually incorporate labyrinth seal type of the piston and are slow running costly machines with relatively low efficiency due to the occurring inherent leakage losses. An example of a small oil-free semi hermetic piston compressor for supercritical CO_2 heat pump applications is presented by Baumann and Conzett (2002). A prototype of a rated shaft power of 500W at 1500 rpm was designed and tested for the inlet pressure of 35 bar and the delivery pressure in a range of 80 – 150 bar. The technology incorporates a combination of high pressure piston/cylinder clearance seal with a minimal gap of 4-6 μm and PEEK-plate valves with flat valve springs. The cylinder head of the machine was manufactured from two different materials to investigate the influence of heat conduction between the pressure and suction side of the cylinder. The first compressor was fitted with stainless steel head, the second one with temperature resistant plastic. In both cases the rest of the machine was manufactured in aluminum. The measurements of isentropic efficiency of the two versions of the compressors are presented in Fig 10. The reference power input is measured from the shaft power, so no electrical losses are taken into account. The figure shows the importance of heat leakage from hot parts of the compressor into the suction section. According to the authors, the test series proved the feasibility of the technology for small oil-free CO_2 compressors. The reported efficiencies are not very high, especially for higher pressure ratios, but show potential of the technology for small scale applications. The authors emphasize that an important focus in the future development should be put on a more compact design and lower production costs. It can be added that high heat transfer coefficient of CO_2 while desirable from the cycle point of view can be problematic on the machinery side of the process.

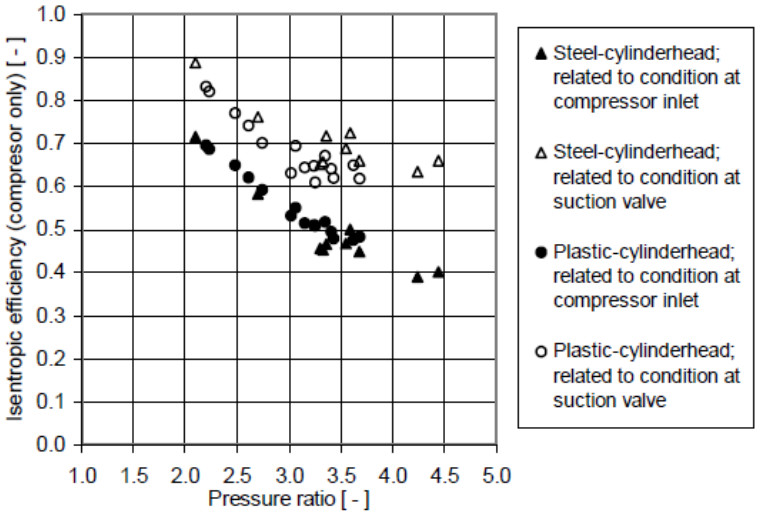

Figure 10. Isentropic efficiency of a small oil-free CO_2 piston compressor at varying pressure ratio for a suction pressure of 35 bar [Baumann and Conzett (2002)]

The performance of oil-free piston compressor can be compared against test data for existing oil-lubricated reciprocating compressors.

Nekså et al. (2000) reported on the development on the series of semi-hermetic reciprocating compressors with swept volumes in the range of 0.5 - 12.6 m^3/h. The single- and two-stage compressors were running at nominal speeds of 2900 rpm and achieving cooling capacities of 0.6 – 15 kW for -35°C evaporating temperature. The measurements of a two-stage compressor in the 4-pole configuration running at 1450 rpm indicated volumetric efficiencies of up to 80% and isentropic efficiencies of up to 60%.

In Christen et al. (2006) performance measurements of five different prototype carbon dioxide compressors are reported. The different compressor designs included:

- a semi-hermetic reciprocating single-stage compressor (Type A) with an nominal cooling capacity of 8.3 kW and displacement of 2 x 20.9 cm^3
- a hermetic rotary two-stage compressor (Type B) with an nominal cooling capacity of 2.4 kW and displacement of 3.33/1.88 cm^3
- a semi-hermetic reciprocating two-stage compressor (Type C) with an nominal cooling capacity of 10.5 kW, intercooling and displacement of 28,8/17.1 cm^3

- a semi-hermetic reciprocating single-stage compressor (Type D) with an nominal cooling capacity of 0.8 kW and displacement of 2.45 cm^3
- a semi-hermetic reciprocating single-stage compressor (Type E) with an nominal cooling capacity of 1.6 kW and displacement of 4.18 cm^3

Compressor tests were conducted for varying suction pressures, superheats and discharge pressures. The comparison of the overall isentropic efficiencies of the compressors is depicted in Fig 11.

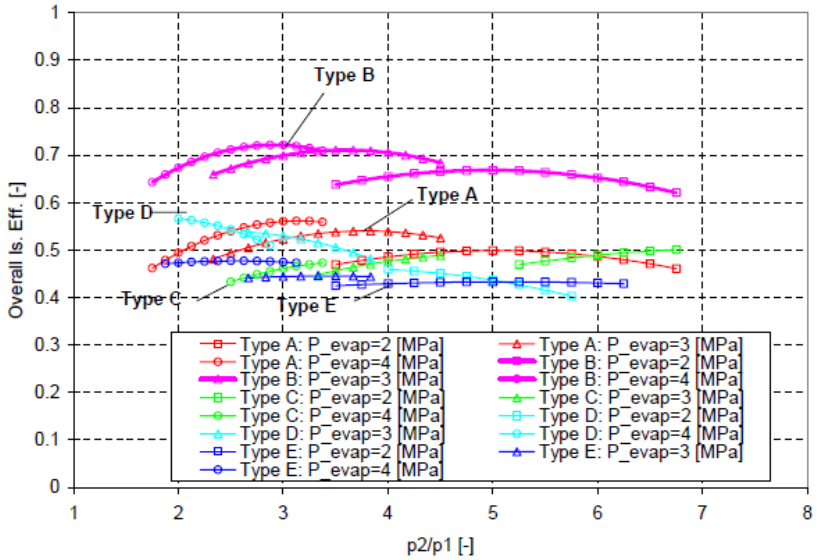

Figure 11. Overall isentropic efficiency of various oil-lubricated rotary and reciprocating compressors. Source: Christen et al. (2006)

It can be seen that overall efficiency of rather small reciprocating compressors presented in the study is low and amounts to below 60% in the full range of pressure ratios. The highest efficiency, in a range of 70%, is reported for the rotary compressor. These high values may seem overly optimistic confronted with the compared piston compressors. The rotary compressor has however an advantage of being equipped in a more efficient DC brushless motor, while the remaining machines are driven by more standard AC motors, 3-phase for compressor types A, C, D and 1-phase for compressor type E. Another factor favoring the rotary compressor in terms of the performance is its double stage configuration, compared to single stage configuration of compressor types A, D and E. Furthermore, the authors do not clarify if and how the heat leak affects the measurements of different types of tested compressors.

An example of the newest generation of semi hermetic piston compressors (see Fig 12) is presented in Hafner et al. (2012 and 2013). The 100 kW 6-cylinder compressor was developed in response to commercial refrigeration market need for a machine capable of delivering flow rates in the range of 10 to 90 m^3/h in a single stage of compression.

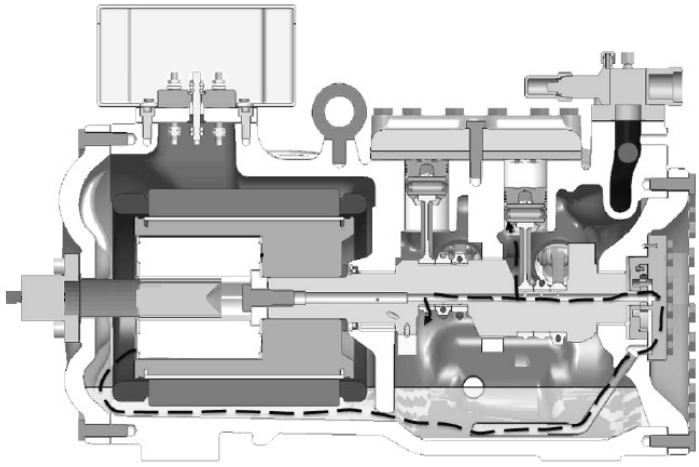

Figure 12. Obrist/Sintef semi hermetic piston compressor

The test results of the compressor, which is still under development, revealed a relatively high overall efficiency. Clear performance advantage of the new compressor over the state-of-art commercial piston compressors for CO_2 applications was shown during the test campaign executed in 2012, see Fig 13. According to the developers, the efficiency improvement can be attributed partially to the application of a new generation of a permanent magnet motor and partially to the careful design of the valves and internal parts of the compressor.

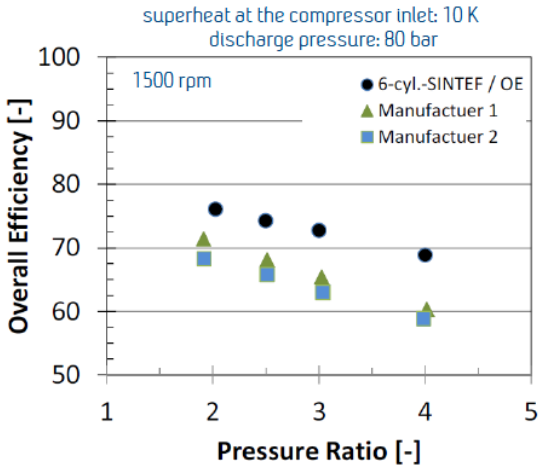

Figure 13. Isentropic efficiency of the new generation of semi hermetic CO_2 piston compressor

Depending on the operating conditions, the compressor can reach isentropic efficiencies up to almost 80%. High efficiency potential is reduced towards higher speeds and operating pressures, which is typical for reciprocating type of compressor. A room for further improvements of the design focusing on the optimization of the piston clearance and the valve area is indicated by the authors. Significance of a careful design of the cylinder sealing for piston compressors with very high pressure difference between suction and discharge is emphasized in Suess and Kruse (1998). The authors show how cylinder leakage losses depend on the difference between the squares of the pressure before and after cylinder. In the case of CO_2 the difference between suction and discharge pressure can easily reach 100 bar. An impact of the rotational speed and operating pressures on the Obrist/Sintef compressor isentropic efficiency is depicted in Fig 14.

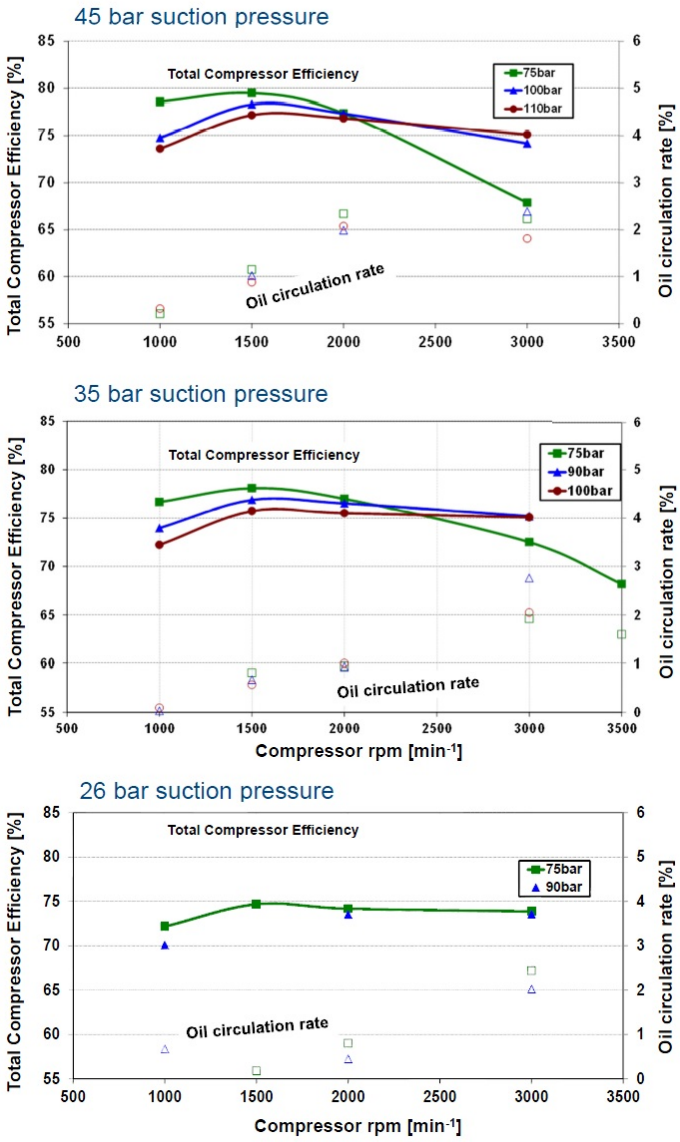

Figure 14. An impact of speed and operating pressure on the isentropic efficiency of a new generation of semi hermetic CO_2 piston compressor. Source: Hafner et al (2013)

Screw compressors

Another class of compressors that can operate without oil is screw compressors. These are, like piston compressors, positive displacement type machines typically used when large volumes of gas need to be handled. The twin screw technology has been identified as a one that could serve both compression and expansion processes when using more conventional halocarbon refrigerants. Unfortunately, when applied to CO_2 the technology appears less suitable due to the significant axial and radial forces generated by the large pressure differences between suction and discharge side of the compressor as well as high leakage losses due to the high pressure differences. Current practice for the twin screw technology has been to use 85 bar as a maximum discharge pressure and a maximum of 35 bar pressure difference between single stage inlet and discharge. It is clear that many CO_2 cycles require both maximum pressures and pressure differences beyond these limits. In Stosic et al. (2002) an analysis is presented showing how the rotor forces created by the compression and expansion processes can be partially balanced to improve the suitability of the technology for high pressure applications. The novelty of the proposed arrangement is the distribution of the admission and exit ports, depicted in Fig 15.

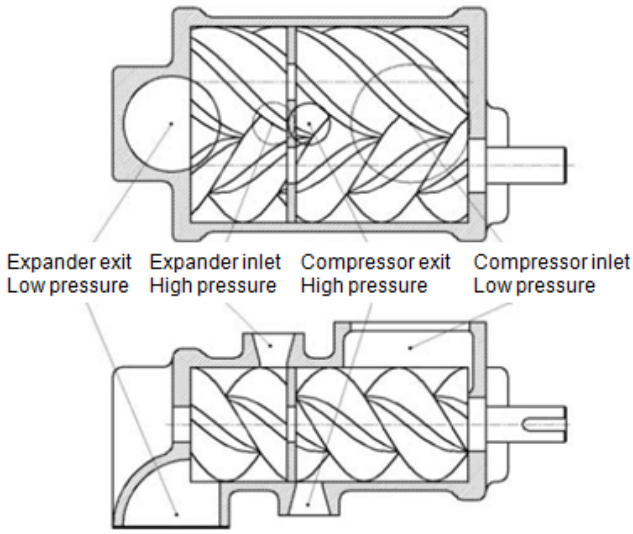

Figure 15. Schematic view of the balanced rotor compressor-expander. Source: Stosic et al. (2002)

Around 20% reduction of the radial bearing loads and elimination of axial loads has been achieved in the course of the computer simulations for a machine designed for a flow rate of 2.75 m^3/min dry saturated vapor at a suction pressure of 35 bar. This would correspond to around 1000 kW of cooling capacity. Still, the remaining loads are huge and amount to tens of kN. Such high loads indicate that high load capability bearings must be used if twin screw technology was to be used for CO_2. Additionally, space available for bearing installation is very limited due to the direct contact of both screws. In effect, the choice of an appropriate bearing technology seems to be limited to roller bearings.

Examples of oil-free screw compressors are known, but not for CO_2 as refrigerant. Oil-free air compressors are used in applications where entrained oil carry-over is not acceptable, such as in medical research, food and beverages industry, textile or semiconductor manufacturing. They are manufactured by several major compressor vendors, but their performance figures are difficult to obtain. The compressors can be equipped with standard oil-lubricated bearings with special seals guaranteeing 100% oil-free operation (Atlas Copco ZR/ZT series) or completely oil-free bearing support (CompAir DH series). In the first case the flow rates processed by the compressor (>300 m^3/h) exceed those typically met in commercial applications. In the later case, water is injected into the compression element to provide lubrication and cooling, hence making the technology unsuitable for CO_2 applications.

2.2.2 Turbocompressors

Turbocompressors belong to the group of machinery that features the continuous flow of a fluid through one or more rotating blade rows. The work is imparted to the fluid by the dynamic action of the blades. The most general classification of turbocompressors can be made based on the direction of fluid flow through them. In a radial (centrifugal) compressor the fluid typically flows towards the larger radius and in an axial compressor it is mainly parallel to the axis of rotation of the machine.

One of the basic turbomachinery equations which relate the work transfer between the fluid and the machine stage is the Euler turbomachinery equation. It is derived from Newton's second law of motion applied to the fluid passing through a control volume. It states that the rate of change of momentum of the fluid is equal to the net applied force F_x on the fluid in the control volume in the direction x of the flow,

$$F_x = \frac{d(mC_x)}{dt} \tag{3}$$

For the steady flow between state 1 and 2, the above equation can be written as

$$F_x = \dot{m}(C_{x2} - C_{x1}) \tag{4}$$

To relate the change of angular momentum of the fluid to the work done by the machine due to the torque τ at the shaft, the right hand side of the equation is multiplied by the local moment arm of the torque, *r*.

$$\tau = \dot{m}(r_2\, C_{\theta 2} - r_1 C_{\theta 1}) \tag{5}$$

The specific work transfer is then given by the equation applicable both for radial and axial machines, generally known as Euler turbomachinery equation.

$$\frac{\dot{W}}{\dot{m}} = \frac{\tau\omega}{\dot{m}} = U_2 C_{\theta 2} - U_1 C_{\theta 1} = \\ = 0.5\left[\left(U_2^2 - U_1^2\right) - \left(W_2^2 - W_1^2\right) + \left(C_2^2 - C_1^2\right)\right] \tag{6}$$

For an axial machine the *U* component of the velocity triangle is constant and this term equals zero, see Fig 16. This is why the work input and pressure ratio will be higher for a radial stage assuming equal diameters of both stages and equal gas velocities. It follows that absolute velocities in an axial compressor must be higher for comparable mass flow rates and pressure ratios. This, together with the inherently higher admission radius of an axial machine, means that to maintain similar efficiency levels for both machines, the mass flow in an axial machine will be significantly higher than in a radial one.

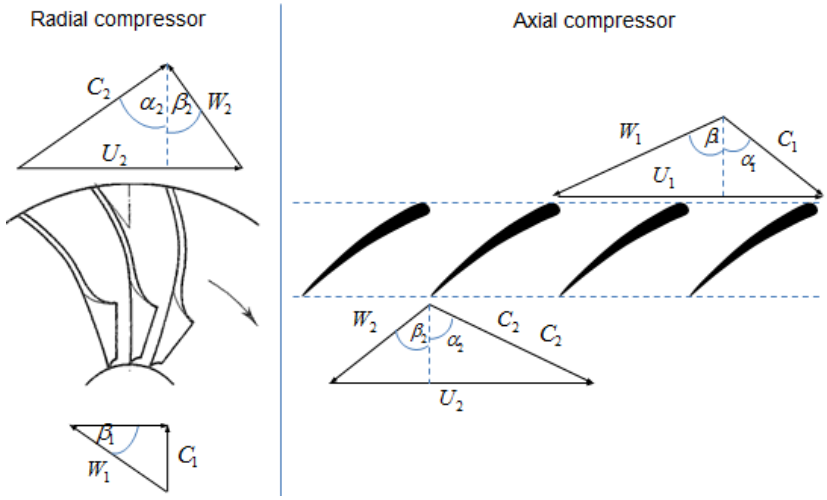

Figure 16. Velocity triangles in radial and axial turbo-compressors

Axial machines are therefore preferable for multi-MW industrial applications, while radial machines are better suited for smaller, lighter, commercial installations. In course of the present thesis it should also become apparent that challenges related to the oil-free operation become more difficult to overcome when smaller applications are in focus.

Radial compressors

A radial compressor is a typical example of turbomachinery often applied in the industry. It has been successfully serving in wide range of applications including aircraft and industrial gas turbines, turbochargers and industrial compressors. Widespread popularity of centrifugal compressor can be attributed to its high efficiency, wide range of operating conditions, compact design and high stage pressure ratios (up to 10:1).

The precursor of a centrifugal compressor was a radial hydraulic pump, later followed by fans and blowers used for ventilation. It is recorded [Cheshire (1945)] that one of the first turbojet engines, the Wittle engine, that was first flown on May 15, 1941 at Cranwell, England , incorporated a centrifugal compressor. Although development of the centrifugal compressor based turbojet engine continued, it soon became clear that axial machines were more suitable for increasingly larger aircrafts. Further acceleration of centrifugal compressor development was fostered in mid-1960s by the need for advanced military helicopters powered by small light turbine engines. Soon centrifugal compressors became a popular choice for small gas turbines for road vehicles and commercial helicopters, as well as for diesel engine turbochargers, chemical plant processes, workshop and factory air supplies and large scale air conditioning plants [Dixon (2005)].

Essential parts of a centrifugal compressor include; an impeller where energy is transferred to the fluid increasing its kinetic energy, and a diffuser where high velocity fluid is decelerated in a diverging duct and converted into a static pressure head, see Fig 17. The fluid from the diffuser is collected in the volute where it is guided as efficiently as possible to the compressor outlet or to the next stage of compression. In multistage compressors the return channel is usually used as an intermediate duct between the diffuser of one stage and the inlet of another.

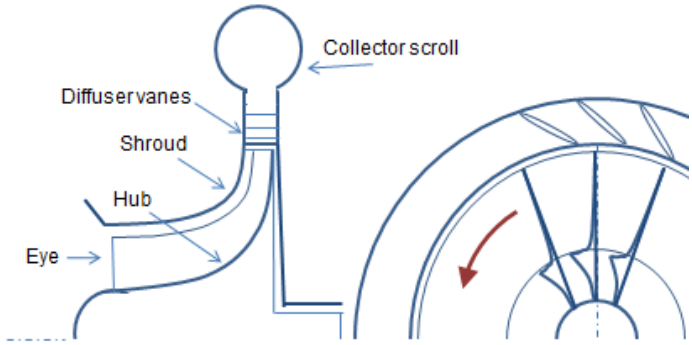

Figure 17. Radial compressor stage

The operating behavior of a centrifugal compressor can be shown in form of a map displaying the relation between pressure ratio and volume or mass flow rate. The region where the compressor can operate is limited by the surge and choke lines and the maximum permissible compressor speed. Typically, such a map includes lines of constant speed and constant efficiency, as shown in Fig 18. The surge line indicates the lowest feasible mass flow at a given speed. The compressor start surging if the flow rate drops below a certain level and the discharge process is interrupted. The surge phenomenon is associated with a sudden drop in delivery pressure and with violent aerodynamic pulsations which are transmitted throughout the whole compressor and may end up in damaging the machine.

The limitation of the maximum compressor volume flow rate is indicated by the choke line. As the mass flow increases at a given speed, the density reduction results in an increase in velocity. At some point the incidence at the leading edge of the impeller and/or diffuser vanes (depending on the type of the diffuser) reaches its maximum and further increase in mass flow becomes impossible. During choking a local velocity in the vaned diffuser or the impeller throat becomes equal to the acoustic velocity. This point represents the maximum gas delivery obtainable at the particular rotational speed.

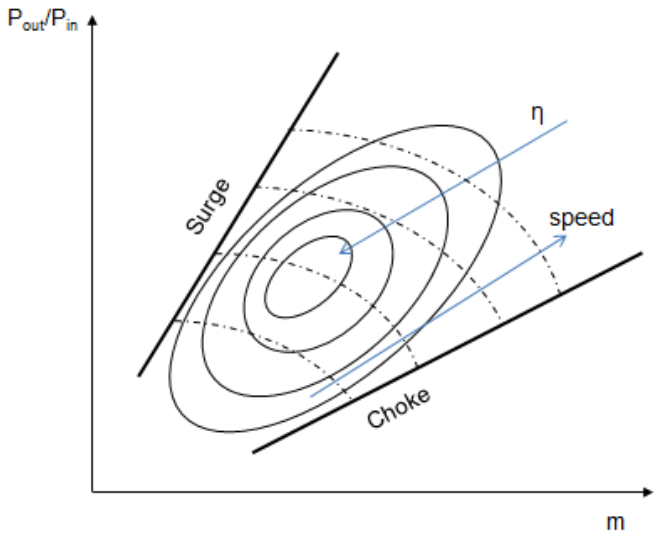

Figure 18. A typical centrifugal compressor characteristic

2.2.3 Industrial scale CO_2 turbomachinery

While CO_2 is now attracting a great deal of interest for being used as working fluid within refrigeration and power production, it has been used for many decades as a support fluid for enhanced oil recovery (EOR). Since its introduction in the early 1970s, CO_2 injection has proven to be one of the most efficient EOR methods. Its good characteristics regarding flowability in porous structures and its ability to dissolve and reduce the viscosity of the oil components make it superior to water which is often an alternative used for EOR. One of the more recent mega-Watt-class applications for compression of CO_2 is carbon capture and storage (CCS) for the purpose of preventing accelerated climate changes. The Sleipner platform was the first to feature CO_2 reinjection compressor for the exclusive purpose of mitigating greenhouse emissions, with about one million tonnes per year of CO_2 injected since 1996.

The traditional approach for compressing CO_2 in large quantities was to use high-speed reciprocating compressors. The main reasons for that included:

- Ability to work across wide range of pressure ratios and capacities
- Short delivery times due to relatively flexible assembly from a selection of frames and cylinders on stock
- Familiarity of the field operators with this type of machinery

An increasing demand for new technologies to meet the demand for clean and sustainable power generation created a room for a new class of machinery capable of handling even higher quantities of carbon dioxide in a more effective manner. Where reciprocating technology reaches its limits, turbocompressors become an interesting alternative. Factors favoring centrifugal compressors include:

- Achievable capacities can reach up to 100 kg/s, exceeding the reciprocating technology for which the maximum is about 12 kg/s
- More reliable and oil-free design reduces maintenance intensity and extends intervals between overhauls
- Superior efficiency
- Higher speeds, that better match to the high speed drivers (electric motors or gas/steam turbines) commonly used in the 10-40 MW range

Within the industrial centrifugal compressors market, two technologies can be distinguished, namely single-shaft and multi-shaft internally-geared machines.

An example of aerodynamic, mechanical and rotordynamic performance of a large single-shaft high pressure centrifugal compressor for CO_2 reinjection is presented in Soulas et al. (2011). The 5.2 MW (7000 hp) compressor was configured as a back-to-back, eight-stage barrel-type machine, with impeller tip width as narrow as two millimeters, see Fig 19.

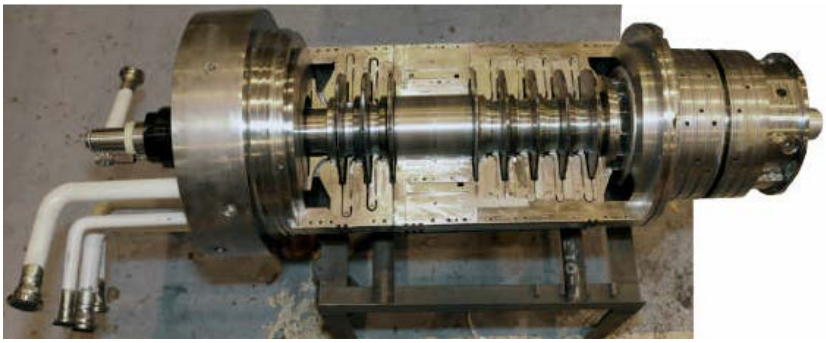

Figure 19. The assembly of the 5.2 MW CCS compressor. Photo courtesy of Dresser-Rand

The compressor was equipped with offset-pivot tilt-pad journal bearings with squeeze film dampers and dry gas seals. During testing of the compressor a good correlation was observed between experimental data and analytical predictions, confirming predicted performance levels and sound rotordynamic characteristic of

the compressor. The machine was capable of compressing CO_2 to a pressure of 310 bar in two main sections, achieving overall pressure ratio of around 8:1. After successful testing the subject compressor was supplied to the end user for a Floating Production Storage and Offloading (FPSO) unit, off the coast of Brazil.

Examples of various integrally-geared compressors, for which a schematic representation is shown in Fig 20, for large capacity CO_2 applications can be found in Habel (2011). According to the author, there are several factors favoring internal-gear design over its single shaft counterpart. These include, among others:

- An axial in-flow to each stage contributing to better impeller efficiency
- More optimal impeller flow coefficients due to the flexible speed selection for each compressor stage
- Possible intercooling between the stages

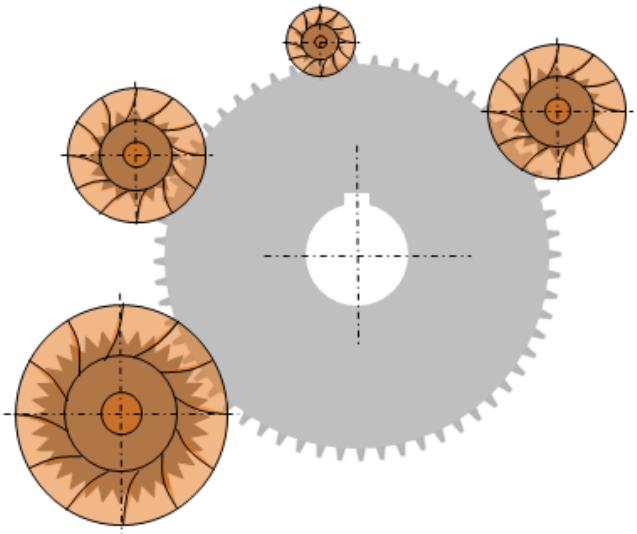

Figure 20. The schematic representation of integrally-geared turbo-compressor.

An example of integrally geared compressors can be the RG series from MAN Turbo. The manufacturer claims that above 80% overall efficiency is possible for the technology. Up to 10 stages are possible within a single unit with impellers measuring from 100 to 1600 mm in diameter. Machines with up to 350 000 m^3/h capacity and shaft power of up to 44 MW are offered. The vendor offers several different sealing options, e.g. carbon ring, single and tandem dry gas seals and labyrinth seals.

Ramgen compressor

Innovative approaches to CO_2 compression are sought not only for commercial scale applications. Although much has been achieved within the field of turbomachinery the below example will show that the room for non-conventional solutions still exists. And although the presented concept is still in the development phase, it may turn out to be a breakthrough when low footprint and high efficiency compression solutions are demanded.

The Ramgen supersonic compressor combines many of the aspects of shock compression systems commonly used in supersonic flight inlets with turbomachinery design practices employed in conventional axial and centrifugal compressor design. According to the analytical predictions and design studies, the novel type of machine has a potential to deliver higher single stage pressure ratios at greater efficiencies than both conventional axial or centrifugal compressor stages [Lawlor and Baldwin (2005)]. The proof-of-concept system was designed to process 1.43 kg/s of air and to produce a pressure ratio of 2.41. Based on that effort an industrial CO_2 compressor has been proposed that could offer both significant purchase savings and efficiency advantages over standard industrial CO_2 compression technology.

The conceptual rotor was configured with an oblique shock system and a terminal shock; according to the principle found in supersonic flight inlet designs, see Fig 21.

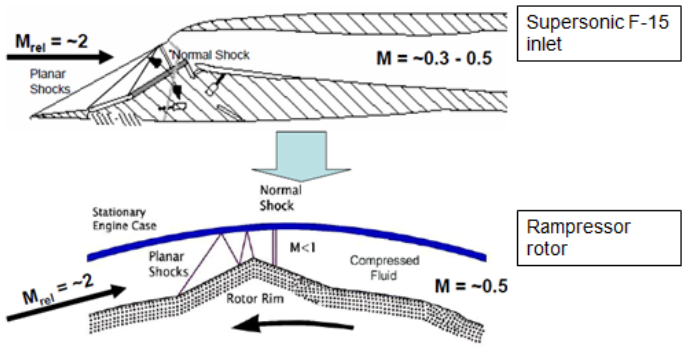

Figure 21. Supersonic flight inlet and supersonic compressor principle. Source: Lawlor and Baldwin (2005)

The rotor flow path is determined by the shape of three elongated blades or strakes mounted on the rim of the rotor, as shown in Fig 22. The main purpose of the blade, unlike in conventional turbo-compressors, is to guide the gas stream, not to compress it. The principal compression work is done by the shock system generated by a compressive ramp or largely planar surface integrated into the rim

of the rotor. The oblique shock is generated by a ramp, and the normal shock is produced downstream of the throat where the subsonic diffusion process commences.

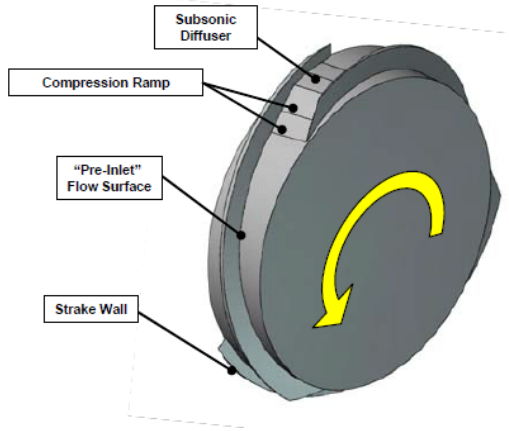

Figure 22. Supersonic compressor stage rotor. Source: Lawlor and Baldwin (2005)

The designers' expectations about the high efficiency of such a system stem from the experience with supersonic flight inlet systems. In Fig 23 the comparison between the flight inlet performance and the performance of conventional industrial compressors is shown. The adiabatic efficiency levels for Point A and the "Military Standard" performance trend do not include impact of the pre-swirl, de-swirl or diffusion losses associated with the stator elements that will be present in a stationary machine. Efficient execution of the above processes will therefore be crucial to realizing the potential performance suggested in Fig 23.

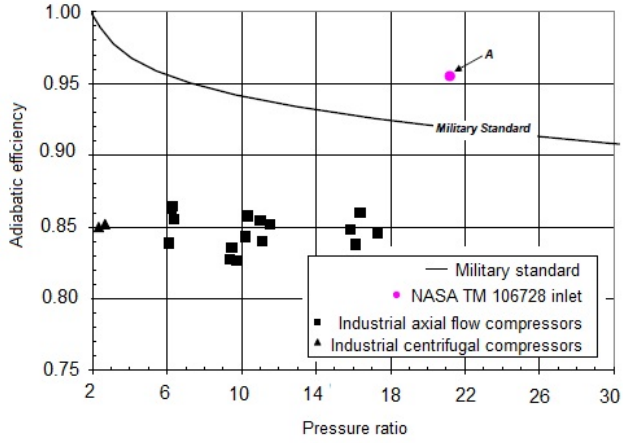

Figure 23. Comparison of the performance of the flight inlet systems with conventional industrial compressor efficiencies. Source: Lawlor and Baldwin (2005)

Initial tests of the novel compressor have shown that the analytical tools used to design the system deliver predictions consistent with the experimental data. The measurements obtained for relatively low total pressure ratios for the rotor, below 2.5, indicate that that the system performance will be sensitive to the tip gap, especially as the future pressure ratios per single stage are expected to reach 10:1.

2.2.4 Small and medium size CO_2 turbomachinery

Only a few examples of small- and medium-scale CO_2 turbo machinery can be found and generally they are limited to laboratory tested prototypes. A probably most detailed report within the field was released by Sandia National Laboratories in USA [(Wright et al. (2010)]. That report is cited extensively in the attached papers. Some of the remaining experience within the field of small-scale CO_2 turbomachinery will be mentioned in the present chapter as well.

It is known that for certain refrigeration applications CO_2 cycles could benefit relatively much from introducing an expander to replace the throttling valve [Yang et al. (2005)]. The study of Robinson and Groll (1998) indicated that an efficient design of the CO_2 expander would be needed.

Hays and Brasz (2004) presented and tested a one-stage two-phase axial-flow impulse turbine with a view to improving efficiency of CO_2-based cycles. A small scale prototype (see Fig 24) with the rotor diameter of 7.1 cm (2.8 inch) and the

blade height of 0.76 cm (0.3 inch) was operated at a maximum speed of 12 800 rpm.

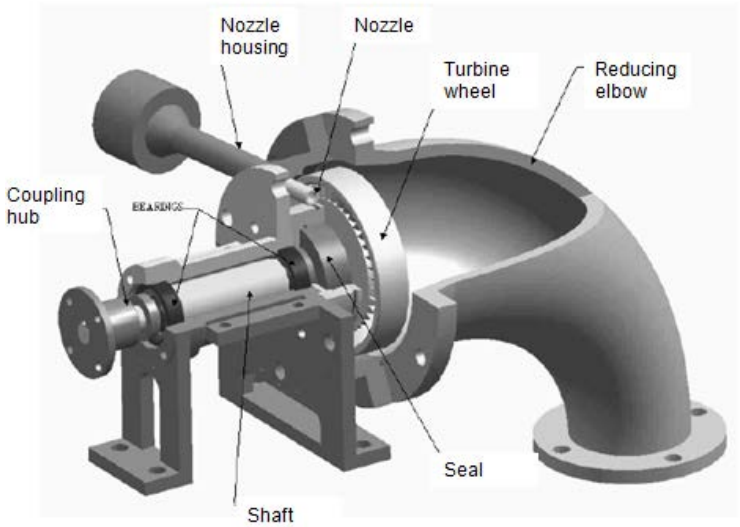

Figure 24. A depiction of a small impulse-type axial CO_2 turbine. Source: Hays and Brasz (2004)

The measured isentropic efficiency of 56 % at the power output of 310 watts was close to the predicted efficiency of 61 %. The authors attribute the discrepancy between the predictions and test data to the relatively large degree of sub-cooling at the inlet compared to the saturated conditions assumed for the calculations.

Another study, this time for a radial outflow impulse turbine designed for a CO_2 refrigeration process with relatively low capacities, was presented by Tøndell (2005). The test conditions, given in Table 2, were chosen to approximate the real conditions in CO_2 based refrigeration, i.e. mobile air conditioning, with corresponding cooling capacity of around 10 kW.

Table 2. Process conditions for expander design

Property	Unit	Value
Inlet temperature	°C	30
Inlet pressure	Bara	100
Outlet pressure	Bara	40
Mass flow	Kg/s	0.05
Jet velocity	m/s	133

The turbine principle geometry is shown in Fig 25. The nozzle jet is represented by line ED and the tangent where the nozzle jet hits the turbine wheel by the line AB.

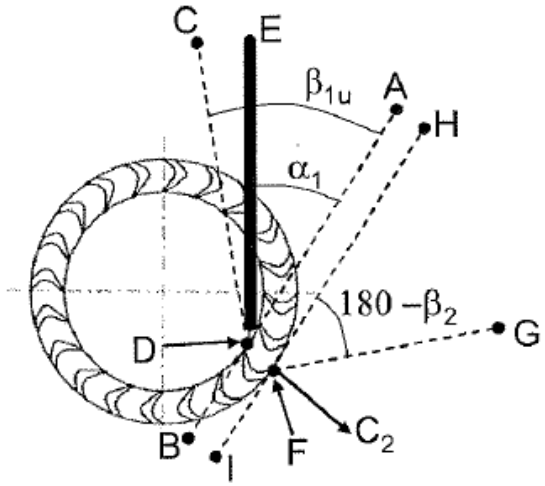

Figure 25. The working principle of a radial outflow impulse turbine. Source: Tøndell (2005)

The experimental campaign showed low turbine efficiency, in the range of 24-30%. Poor performance of the machine is attributed by the author to the three main loss mechanisms: the exit loss, the loss from jet not hitting the blade and the rotational losses. It is also pointed out that the nozzle efficiency is only 60 %, while up to 84 % nozzle efficiencies are reported for other working fluids [Hays & Brasz (1996)]. The author supposes that conical nozzle jet caused considerable fractions of the jet to by-pass the turbine blade. Further improvements could involve optional shaft support, which in this case, comprised the standard grease lubricated

roller bearings generating considerable friction loss. It is also pointed out that the velocity triangles achieved during the test runs deviated from the design ones as the machine did not reach its intended speed.

2.3 Windage in CO_2 machines

Rotational losses or windage losses can be of significant magnitude in CO_2 machinery [Tøndell (2006), Briggs (2008), Wright et al. (2010), Paper I, Paper II]. Vrancik (1968) developed an equation to predict the windage losses for a cylindrical rotor and modified it with empirical relations to take into account the effects of the salient poles and shrouds of the homopolar induction alternator. Measurements of the windage loss of a shrouded homopolar inductor alternator conducted at NASA Lewis Research Center agreed with ± 10 % for a range of pressure from standard atmospheric to 2.75 bar. The developed method assumed that the gap is small compared to the radius and length of the rotor and that the flow in the gap is laminar. The rotor moves with respect to the stator with a velocity V thanks to a driving force F. An action of force F must be counterbalanced by an equal in magnitude and opposite in direction force coming from the shearing stress of the fluid, as shown in Fig 26.

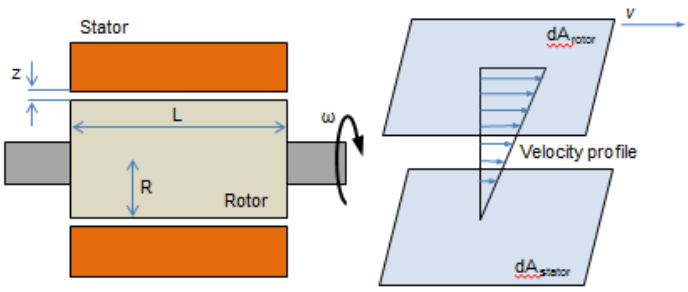

Figure 26. Depiction of assumptions for calculation of windage of a rotating cylinder

The shearing stress was defined as the force per unit area dF/dA and the strain as a ratio of the displacement due to the stress to the transverse dimension z. The shear stress in a fluid having laminar flow is proportional to the rate of change of shear strain $v \cdot t/z$, therefore:

$$\frac{d}{dt}\frac{Vt}{z} = \frac{V}{z} \tag{7}$$

and

$$\frac{dF}{dA} \propto \frac{V}{z} = \mu\frac{V}{z} \tag{8}$$

where viscosity μ is treated as constant of proportionality. Integration results in

$$F = \mu\frac{VA}{z} \tag{9}$$

where $A = 2\pi RL$ and $V = R\omega$ or

$$F = \frac{2\pi\mu R^2\omega L}{z} \tag{10}$$

The windage power is

$$W = FR\omega = \frac{2\pi\rho R^4\omega^3 L}{\mathrm{Re}} \tag{11}$$

where

$$\mathrm{Re} = Rz\omega/v \tag{12}$$

Finally, if $2/\mathrm{Re} = Cd$ where Cd is understood as the skin friction coefficient, the windage loss is defined as

$$W = \pi Cd\rho R^4\omega^3 L \tag{13}$$

The equation developed for a laminar flow ceases to be valid for fast rotating rotors. It was shown that sufficient approximation of windage for turbulent case is obtained when the theoretical skin friction coefficient for turbulent flow between two parallel plates is applied

$$\frac{1}{\sqrt{Cd}} = 2.04 + 1.768\ln(\mathrm{Re}\sqrt{Cd}) \tag{14}$$

The model developed by Vrancik was later validated by Wright et al. (2010) for a rotor spinning at 35,000 rpm in the CO_2 atmosphere at pressures ranging from 32.4 – 55.15 bar. The comparison of measured and modeled windage losses are shown in Fig 27.

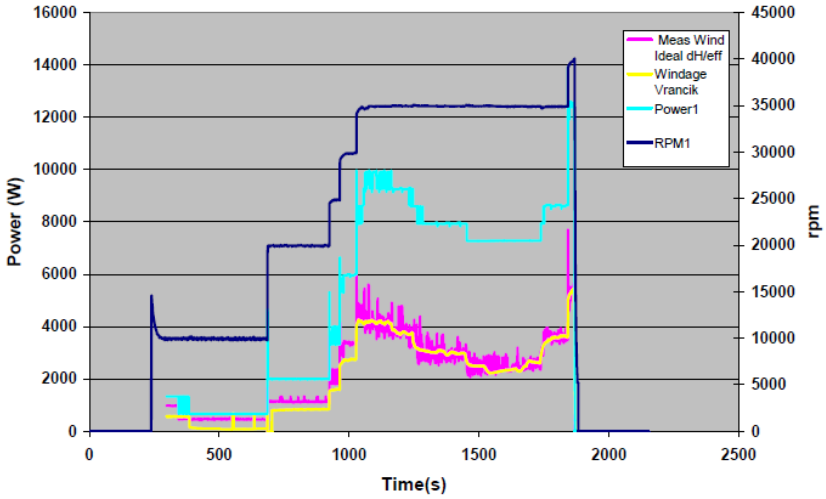

Figure 27. Comparison of windage estimates based on measured data (magenta) with the Vrancik model (yellow). Source: Wright et al. (2010)

The windage loss is proportional to the density of the ambient fluid and increase with third power of rotational speed. The magnitude of the loss may be significant, thus it cannot be neglected during the design process of a hermetic type machine. Examples of efficient high speed radial turbo-compressor designed for R134-based cycles are known [Schiffmann and Favrat (2009, 2010), Alvares (2010)]. However, if one realizes that carbon dioxide have around 7 times higher vapor density at -5 °C than R134, it becomes clear that previous experiences do not necessarily guarantee achieving good efficiencies for CO_2 applications.

2.4 Seals and bearing concepts for oil-free operation

Several configurations enabling oil-free compression can be distinguished depending on the size of the compressor and particular technology choices. It should be further clarified that a compressor enabling oil-free processing of the gas is not necessarily an oil-free machine. Some vendors use the term oil-free compressor for machines providing “clean” gas compression but supported on oil-lubricated bearings. To avoid confusion we will distinguish between an oil-free compressor and a compressor providing oil-free compression. To picture the importance of such a distinction let us consider the following examples.

Typically, to avoid losses of the gas or losses of the energy transferred to the gas in the impeller any leakage from the compressor stage to its surroundings should be prevented. In large MW-class machines this can be realized through application of dry gas seals. This technology has been serving in turbocompressors for already more than 30 years. It is estimated that that over 80% of centrifugal gas compressors manufactured today are equipped with some variation of a dry gas seal [Stahley (2003)].

Dry gas seals are non-contacting, dry-running mechanical face seals. The “running gap” of the seal is created between a stationary and a rotating face of the seal by fluid-dynamic force generated by the grooves of a rotating face. There is a variety of dry gas seals configurations, among which the “tandem” style seal, see Fig 28, is typically applied in process gas services.

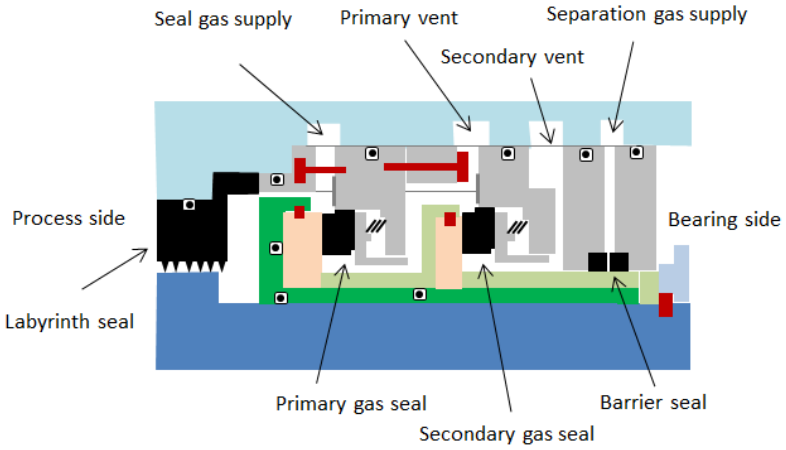

Figure 28. Tandem style dry gas seal

The tandem seal consists of a primary and a secondary seal, placed in a single cartridge. The task of a primary seal is to absorb the total pressure drop to the vent system. The secondary seal serves as backup should the primary seal fail. A sealing gas is supplied between the inner labyrinth seal and the gas seal providing the working fluid for the running gap and the seal between the atmosphere and the compressor internal process. The separation of the process gas from the seal gas is ensured by the inner labyrinth seal. The dry gas seal is accompanied by a barrier seal, which separates the gas seal from the compressor shaft bearings. The separation gas used in a barrier seal is typically air or nitrogen. The primary function of the barrier seal is to prevent lubrication oil migration into the gas seal. Secondary function of the barrier seal is to serve as a last defense in the event of a serious failure if both primary and secondary gas seals.

The schematic representation of a compressor providing oil-free compression, equipped with dry gas seals is presented in Fig 29.

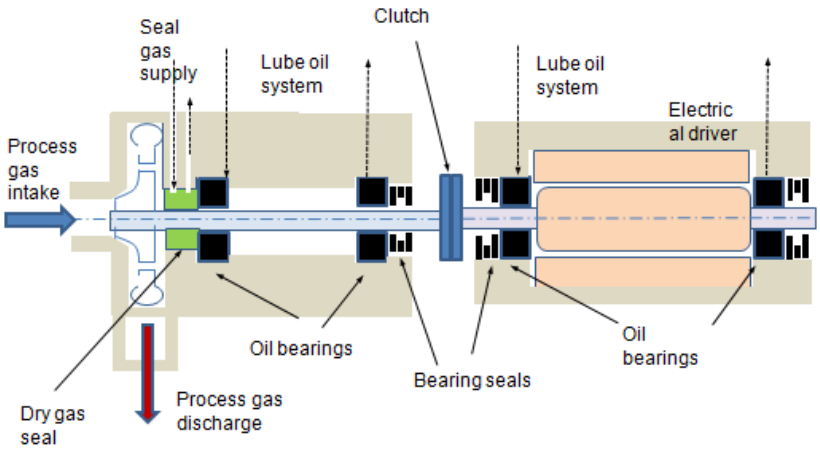

Figure 29. Industrial turbo-compressor equipped with dry gas seals

For smaller compressors, in a few tens to a few hundreds kW class shaft power, for which dry gas seals are not available, a different strategy must be applied to avoid leakage to the atmosphere or contamination of the process gas. For example, a hermetic configuration, with oil free bearings and electrical motor contained in a single housing is used. The leakage of the compressed gas between impeller space and motor cavity is limited through the application of labyrinth seals. Labyrinth seals are most widely used and the simplest among the annular type gas seals. They are made of a series of blades and cavities, as shown in Fig 30.

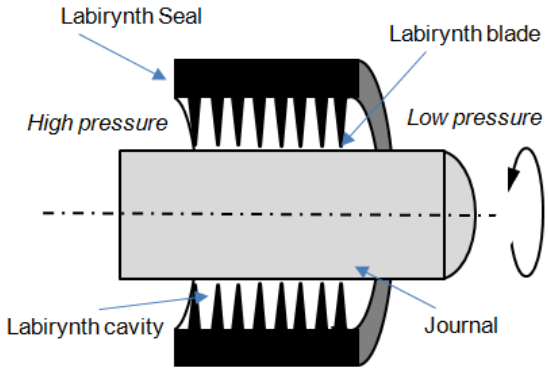

Figure 30. Cross/section of a labyrinth seal

The working fluid is throttled and expanded repeatedly in the annular constrictions formed by the seal blades, thus reducing the total pressure of the fluid from one cavity to the subsequent one, limiting the overall axial leakage rate. Although labyrinth seals have been successfully serving in various types of turbo-machinery for decades, they do not eliminate the leakage completely. In hermetic CO_2 compressors this feature is actually desirable as some part of the process gas has to be throttled into the cavity in order to provide at least the fraction of the cooling capacity needed to remove friction heat generated by the gas bearings and the rotor, see Fig 31.

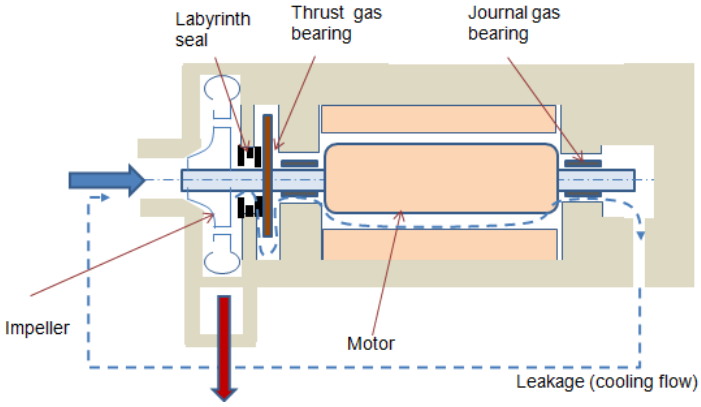

Figure 31. An example of a hermetic oil-free compressor configuration

The above examples illustrate that oil-free compression might incorporate significantly different solutions. Dry gas bearings enable separation of a process gas from the motor and bearings, but require relatively low shaft speeds and relatively large diameters. Due to not complete elimination of a leakage, a working fluid make-up system will also have to be considered. The CO_2 compressor in such a case is not expected to suffer from high windage losses of a rotor. On the other hand, choice of the specific speed for each impeller might be more constrained, and the overall design of the machine with its auxiliary systems, e.g. lube oil distribution and seal gas delivery, more complex.

Hermetic oil-free concepts favor smaller machines, in theory giving more freedom in selecting compressor speed and in making the overall design more compact and simpler.

An attempt to categorize the appropriate technologies that might be suitable for oil-free compression based on the size of the machinery is presented in Fig 32. The dotted line represents the compressor range that seems especially challenging in terms of achieving high efficiencies due to the windage issues.

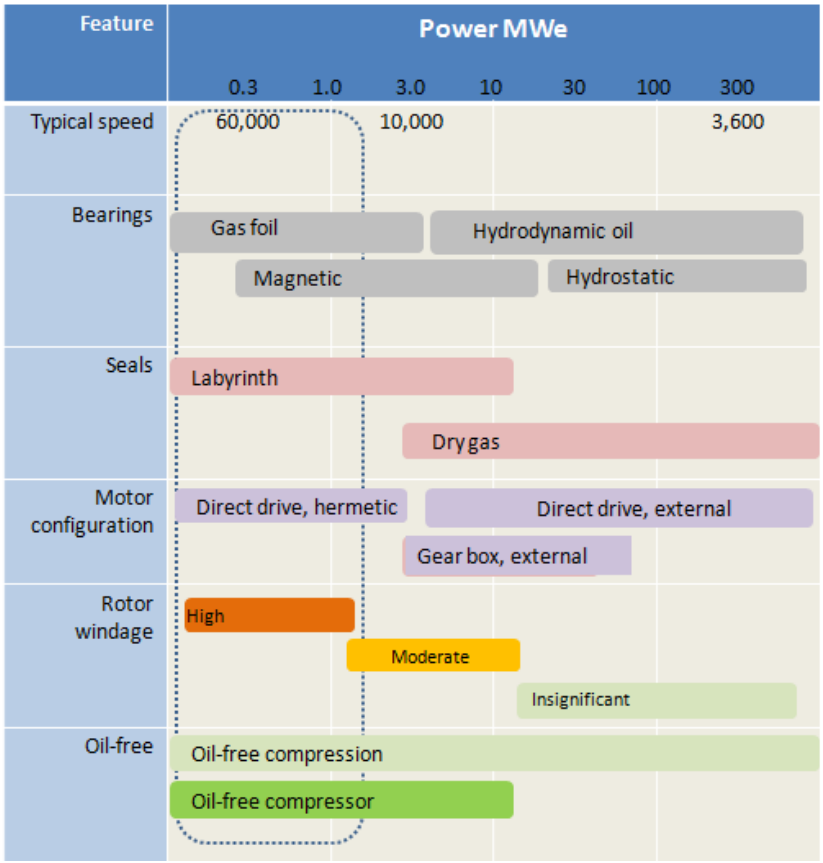

Figure 32. Overview of the potential technology choices for oil-free CO_2 compression systems

2.5 Oil free bearing technology for commercial applications

Oil-free bearings are an integral part of oil-free machines. Two main categories of the technology enabling oil-free operation can be extinguished among the bearing alternatives: active magnetic bearings and fluid film bearings. Regardless of the technology choice, oil-free bearings offer the following advantages over its lubricant based competitors. These include:

- No speed limitation
- Quiet operation
- Wide operating temperature range
- No scheduled maintenance
- Virtually no wear once they are in operation

Magnetic bearings

Active magnetic bearings (AMB) offer a relatively novel way of solving classical problems of rotor dynamics by supporting the rotating rotor with no contact, wear and lubrication, and controlling its behavior through an electronic system. Although the early history of AMB can be traced back to as far as 1840s when Earnshaw (1842) and later Braunbek (1939) were investigating the magnetic forces acting on a freely suspended body, the first industrial applications came much later, when Haberman and Liard (1977) introduced AMBs to aerospace momentum wheels applications. The pronounced growth of interest in AMB followed the implementation of digital control becoming a standard element of modern machinery. The availability of the design tools for modeling rotor dynamics and advances of hardware for power electronics led to industrialization of the technology some 20 years ago. Today, AMBs are used in a number of applications including high-speed turbines and compressors, pumps and jet engines and flywheels for energy storage. The bearings are inherently unstable and a feedback control system is needed to provide stable operation.

The principle of the active magnetic bearing is shown in Fig 33. Main components of the system include: a gap sensor measuring the displacement of the rotor from its reference position, a microprocessor control unit deriving a control signal from the sensor and a power amplifier transforming the signal into a control current generating the magnetic field responsible for maintaining the rotor in its hovering position. Of course, the support of a full rotor requires several magnets connected to one another by a multivariable controller.

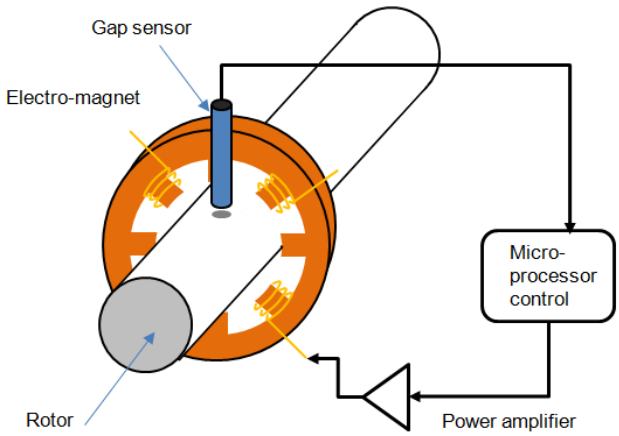

Figure 33. Principle of actively controlled magnetic bearing

The characteristics of the system are determined by the software allowing for adjustments of stiffness and damping, also during operation of the bearing. Magnetic bearings require electromagnetic coils to generate magnetic forces sustaining the rotor in levitation. Additional stacked laminations are required on the rotor to reduce the eddy currents and hysteresis losses. As a result static parts of the bearing are larger than those of a competing technology. The relative footprint of the machine using AMBs increases with decreasing rotor size, which makes the technology less suited for very small capacity applications. Another drawback of a magnetic bearing system is the need for touch-down bearings in case a power failure occurs, and these are difficult to design, increase the length of the motor and add complexity to the system. At present, touch-down bearings are manufactured by only a handful of companies around the world. Typical design of a backup bearing comprises ceramic tightly packed balls, without ball separators. The racers are manufactured in corrosion resistant steel to protect the bearing from aggressive gases. For particularly harsh environments zirconia balls can also be used. The touch-down bearing system must be capable of fulfilling several strict design criteria, including extremely high accelerations from zero to nominal speed, high-impulse radial and axial forces, limited dimensions, poor lubrication and reasonable manufacturing costs.

Fluid film bearings

The Fluid Film Bearing represents the second category of non-contact bearing technology. Depending on the working principle two further sub-categories can be distinguished: dynamic or static bearings.

In the **dynamic bearing** the lifting force is generated through the rotation of the shaft thanks to the viscosity of the lubricant dragged along with the moving surface. During the relative movement of the bearing surfaces wedge is formed, in which pressure is generated due to the hydrodynamic action of the fluid, see Fig 34. The combination of Couette (shear driven) and Poisselle (pressure driven) flows in the gap produce a distribution of pressure allowing to keep the two surfaces separated.

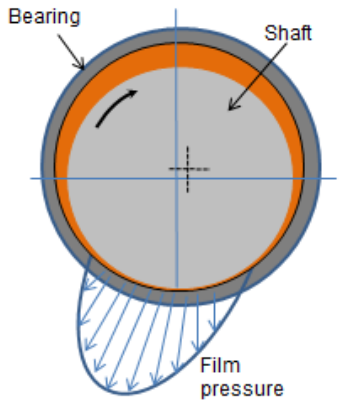

Figure 34. Hydrodynamic pressure generation

In a **static bearing** a pressurized fluid is delivered to the space between the surfaces assuring continuous flow through the bearing. Unlike the hydrodynamic bearing the hydrostatic one avoids the slip resistance during the start-up and rundown, thus reducing the wear of the bearing. The hydrodynamic effect gets involved also at zero rotational speeds thanks to the circumferential difference in the fluid flow resistance. The drawback of a static bearing is an additional consumption of energy, as the continuous work of a lubricant delivery pump is required. Systems involving continuous oil circulation can typically be found in smaller capacity compressors for refrigeration applications.

Foil bearings

Foil bearings have been selected as a potential technology for enabling cost efficient oil-free CO_2 compression for various commercial applications (Paper II). They belong to the group of self-acting hydrodynamic fluid film bearings. The lubricating fluid film is generated by the viscous pumping action of a moving

runner, a mechanism common for all hydrodynamic bearings. The distinctive feature of the bearing is the combination of a sheet metal foil layer and a series of supporting spring (bump) foils depicted in Fig 35.

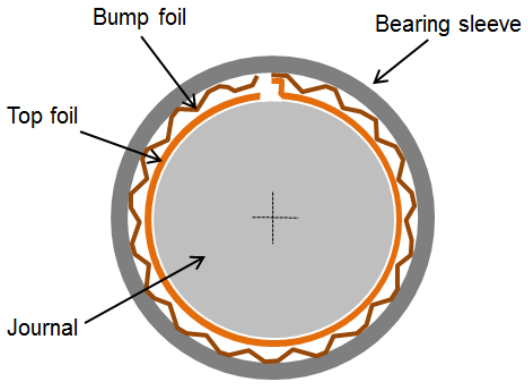

Figure 35. Cross section view of simple radial foil bearing

The top foil's primary function is to trap the gas film and enable generation of the hydrodynamic pressure required to push the shaft ensuring the non-contacting movement. The major benefit of the foil surface being compliant is larger thickness of the film than would be present in a geometrically identical rigid bearing. The thicker fluid film and compliant surface make the bearing less susceptible to damage by ingested dirt particles.

The spring foils play multiple roles providing compliance, tolerance to misalignment and distortion, and external damping. Through a relatively simple and robust design a high tolerance to misalignment, shock and excessive vibrations is achieved. When the machine is in operation the fluid film protects the surfaces from wear. During stop/start sequences, when the foil surface is in contact with the shaft, special coatings minimize the wear. The modeling of foil bearings is rather complicated due to the complex non-linear structural, hydrodynamic and thermal interactions between the foils and the fluid film. Thermal management can sometimes also be an issue. Typically used materials such as nickel based super-alloys are characterized by low thermal conductivity and high thermal expansion coefficients. In effect, localized overheating of the bearing can lead to foil distortion, rupture of the fluid film, and bearing failure (DellaCorte and Bruckner, 2010).

Main advantages of foil-bearing technology

High reliability – Only a few parts needed to support the rotating assembly results in increased reliability of the machine supported on foil gas bearings. Elimination of the components responsible for lubricant distribution further simplifies the system architecture.

No scheduled maintenance – During operation of the machine there is no direct contact between metallic surfaces of the bearing, hence the wear is minimized. Since there is no oil in the system, there is no need to check and replace the lubricant. This results in lower operating costs.

Soft failure – In case any failure occurs, the overall damage is quickly restrained by the bearing design that due to the inherently low clearances and tolerances prevents the shaft from excessive movement. As a result, the main part of the impact is confided to bearings and shaft surfaces, and the damage to other parts of the assembly is minimal and usually repairable during overhaul.

Low and high temperature capabilities - Many oil lubricants will not operate at very high temperatures as they will decompose. At very low temperatures they will become too viscous to provide efficient operation or they will simply freeze. Foil bearings can provide reliable operation at severely high temperatures as well as at cryogenic temperatures.

Pure process fluid operation – Foil bearings have operated in various applications utilizing fluids such as air, refrigerants, helium, xenon, and oxygen and nitrogen and operating down to cryogenic temperatures. Often a fraction of working fluid can be used to lubricate the bearings without the need for any additional lubrication system or additives to the working fluid. As a result, the system can operate efficiently without contamination of internal surfaces of the installation, which is often the main motivation for pursuing oil-free system concepts.

2.6 Partial admission turbines

A significant portion of the original work presented in this thesis (Paper III and IV) explores an idea of partial admission applied to a radial type turbocompressor. Unfortunately, rather scanty amount of experience on this subject is made publicly available. Examples of radial blowers and compressor with either partial admission or emission are presented in Paper III. None of the mentioned technologies seems, however, to have a potential of achieving reasonably high efficiencies at pressure ratios required in commercial scale CO_2 applications. On the other hand, rather rich experience exists within the field of partially admitted axial turbines. While that experience may not be, in all of its aspects, directly transferable to the design of a novel turbocompressor, it is believed that analogies between the two technologies

can be found, and hence an extended introduction to the subject should be provided at this place.

Where small volumetric flow rates and low rotational speeds are design constraints, partial admission machines should be considered. In fact, partial admission has been applied for more than a century and, over the years, has been studied by many researchers [Stodola (1927), Ohlsson (1962), Traupel (1977)] whose insights provided a general physical understanding of the phenomena accompanying operation of partial admission turbines.

It is commonly adopted practice to use partial admission turbines in high pressure stages of small axial steam and gas turbines. Such a configuration allows using relatively high blades and avoiding significant blade losses that would occur if the flow was admitted in full arc but with smaller blades.

Partial admission is also routinely applied for industrial steam turbines in CHP (combined heat and power) plants which frequently operate at partial load, thus enabling the district heating grid to act as a heat sink. When rapid load changes occur, the inlet steam flow is individually throttled with control valves into separate annular arcs of the first stator row. If a partial admission stage is applied as a first admission stage in an industrial turbine it is commonly referred to as a control stage. High part load efficiencies are possible due to the maintained high pressure at the turbine inlet [Fridh et al. (2012)]

Performance of a turbomachine is limited by various loss mechanisms. While some of them are common for all types of turbomachinery, operation in partial admission mode introduces additional forms of irreversibility. A general division and brief characterization of losses occurring in full- and partially admitted axial turbine are listed below.

Losses in a full admission turbine stage

- **Endwall losses**. Occur on surfaces having direct contact with a fluid in motion due to the separation of the boundary layer formed on the end-wall of hub and casing when it is hit by the blades.
- **Profile losses**. Generated through viscous interaction between the boundary layer around the blade profile and the main through-flow. The loss is calculated in a similar manner as a pipe flow friction and is mainly dependent on the flow velocity and surface roughness
- **Mixing losses**. Occur in turbomachinery due to the shear strain between the fluid streams having different velocities. Mixing losses are especially pronounced in separated flows, such as in the jet/wake zones at the discharge of the blades
- **Leakage losses**. For unshrouded rotors they are generated by undesirable fluid flow over the tip of the blade driven mainly by the pressure difference

across the gap. For shrouded blades the leakage takes place in the space between blade the rings and the turbine casing

- **Disc friction losses**. Occur due to the relative motion between the disc and the housing of the turbine as a product of interaction between the skin friction and circulation of the fluid between these two surfaces.
- **Shock wave losses**. Result from viscous dissipation across a shock. In a transonic turbine stages the trailing edge shock from the upstream blade rows are one of the most important sources of unsteadiness (Denton, 1993). Due to the interaction of the shock with the boundary layer indirect sources of the loss are also present.

Losses due to the partial admission

Depending on the author, various classifications of the partial admission losses can be found. A comprehensive list of mechanisms arising from partial admission operation is cited below, after Yahya (1967).

- Pumping loss
- Nozzle jet dispersion loss
- Sudden expansion loss
- Mixing loss
- Leakage loss
- Shear flow loss
- Loss due to change of reaction
- Interstage losses in multistage turbines
- Induced pumping and friction losses

In Yahya (1969) a method for predicting the stage efficiency of a partial admission turbine is given. The derived loss correlations are verified using three turbine rotors with different blade pitches. They are shown to be approximately correct and the effect of blade pitching is shown to be negligible. It is concluded that the mixing, leakage and sudden expansion losses are primarily responsible for the lowered efficiency of a partially admitted machine. While the literature on the similar partial admission concept applied to an axial compressor is lacking, it is expected that similar loss mechanisms will be present.

A review of the analysis and the design of an axial partially admitted impulse turbine, substantiated by the test data, is presented in Linhardt and Silvern (1961). The working principle of an impulse turbine is understood in the following way. The turbine converts its available pressure energy completely in the nozzle and then extracts the resultant kinetic energy in the rotor by turning of the relative flow (110 to 140 deg) under constant static pressure. A typical blade configuration of an impulse turbine together with its velocity triangles is shown in Fig 36.

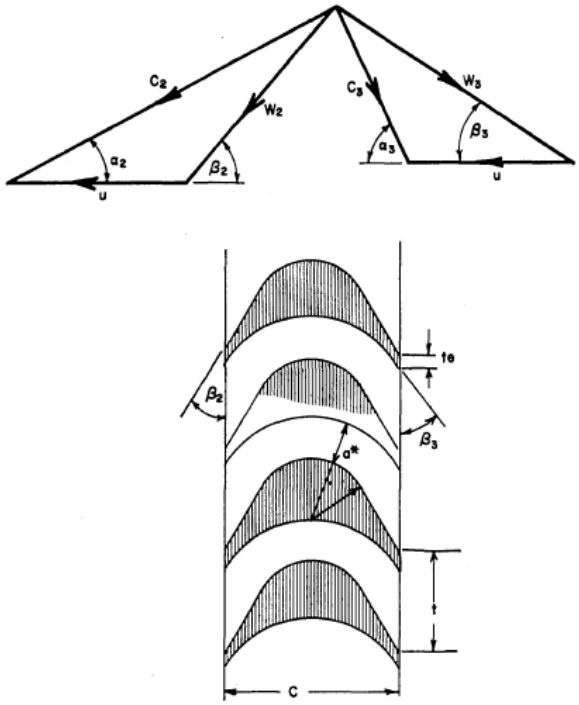

Figure 36. Typical velocity triangle and blade configuration of an impulse turbine. Source: Linhardt and Silvern (1961)

The authors propose combining several partial admission impulse stages within a single disc, introducing a so-called “re-entry-type-turbine”, as shown in Fig 37. In such a configuration the gas is admitted on one side of the rotor, passes through the blade row, is collected and passed through the rotor again. The fluid leaves the turbine at the same side at which it is admitted. The advantage of such a re-entry is that the disc friction is reduced compared to the conventional multidisc turbine. Both test and theoretical analysis illustrated that leakage is the most important parameter affecting the performance of a two-stage high pressure ratio (pr = 300:1) re-entry turbine. It was shown that the tangential and radial leakage occurs between the first stage nozzle exit and the exhaust port of the second stage, due to the significant pressure gradient. In order to reduce the driving force of a leakage it is suggested that the nozzles of the first stage and second stage should be located on the same side of the rotor through the application of the cross-over duct. Further improvement potential, according to the authors, lies in a proper redesign of the

blades for the supersonic conditions. Efficiencies of more than 60% were cited for the two-stage turbine prior to the mentioned design modifications.

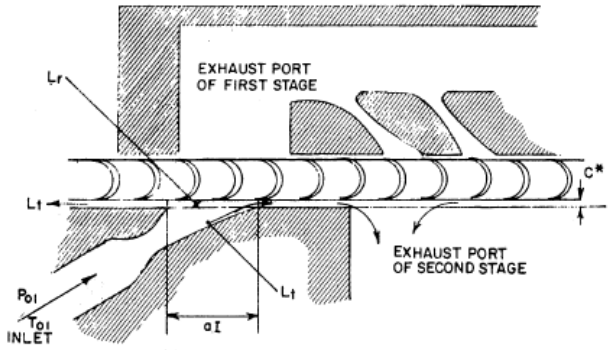

Figure 37. Two-stage re-entry partial admission impulse turbine. Source: Linhardt and Silvern (1961)

Vibrations in partial admission machinery

One of the main drawbacks of the partial admission is the inherently unsteady nature of the flow generating unsteady forcing on the rotor. Due to the unforeseen excitation frequencies, underestimated force magnitudes, or a combination of both, the risk for a so called high cycle fatigue (HCF) leading to a failure of machine elements exists.

When rotating blades of a partial admission machine enter and leave the active arc they receive a rapid load increase and then a rapid load decrease. This can lead to several problems. In the early 1940s, the introduction of partially admitted machines resulted in industry-wide problem of shroud and blade failures. These experiences initiated the early investigations into the vibration of turbine blades due to the partial admission [Allen (1940), Kroon (1940)]. The conclusions of this early research were that the problem was a result of an increase in the rotational speed of the high capacity machines to 3600 rpm. As a result of increased speed the blade heights also increased, making the blades more susceptible to shock induced vibrations. The new challenge was encountered again in the early 1960s. At that time, the resonances with the nozzle wake frequency were identified as a source of the problem [Vuksta (1961)]. The comprehensive analysis of both the shock load and nozzle resonance stresses was presented by Pigott (1980). He found that the shock amplification was independent of the degree of admission and that the unwanted resonances can be eliminated by changing the number of blades per group, the number of nozzles or the basic design. These modifications will affect the blade group response to the shock loading. Hence, the optimization of the

design should involve analysis of both the nozzle wake response and the shock loading response. It was also observed that the severity of the transients was strongly coupled to the loading/unloading time and the natural periods of the blade's eigenfrequency. The depiction of general character of the blade forces acting in a partial admission stage are shown in Fig 38.

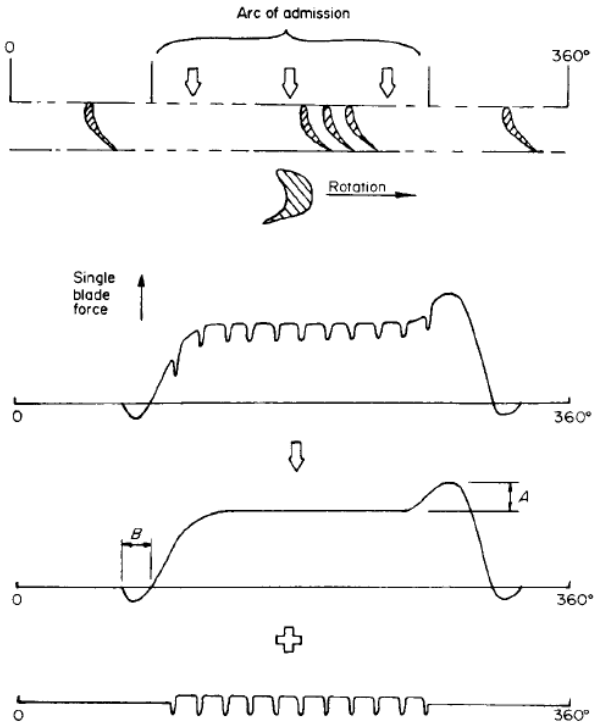

Figure 38. General character of blade forces in partial admission stage. Source: Pigott (1980)

In his recent paper Fridh et al. (2012) gives an extended design criteria toolbox, as well as validation data, for control stage design based on experimental data to reduce HCF incidents in partial-admission turbines. For that purpose a forced-response analysis of a two-stage air test turbine is performed and results are presented in Cambell diagrams (rotational speed vs frequency). It is observed that partial admission creates a large number of low-engine-order forced responses due to the blockage, pumping, loading and unloading processes (see Fig 39).

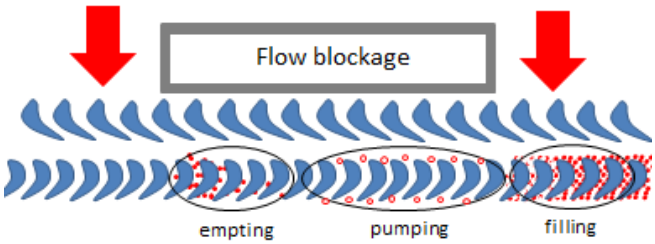

Figure 39. Illustrated emptying, pumping and filling processes for a partial admission stage

According to the author, the excitation pattern can be altered changing the stator and/or rotor pitches. Also a relationship between the circumferential lengths of the admitted and non-admitted parts dictates the excitation forces and may serve as a design parameter.

2.7 Design and analytical methods

The complete design of a turbo-compressor is a multidisciplinary undertaking involving knowledge of thermodynamics, fluid dynamics, rotordynamics, material and numerical sciences. Although the tools may differ, the essential procedures remain similar.

2.7.1 Aerodynamic design procedures

Typically, the design activity starts with the aerodynamic analysis that, depending on complexity, may include 3 steps: 1D, 2D and 3D modeling.

1D modeling

A one-dimensional (1D) approach to the design and analysis of the compressor is a combination of fundamental fluid flow equations, thermodynamic equations and empirical relationships.

Its main aim is to establish the main geometrical outline of the compressor stage including diameters, passage height and blade angles. Empirical loss models allow

calculating losses occurring in subsequent ducts of the compressor and estimating overall compressor efficiency. A 1D study can be expanded to include off-design performance and present behavior of a compressor in its full range, between the surge and choke margins. Some prior knowledge of good design practice is essential to provide a reasonably good starting point for the design assumptions. In terms of the time required for completion of each design stage, a 1D procedure is the most convenient one for the designer. A detailed overview of one-dimensional design procedures can be found in several turbo-machinery textbooks, i.e. Dixon (2005), Whitfield and Baines (1990), Japikse and Baines (1994).

2D analysis

Two-dimensional or hub-to-shroud analysis predicts the evolution of the velocity in the impeller passage and can be used as a first estimate for more detailed analysis and refinement of the design.

3D CFD

Further aerodynamic improvements can be obtained by means of a three-dimensional computational fluid dynamics (CFD). This stage of the design process is usually the most time consuming and least suited for multiple optimization iterations. It is therefore important to achieve a reliable design already during the preliminary phase of the process.

2.7.2 Introduction to the applied CFD method

CFD methods have been of great importance during the present work. A more detailed introduction to CFD is therefore important.

There are five equations describing the physical behavior that a fluid must abide. First, the continuity equation (15) states that the rate of change of density in a control region equals the net flow of mass into that region. Second equation (16) – the momentum equation - is based on Newton's second law and states that the change of momentum of a particle is equal to the sum of forces acting on the particle. The third equation (17) – the energy equation – stems from the first law of thermodynamics and states that the rate of change of energy within a fluid region convected with the flow equals the rate of energy received or rejected by heat and the work transfer.

$$\frac{D\rho_1}{Dt} = -\rho\partial_i\upsilon_i \tag{15}$$

$$\rho\frac{D\upsilon_i}{Dt} = -\partial_i p + \partial_j\tau_{ji} + \rho F_i \tag{16}$$

$$\rho \frac{DE}{Dt} = -p\partial_i \upsilon_i + \tau_{ji}\partial_j \upsilon_i - \partial_i q_i \tag{17}$$

Where τ_{ji} is the viscous stress tensor, defined by

$$\tau_{ji} = \mu\left(-\frac{2}{3}\delta_{ij}\partial_k \upsilon_k + \partial_j \upsilon_i + \partial_i \upsilon_j\right) \tag{18}$$

The above equations are impossible to solve analytically, except for simplified laminar flow. The main reason of difficulties with real flow is their complex nature, often including turbulent behavior. By turbulence, we understand the flow that is unsteady, irregular, swirly and occurring above a certain Reynolds number. The chaotic nature of turbulence results in difficulties in its modeling.

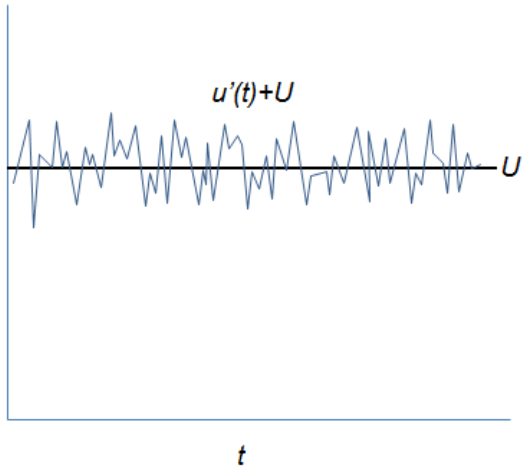

Figure 40. Time averaging of velocity

To model it directly is usually too demanding in terms of computational time and recourses. Fortunately, for industrial problems, it is rarely necessary to predict turbulence to its smallest eddies or for the smallest time scales. In practice, short-scale influence of turbulence is smeared by time-averaging the set of equations. The velocity is split into a constant part *U* and a part varying in time, *u'(t), as* shown in Fig 40. The turbulent part is considered truly random and therefore the time average of *u'(t),* equals zero.

$$u'(t) = \frac{1}{T}\int_0^T u'(t)dt = 0 \tag{19}$$

The pressure is treated in a similar fashion and *p'(t)+P* is substituted for *p*. Reformulation of the instantaneous continuity and momentum equation can be now given.

$$\partial_i Ui = \partial_i \overline{u'_i} = 0 \tag{20}$$

$$p\partial_j \left(U_j U_i\right) = -\partial_i P + \mu\partial_j \partial_j U_i - \rho\partial_j \left(\overline{u'_j u'_i}\right) \tag{21}$$

When the equations are averaged, six new terms emerge as $\rho\left(\overline{u'_j u'_i}\right)$, known as the Reynolds stresses. These stresses are calculated through a turbulence model, which adds from one to seven extra equations to the set.

Turbulence models

The choice of turbulence model is a compromise between computing time and the level of detail. Detailed description of various turbulence models can be found in handbooks, i.e. Versteeg and Malalasekera (1995), Ferziger and Perić (1996), Chung (2010).

The Fluent code used for this thesis offers multiple choices for turbulence modeling:

- Spalart-Allmaras model
- Standard k-ε model
- RNG k-ε model
- Realizable k-ε model
- RSM
- Large eddy simulation model

An appropriate model has to be selected with respect to the flow problem in consideration, since not every model is suited for every problem. The k-ε used extensively in this thesis adds two equations, for the kinetic energy, k and its rate of dissipation, ε, to the set of equations solved by the Fluent solver.

$$\rho\frac{Dk}{Dt} = \frac{\partial}{\partial x_i}\left[\left(\mu + \frac{\mu t}{\sigma_k}\right)\frac{\partial k}{\partial x_i}\right] + G_k + G_b - \rho\varepsilon - Y_M \tag{22}$$

$$\rho\frac{D\varepsilon}{Dt} = \frac{\partial}{\partial x_i}\left[\left(\mu + \frac{\mu t}{\sigma_\varepsilon}\right)\frac{\partial \varepsilon}{\partial x_i}\right] + C_{1\varepsilon}\frac{\varepsilon}{k}\left(G_k + C_{3\varepsilon}G_b\right) - C_{2\varepsilon}\rho\frac{\varepsilon^2}{k} \tag{23}$$

In the above equations, Gk represents the generation of turbulent kinetic energy due to the mean velocity gradients, Gb represents the generation of turbulent kinetic energy due to the buoyancy and Y_M is the contribution of the fluctuating dilatation in compressible turbulence to the overall dissipation rate. σ_k, σ_ε are

turbulent Prandtl numbers for k and ε and $C_{1\varepsilon}$, $C_{2\varepsilon}$ and $C_{3\varepsilon}$ are constants [(Tousi and Tourani (2008)].

Finite volume method

To solve the averaged – non-linear set of equations, a numerical method for discretizing and solving differential equations must be applied. In many commercial codes, including Fluent, a robust and proven finite volume method (FVM) is used. The procedure comprises three main steps. Mesh generation is the first step in the CFD FVM procedure, where the computational domain is divided into small control volumes (CV). Physical properties such as velocity and pressure are calculated for each control volume, some of them in the central point of it, some on the volume faces. The second step involves integration of underlying equations for the given CV. The parameters are considered to be known at the central points of each control volume, while the values at the faces are determined by means of interpolation. More, second order, or less accurate, first order, methods of interpolation can be used. To increase the accuracy of the solution, the size of the mesh should be as small as possible, as the interpolation accuracy is dependent on the distance between the grid points. Finally, the solver integrates the governing equations for the unknowns (p, v, t, and conserved scalars) and the linearized set of discretized equations is solved to yield updated values of the dependent variables [Ansys, Inc (2011)].

Solver

In Ansys Fluent the user has a choice of two numerical solvers, pressure-based and density-based solver. The velocity field, in both methods, is calculated from the momentum equation. In the density based solver, the density field is determined based on the continuity equation, while the pressure field is based on the equation of state. In the pressure-based approach, the continuity and momentum equations are manipulated to obtain a pressure field from pressure or pressure correction equations. The outline of the pressure-based solver procedure is presented below.

The pressure-based solver algorithm

The pressure based algorithm implemented in Fluent belongs to the segregated algorithms, which means that the governing equations are solved sequentially. A converged solution is found iteratively as the non-linear and coupled equations cannot be solved directly. Each governing equation must be “decoupled” and “segregated” during the solving process. Since the discretized equations must be stored in the memory only at the time they are segregated and solved, it makes it memory-efficient. Each solver’s iteration consists of the following steps:

1. Update fluid properties (e,g, density, viscosity, specific heat) including turbulent viscosity (diffusivity) based on the current solution.
2. Solve the momentum equations, one after another, using the recently updated values of pressure and interfacial mass fluxes.

3. Solve the pressure correction equation using the recently obtained velocity field and mass-fluxes.
4. Correct interfacial mass fluxes, pressure, and the velocity field using the pressure correction obtained from Step 3.
5. Solve the equations for additional scalars, if any, such as turbulent quantities, energy, species, and radiation intensity using the current values of the solution variables.
6. Update the source terms arising from the interactions between different phases (e.g., source term for the carrier phase due to discrete particles).
7. Check for the convergence of the equations

Grid sensitivity

A very important part of the numerical procedure is the grid independence study. Theoretically, the errors in the solution related to the grid should decrease as the number of cells is increased. When the numerical solution obtained on different grids agree to some reasonable level of tolerance, it may be referred as a grid converged solution.

To validate the numerical results one must also ensure that the computational domain complies with the requirements of the turbulent models used. The standard k-ε model ceases to be valid in the vicinity of the wall, where viscous stresses exceed the turbulent Reynolds-stresses. The approach employed in the k-ε model in the concerned region is to use a semi-empirical formula instead of resolving the flow. The standard wall functions using a logarithmic formula to solve the mean velocity are used. It is therefore essential that the distance from the wall for the wall adjacent cell must be within the range in which the formula is applicable. To measure this distance the dimensionless wall distance y+ is defined.

$$y^{+} = \frac{u_{*} y}{\upsilon} \tag{24}$$

Where u_{*} is the friction velocity at the nearest wall, y is the distance to the nearest wall and υ is the local kinematic viscosity of the fluid.

Based on experimental work, the law-of-the-wall is known to be valid in the range of $30<y+<60$ (Tamm et al., 1996). Some authors suggest that higher values are also permissible. In practice, values of y+ above 200 should be avoided due to the substantially large wake above the log layer [Ansys, Inc. (2011)].

Numerical approaches to turbo-machinery

There are different modeling approaches to the problems involving rotating elements, such as blades of a turbo-compressor. The so-called multiple frames problems can be treated with the following models:

- The frozen rotor model
- The mixing plane model
- The sliding mesh model

The two first models belong to the multiple frames of reference (MFR) technique in which the rotating element (impeller) is modeled in a rotating frame of reference, while the stationary components (inlet duct, diffuser) are assigned to the to a stationary frame of reference. Between each zone an interface is applied. The first type of interface implemented in the MFR analysis is called the frozen rotor model. The model preserves the flow profile variation in the circumferential direction before transferring the information to the downstream frame of reference. This interface however does not consider any circumferential flow distribution change due to the variation of the relative position between the two involved zones.

The second type of interface is called the mixing model or circumferential averaging. It means that before the information is transferred to the downstream zone, the upstream velocity profile is averaged circumferentially. It is assumed that the flow is steady and axisymmetric. None non-uniformity or distortion of the flow in the circumferential direction is preserved across the interface (mixing plane).

Both the mixing plane model and the frozen rotor model are steady state representations of rotating parts and therefore cannot simulate adequately all transient effects occurring in turbo-machines.

The third type of the interface, called the transient sliding mesh interface is able to predict the fluid motion caused by the relative movement between a rotor and stationary ducts of the turbo-machine. In this approach, a moving mesh of a rotating part is coupled with a stationary zone mesh with sliding interface. The flow field unsteadiness in both time and space is fully taken into account in the transient sliding mesh methodology.

The selection of appropriate model for simulation of turbo-machinery is essential. Liu and Hill (2000) compared the results of all three models obtained for a centrifugal compressor. Firstly, the effects in the impeller inlet interface were examined for two cases, radial and axial inflow. Secondly, the impeller-diffuser interaction was analyzed for different gaps between the impeller and the diffuser vanes. In general, it was concluded that when the coupling effects between moving and stationary zones is weak, then all three interfaces give similar results. The deviations between the three models are displayed in circumferential flow field for a radial inlet interface. For the case of impeller-diffuser interface, the frozen rotor model tends to predict the flow field to be very different from the other solution when the gap is decreased. It is also concluded, that only the transient approach is capable of simulating the aerodynamic interactions between the impeller and inlet guide vanes or downstream discharge vanes.

3 Summary of papers

3.1 Paper I

Kus, B., & Nekså, P. (2013). Development Of One-Dimensional Model For Initial Design And Evaluation Of Oil-Free CO_2 Turbo-Compressor. *International Journal of Refrigeration. Available online. In press.*

In the first paper a 1-dimensional tool for preliminary design and performance prediction of an oil-free CO_2 compressor is presented. A radial 2-stage machine with the rotor supported on gas foil bearings lubricated by a fraction of a compressed gas is modeled. In order to give a possibly comprehensive overview of the technology, a wide range of loss mechanisms is considered. Well established semi-empirical correlations are used to calculate compressor stage efficiency as well as the remaining non-stage losses, such as windage of a motor and gas bearings, cooling and electrical losses. It is reasoned that only an inclusion of a full scope of loss generating mechanisms enables comparison of a new compressor concept with existing commercial alternatives. To validate the accuracy of the analytical model three methods are used. 3D numerical modeling of the three different centrifugal stages is carried out to verify the 1D predictions of the stage efficiency. The maximal discrepancy between analytical and numerical method amounts to 2% for efficiency and 5% for pressure ratio, while the largest disagreement is observed for supercritical compression to a supercritical pressure. Without experimental verification it is difficult to conclude which method is more accurate in this case. It can however be expected that some general approximation present in the 1D model tend to reduce accuracy prediction in the supercritical region where small under- or over-prediction of one thermodynamic property can result in significant variation of another. The main non-dimensional performance coefficients are also calculated for the analyzed geometries to compare obtained stage efficiencies with those of existing machines. Also here reasonable match is found. The 1D prediction of the total compressor efficiency is compared with the test data from a 50kW compressor published by Sandia Laboratories. The predicted peak efficiencies are between 66-67.5% while experimentally measured values are within 65-70%. The paper identifies the need for fast accurate methods of thrust prediction. When using typical 1D correlations to calculate thrust acting on a radial impeller operating with CO_2, one risks both wrong prediction of its magnitude, and even its direction. At the present stage of the tool development values of axial thrust were assumed in order to calculate size and windage of a thrust bearing.

3.2 Paper II

Kus, B., & Nekså, P. (2013). Oil Free Turbo-Compressors For CO_2 Refrigeration Applications. *International Journal of Refrigeration. Volume 36, Issue 5, August 2013, Pages 1576–1583*

The model developed and described in Paper I is used to assess feasibility of replacing oil-lubricated compressing equipment in CO_2 based refrigeration systems with oil-free turbocompressors. The peak efficiency is predicted for compressors designed for different system capacities and operating between different pressure levels. According to the 1D study, high compression efficiencies (>70%) are possible for the oil-free concept in a wide range of capacities provided that the inlet pressure is low, around 1 MPa, and the pressure ratio is moderate, below 3. Potential for good efficiency deteriorates with increasing operational pressures. As the density of the fluid increases so does the required rotational speed of the impeller. In turn, the windage exerted by the rotating elements of the machine increases rapidly introducing pronounced friction losses. Depending on the case, it may occur that the optimal speed of the compressor is different than the one providing the best aerodynamic performance. The aim of the designer is therefore to find the trade-off between aerodynamic performance and the remaining non-stage parasitic losses. An approach to reduce windage losses by incorporating a 2-times longer motor is also applied to a compressor with inlet pressure of 3 MPa and pressure ratios of 2 and 2.56, respectively. Such a strategy could be beneficial for compressor efficiency but may require special rotordynamic solutions or supporting each impeller-rotor pair on a separate set of bearings. The latter option while theoretically easier to realize, is likely to suffer from unbalanced impeller thrust, due to the lack of a balancing action of a second impeller, as well as increased investment cost. A double shaft approach can be expanded by increasing the number of impellers to four and thus improving aerodynamic efficiency while reducing thrust values at the same time. In effect, one ends up with two two-stage compressors in series. Whether such a strategy is reasonable from an economical point of view it is yet to be answered. It is nevertheless apparent, that there is no obvious solution assuring reasonably high efficiency of an oil-free CO_2 commercial scale turbocompressor while maintaining a relative simplicity of the system.

3.3 Paper III

Kus, B., & Nekså, P. (2013). Novel partial admission radial compressor for CO_2 applications. *International Journal of Refrigeration. Available online. In press.*

In this paper a different approach is proposed for reduction of the high windage losses affecting performance of an oil-free CO_2 compressor. The concept of a partially admitted radial flow machine is analyzed by means of a numerical method. The rationale behind applying a partial admission stage is to enable operation at speeds that will be lower compared to a fully admitted centrifugal stage of a commercial size compressor. It is clear that an electrical motor designed for a certain rated power, but operating at different speeds will generate significantly lower windage friction losses at lower speeds, despite its bigger dimensions. The aim was to find a design where the aerodynamic performance of an inward flow partial admission stage was at levels similar to that of a competing centrifugal counterpart. The overall performance of a novel compressor should benefit from reduced non-stage losses. To initially assess the performance potential of a novel partial admission stage, a 2D transient analysis of a wheel bladed with 200 blades and rotating at 13000 revolutions per minute was carried out. The base stage efficiency without the diffuser, namely the wheel efficiency, was according to the simulations, higher than 80% at around 1.4 total pressure ratio. Depending on the 3D depth the profile (blade height), a drop in the base efficiency caused by the wall effects and other 3D effects can be expected. These aspects should be analyzed more extensively in future research. It is initially assessed that a more pronounced drop in efficiency occurs for blade heights of less than 5 mm. It accounts for volumetric flow rates of less than 0.02 m3 s-1, corresponding to cooling capacity of around 500 kW at 60 bar.

The proposed impeller design is characterized by a low degree of reaction which means that the major part of the static head must be created in the diffuser. It is therefore concluded that a careful design of the diffuser will be crucial to the overall stage efficiency. The paper does not include predictions of the diffuser performance but shows how the overall stage efficiency depends on the diffuser total loss coefficient. Additional steady state simulations show a potential for wheel efficiency improvement by optimization of the shape and the number of blades. For the selected shape of a blade an initial structural analysis of safety factor is also presented. Depending on the factual load that will act on a very short and thin blade, the usage of very strong and expensive materials might be necessary in order to safely transfer the loads. It is expected that a small size of the blades and small distances between them may require electrochemical machining especially when difficult-to-machine alloys would be used.

3.4 Paper IV

Kus, B., & Nekså, P. (2013). Numerical study of diffuser systems for a novel partial admission compressor using CO_2 as refrigerant. *Submitted to International Journal of Refrigeration.*

To get a better impression of the level of the overall efficiency for a partial admission stage, the performance of the diffuser system must be assessed. A 3D numerical study of various diffuser systems that could be applicable for the novel compressor is therefore presented. For each diffuser a non-uniform inlet velocity profile resembling that at the partial admission wheel discharge is applied. Each geometry is characterized by the bend section necessary to direct the gas outside the wheel and design of a proper diffuser duct. Designs with rectangular and circular cross sections, different lengths and area ratios are analyzed with regard to pressure recovery and total pressure loss coefficients. For the best geometries within the given area ratio, return channels are added and the performance of the diffuser/return channel assessed. For the applied inlet conditions the most efficient system, characterized by the circular diffuser with an area ratio of 3.9 and non-dimensional length of 15.3, achieves total pressure loss and pressure recovery coefficients of 0.13 and 0.82, respectively. It is believed that a redesign of the impeller discharge angles should improve the performance of the diffuser due to the lower curvature of the channel. It was expected that application of a pinch to the rectangular assembly would improve the uniformity of the flow across the diffuser channel and therefore improve its performance. It turned out however, that introduction of a 3% pinch to the 2.8 area ratio diffuser, while improved the uniformity of the flow, actually increased the overall loss across the channel. It is believed that this can be attributed to the increase of already high friction losses in the initial segment of the rectangular duct, were the deceleration of the gas is minimal.

4 Conclusions

The objective of the present work was to propose the design for an efficient oil-free compressor for commercial scale CO2 refrigeration applications. It was shown that for higher operating pressures, around supercritical pressure, an ordinary radial compressor in hermetic configuration will not provide the aimed efficiency level. A novel concept of a partially admitted compressor was therefore proposed as an alternative solution for high pressure medium capacity applications. The important parts of the present work comprised:

- Development of a 1D tool for preliminary design and performance prediction of two-stage hermetic radial turboconmpressor
- Evaluation of the 1D tool based on CFD aerodynamic efficiency predictions and experimental data for a 50kW hermetic CO2 turbocompressor
- Development of a novel partially admitted radial turbocompressor concept
- Numerical investigations of the novel compressor's wheel and diffuser systems
- Analytical predictions of the novel compressor overall efficiency

The more detailed outline of subsequently achieved objectives for the present research is given below.

In the course of the present study turbo-type technology was identified as the most feasible candidate for oil-free operation. An overview of other technologies that have been considered, but not necessarily recommended as cost- and energy-effective alternatives, such as custom designed oil-free piston compressors, has been also provided.

A 1D model of a two-stage radial turbo-compressor supported on oil-free foil gas bearings was built to predict compression efficiencies that could be achievable for different CO2 based applications. To validate aerodynamic predictions of the 1D model, three compressor stages with specific speeds ranging from 0.34 to 0.66 were generated and investigated with a 3D CFD method. Maximal discrepancy between analytical and numerical predictions amounted 2% for efficiency and 5% for pressure ratio. The 1D prediction of the total compressor efficiency was compared with test data from a 50 kW compressor published by Sandia National Laboratories. The analytically predicted peak compressor efficiencies were between 66 and 67.5% while experimentally measured values were within 65-70% region. The validation procedure confirmed acceptable accuracy of the model, which was subsequently used to investigate the performance of compressors designed for various operating conditions and capacities corresponding to shaft power from a few tens of kilowatts to a few megawatts.

It was found that high overall isentropic efficiencies, exceeding 70%, are possible for the 2-stage radial compressor concept, but within limited range of applications. For low inlet pressures and low to moderate pressure ratios (Pin = 1 Mpa, Pout = 2

or 3) the compressor is expected to achieve good efficiency in a wide range of system capacities, corresponding to shaft powers from 50kW up to a few MW. The potential for a good overall efficiency deteriorates with increasing operational pressures. It is an effect of reduced volumetric flows requiring higher shaft speeds and thus triggering pronounced windage losses. For example, for a 100kW shaft power machine designed for inlet pressure of 3 MPa and pressure ratio of 2.5, the overall isentropic efficiency is expected to be of around 60%. This is not a satisfactory value, especially when compared to the new generation of commercial oil-lubricated CO2 piston compressors.

The higher the capacities of the system, the lower the parasitic windage losses triggered by high shaft speeds and the more we approach the performance levels typical for centrifugal compressor concepts for other applications. As we move towards multi-mega-Watt applications, the aerodynamic stage can be much more effectively sealed from the motor compartment by dry gas seals and the windage losses become negligible. As the perfect sealing does not exist, some degree of leakage of the working fluid to the ambient must be taken into account. In such cases an additional installation for a working fluid make-up might turn out necessary.

Pursuing higher compression efficiencies in high pressure commercial size application requires more effort. In these applications, permanent leakage is unacceptable. Designing CO2 hermetic turbocompressor is not a trivial task, as the designer must find the trade-off between the aerodynamic performance and the remaining parasitic losses. It is likely that the specific speed of the compressor optimal from an overall efficiency point of view will be different than that optimal from the stage efficiency point of view. In some cases, the level of windage may still remain unacceptable. It was shown (Paper II) that applying non-standard strategies such as driving each of the impellers with a separate motor, thus assuring higher overall length of the rotor, may prove insufficient in achieving desirable efficiency levels.

Instead, another approach to the reduction of high windage losses was pursued. The presented novel concept of a turbo-compressor employs partial admission principle, radial inward flow configuration and a special type of a curved diffuser. The theoretical analysis has shown that 75% reduction of rotational speed of the motor could result in as much as 90% reduction of the windage, despite bigger dimensions of the slower rotating motor, for the same rated power.

Partially admitted wheel does not guarantee achieving competitive aerodynamic stage efficiency, when compared to typical radial compressor. Essential part of the current work focused therefore on a theoretical prediction of the partial admission stage efficiency. While only limited amount of blade shapes and angles were used for numerical simulations it seems obvious that very short and thin blades similar to those found in an impulse turbine are required to achieve good wheel efficiency. 2D simulations indicated that the wheel isentropic efficiencies of more than 80 % might be expected. To confirm these initial findings detailed structural and manufacturability analysis should be performed. Further analysis should also be

undertaken to take into account a full spectrum of 3D effects, such as end-wall losses, impact of the blade length or radial clearance.

Due to the short passage length and a certain angle at which the flow should be discharged to the diffuser, the degree of reaction will be low. This indicates that the major part of the static head must be produced in the diffuser, the design of which must be executed very carefully, having in mind generally unfavorable conditions for the diffusion process like the non-uniform velocity profile, close to sonic flow conditions and curved shape of the channel. For given inlet conditions, approximating these at the discharge of the previously simulated partial admission wheel, a number of different diffuser systems were analyzed with the 3-dimensional numerical method. The most efficient, among the tested, diffuser/return channel is characterized by the circular diffuser with an area ratio of 3.9 and non-dimensional length of 15.3 and achieves total pressure loss, and pressure recovery coefficients of 0.13 and 0.82, respectively. An impact of introduction of 3% pinch to the rectangular 2.8 area ratio diffuser was also simulated. It turned out, that instead of an expected improvement in the diffuser performance, the level of losses increased. It is believed that this can be attributed to the increase of already high friction losses in the initial segment of the rectangular duct, were the deceleration of the gas is minimal. The contradictory results to these typically found in a diffuser of a centrifugal compressor, where low degree of pinch typically improves the diffuser performance, deserves however more insight.

After the first round of simulations of both the wheel and the diffuser, the target 75% stage efficiency at around 1.4 pressure ratio may seem reachable. Much will however depend on further full stage 3D transient simulations that due to limited scope of this work have not been performed. Detailed structural analysis of the tiny blades undergoing cyclical loads and manufacturability issues will also be crucial to the feasibility of the new concept. At the first glance then, it seems that the partial admission concept could be an interesting alternative for an oil-free hermetic CO2 compressor operating at high, close to critical pressures in commercial applications. To confirm these first observations further modeling and experimental work is however inevitable. It is expected that further improvements of the diffuser shape accompanied by a redesign of the impeller blades and discharge angles are possible.

5 Suggestions for further work

As shown in the present work the development of new machinery requires insight into various fields of science and engineering. During the theoretical analysis of potential alternatives for an oil-free compressor several areas have been identified as interesting from future research opportunities perspective. If it comes to the rapid 1D modeling of a centrifugal compressor, a new method for an axial load prediction seems desirable. It is especially challenging area for CO_2 compressors as one has to deal with very high pressure gradients across the impeller faces. The gained experience could be equally relevant for CO_2 machines as well as for a wide range of different working fluids and applications. Fair amount of research has been devoted recently to foil gas bearings, a technology enabling operation of small to medium-scale oil-free turbo-machinery. Despite numerous advantages of foil gas bearing technology its coupling with turbomachinery is still emerging practice and only a small amount of performance data is accessible publicly. Relatively small number of foil bearing manufacturers has led to the high perception of risk and therefore rather slow industry transition to this technology [Conboy and Wright (2011)]. Recent interest of NASA and the U.S. Army Research Lab in the foil bearing technology encouraged more R&D activity bringing to the public open-source gas foil bearings [DellaCourte (2007)]. Still there is a considerable potential for future research in this area. Modeling of compliant gas foil bearings has been notoriously difficult as the solution of the hydrodynamic pressure fields must iterated together with the solution of the structural model, since the deflection of bearing surfaces and the local pressure are linked together. The present thermal effects make the problem even more demanding as the temperature gradients affect both the pressure distribution and the material expansion and deformation. It is not certain how foil bearings would behave with a partially admitted machine which rotor is expected to be less stable that a fully admitted one due to the cyclic loading and unloading processes. In addition, the speeds selected for the presented conceptual compressor are in the lower range of what is applicable for foil gas bearings. This together with not yet known radial loads of the partially admitted wheel creates an interesting area for a scientific inquiry. But not only prediction of the bearing behavior remains a challenge. The non-standard configuration of the partially admitted wheel and the complex geometry of the diffuser pose rather demanding problem from the fluid dynamics point of view. The transient simulations of a full aerodynamic stage with a properly selected turbulence models seem vital for a better understanding of the phenomena taking place in the novel compressor. It is also reasonable to infer that the numerical procedure, thanks to relative novelty of the problem, should be accompanied by an experimental campaign. Such a campaign could give a comprehensive insight into performance of various components put together in a rather uncommon configuration. The areas linked to the development of a novel compressor that are identified as interesting from both scientific and practical point of view are summarized below:

- Numerical modeling of various stage configurations, including different shapes and number of blades, admission ratios, admission arc position, impeller discharge angles and diffuser curvature
- Impact of cyclic loads on structural and rotordynamic performance of the compressor
- Experimental validation of predicted design and off-design stage efficiencies
- Modeling and measurement of performance and behavior of foil gas bearings operating at relatively low speeds in high pressure CO_2

6 Bibliography

1. Allen, R.C., 1940. Steam turbine blading. Trans. ASME, 62, 689-710
2. Alvares, J. (2010). The Part-Load Efficiency Benefit of Oil-Free, High-Speed, Direct-Drive Centrifugal Compressors.
3. Ansys, Inc., 2011. Ansys Fluent user's guide.
4. Balje, O.E., 1981.Turbomachines: a guide to design, selection, and theory. John Wiley & Sons
5. Baumann, H., Conzett, M., 2002. Small Oil Free Piston Type Compressor For CO_2. International Compressor Engineering Conference. Paper 1611
6. Bäckström, M., 1970, Kylteknikern, Sv Kyltekniska föreningen
7. Braunbek, W., 1939. Frei schwebende Koerper im elektrischen und magnetischen Feld. *Z. Phys.*, 112:753–763
8. Bradshaw, P., 1996. "Turbulence modeling with application to turbomachinery." *Progress in Aerospace Sciences* 32.6 (1996): 575-624.
9. Briggs, Maxwell Henry, 2008. High pressure performance of foil journal bearings in various gases. Diss. Case Western Reserve University
10. Bruckner, Robert J, 2009. "Windage Power Loss in Gas Foil Bearings and the Rotor-Stator Clearance of High Speed Generators Operating in High Pressure Environments." ASME, 2009.
11. Chen, Y, 2011. Thermodynamic Cycles using Carbon Dioxide as Working Fluid. CO2 transcritical power cycle study. PhD Thesis. School of Industrial Engineering and Management. Stockholm
12. Cheshire, L. J. (1945). The design and development of centrifugal compressors for aircraft gas turbines. *Proc. Instn. Mech. Engrs. London*, **153**; reprinted by A.S.M.E. (1947), Lectures on the development of the British gas turbine jet.
13. Christen, Thomas, et al., 2006. "Experimental performance of prototype carbon dioxide compressors." International Compressor Engineering Conference. Paper 1730
14. Chung, T. J. (2010). Computational fluid dynamics. Cambridge university press.
15. DellaCorte, Christopher, and Robert J. Bruckner. Remaining technical challenges and future plans for oil-free turbomachinery. National Aeronautics and Space Administration, Glenn Research Center, 2010.
16. Denton, J. D., and W. N. Dawes. 1998. "Computational fluid dynamics for turbomachinery design." *Proceedings of the Institution of Mechanical Engineers, Part C: Journal of Mechanical Engineering Science* 213.2: 107-124.
17. Denton, John D. "Some limitations of turbomachinery CFD." *ASME Paper No. GT2010-22540* (2010).
18. Dixon, S. Larry, 2005. Fluid mechanics and thermodynamics of turbomachinery. Butterworth-Heinemann.
19. Earnshaw, S., 1842. On the nature of the molecular forces which regulate the constitution of the lumiferous ether. *Trans. Camb. Phil. Soc.*, 7, Part I:97–112
20. EIA, 2011. International Energy Outlook. Energy Information Administration. Report Number: DOE/EIA-0484(2011)

21. Feher EG, 1968. The supercritical thermodynamic power cycle. Energy Conversion 8:85-90
22. Ferziger, Joel H., and Milovan Perić, 1996. *Computational methods for fluid dynamics*. Vol. 3. Berlin: Springer.
23. Fridh, Jens, Björn Laumert, and Torsten Fransson. " Forced response in Axial Turbines Under the Influence of Partial Admission." ASME Turbo Expo 2012-Turbine Technical Conference and Exposition, Copenhagen, June 11-15, 2012. 2012.
24. Fridh, J., 2012. Experimental investigations of performance, flow interactions and rotor forcing in axial partial admission turbines. Doctoral thesis. Royal Institute of Technology, Stockholm, Sweden
25. Galerkin, Y.B., Mitrofanov, V.P., Prokofiev, A.Y., 2003. The experience of CFD calculations for flow analysis in centrifugal compressor stages. Proceedings of the International Gas Turbine Congress, Tokyo
26. Habel, Rolf. "Advanced Compression Solutions for CCS, EOR and Offshore CO2." OTC Brasil (2011).
27. Habermann, H. and Liard, G., 1977 Le palier magn´etique active: un principe r´evolutionaire. SKF Rev. Roulements Nr. 192
28. Hafner, A., Nekså, P., Rekstad, H., 2012. High efficient 100kW shaft power R744 compressor. 10th IIR Gustav Lorentzen conference on natural refrigerants (June 2012) in Delft, the Netherlands
29. Hafner, A., Alonso, M. J., Nekså, P., Schmälzle, C.,2013. High efficient 20-90 m^3/h R744 compressor. Compressors Conferences, Častá Papiernička - Smolenice, Slovakia
30. Hays, L., Brasz, J., 1996. Two-phase turbines for compressor energy recovery, proceedings of the 1996 International Compressor Engineering Conference at Purdue, Vol. II, pp. 657-662
31. Hays, L., Brasz, J., 2004. A transcritical CO_2 turbine-compressor. *International Compressor Engineering Conference.* Paper 1628.
32. Hejzlar P, Dostal V, Driscoll MJ, Dumaz P, Poullennec G, Alpy N, 2006. Assessment of gas cooled fast reactor with indirect supercritical CO2 cycle. Nuclear Engineering and Technology 38:109-18
33. Howard, Samuel A., et al., 2007. "Gas foil bearing technology advancements for closed Brayton cycle turbines." AIP Conference Proceedings. Vol. 880. 2007.
34. IIR, 2010. Statement given by Didier Coulomb, Director of International Institute of Refrigeration, United Nations Climate Change Conference, Cancun, Mexico
35. Japikse, David, and Nicholas C. Baines, 1994. *Introduction to turbomachinery*. Concepts Eti.
36. Kim, Y. M., Kim, C. G., Favrat, D., 2012. Transcritical or supercritical CO2 cycles using both low- and high-temperature heat sources. Energy 43 (2012) 402-415
37. Kroon, R.p., 1940. Turbine blade vibration due to the partial admission. J. Appl. Mech. Trans. ASME, 62, A-161

38. Lawlor, S.P., Baldwin, P., 2004. Conceptual design of a supersonic CO_2 compressor. Proceedings of ASME 2005 ASME TURBO EXPO 2005 June 6-9, 2005, Reno, Nevada
39. Linhardt, Hans D, Silvern, D.H., 1961. "Analysis of partial admission axial impulse turbines." ARS Journal 31.3): 297-308.
40. Lorentzen, Gustav, and Jostein Pettersen. 1993. "A new, efficient and environmentally benign system for car air-conditioning." *International Journal of Refrigeration* 16.1: 4-12.
41. Lorentzen, Gustav, 1995. "The use of natural refrigerants: a complete solution to the CFC/HCFC predicament." *International Journal of Refrigeration* 18.3: 190-197.
42. Liu, Z. and Hill, D. L., 2000. "Issues Surrounding Multiple Frames of Reference Models for Turbo ompressor Applications" (2000). *International Compressor Engineering Conference.* Paper 1369.
43. Marquardt, J. T., 2011. Successful Operational Experience Sealing Supercritical CO_2. Supercritical CO2 Power Cycle Symposium May 24-25, 2011 Boulder, Colorado
44. Muntean, Sebastian, Håkan Nilsson, and Romeo F. Susan-Resiga, 2009. "3D numerical analysis of the unsteady turbulent swirling flow in a conical diffuser using Fluent and OpenFOAM." *3rd IAHRWG Meeting, Brno*.
45. Natural refrigerant CO2, 2009. Leonardo Project "NARECO2". KHLim (2009)
46. Nekså, P, Rekstad, H., Zakeri, G. R., Schiefloel, P. A., 1998. "CO_2-heat pump water heater: characteristics, system design and experimental results." *International Journal of Refrigeration* 21.3: 172-179.
47. Nekså, P., Dorin, F., Rekstad, M., and A. Bredesen, 2000 "Development of Two-Stage Semi-Hermetic CO2-Compressors" Proc. of the 4th IIR–Gustav Lorentzen Conference on Natural Working Fluids, Purdue University, West Lafayette, IN, July 25-28, pp. 355-362
48. Nekså, Petter, 2002. CO_2 heat pump systems." International Journal of refrigeration 25.4 (2002): 421-427.
49. Noall, J., Batton, W., 2011. Correlation of Reaction to Isentropic Velocity Ratio for a Subsonic Radial Inflow Turbine. Supercritical CO2 Power Cycle Symposium, Boulder, Colorado
50. Ohlsson, G. O., 1962, "Partial-Admission Turbines," J. Aerosp. Sci., 29(9), pp. 1017–1028.
51. Persichilli, M., Kacludis, A., Zdankiewicz, E., Held, T., 2012. Gen India & Central Asia 2012, 19-21 April, 2012, Pragati Maidan, New Delhi, India
52. Pigott, R., 1980. Turbine blade vibration due to the partial admission. Int. J. Mech. Sci. Vol. 22, pp. 247-264
53. Roberts, D.A., Steed, R., 2004. A comparison of steady-state centrifugal stage CFD analysis to experimental rig data. Int-ANSYS-Conf
54. Robinson, D., Groll, E., 1998. Efficiencies of Transcritical CO2 Cycles With and Without an Expansion
55. Turbine, Int. J. Refrig., Vol. 21, No. 7, pp. 577-589, 1998
56. Schiffmann, J., Favrat, D., 2009. Experimental investigation of a direct driven radial compressor for domestic heat pumps. Int. J. Refrig. 32, 1918 – 1928

57. Schiffmann, J., Favrat, D., 2010. Design, experimental investigation and multi-objective optimization of a small-scale radial compressor for heat pump applications. Energy. 35/8, 436-450
58. Schweitzer, G., 2009. Applications and Research Topics for Active Magnetic Bearings. Proc. IUTAM-Symp. on Emerging Trends in Rotor Dynamics, Indian Institute of Technology, Delhi, India.
59. Stodola, A., 1927, Steam and Gas Turbines, Vol. I (L.C. Loewenstein, trans.), McGraw-Hill Book Co., Inc., Reprinted in 1945 by P. Smith., Magnolia, MA
60. Stosic, N., Smith, I.K, Kovacevic, A., 2002. A twin screw combined compressor and expander for CO_2 refrigeration systems
61. Tamm, A., Gurge, M. and Stoffel, B. (1999), Experimental and 3-D Numerical Analysis of the Flow Field in Turbomachines Part Two, Darmstadt University of Technology, Darmstadt.
62. Traupel, W., 1977, Thermische Turbomaschinen, Vol. 2, 3rd ed., Springer-Verlag, Berlin
63. Schlichting, Hermann. Boundary-layer theory. Vol. 539. New York: McGraw-Hill, 1968.
64. Shi, W., Wang, H., Zhou, L., Zou, P., Wang, C., 2010. The estimation and experiment of axial force in deep well pump basing on numerical simulation. . IJMECS Vol.2, 53-61
65. Simonsen, A. J., Krogstand, P. A., 2004. Experimental–numerical investigation of a bend–diffuser configuration. In: 15th Australian fluid mechanics conference, University of Sydney, Australia; 13–17 December
66. Soulas, T., Colby, G., Desai, A.R., Griffin, T., 2011. CO2 Compression for Capture and Injection in Today's Environmental World. Proceedings of the First Middle East Turbomachinery Symposium February 13-16, 2011, Doha, Qatar
67. Suess J., Kruse H., 1998. Efficiency of the indicated process of CO2 - compressors, International Journal of Refrigeration, Vol. 21, pp. 194-201, 1998
68. Stahley, J. S. (2003). Design, Operation, and Maintenance Considerations for Improved Dry Gas Seal Reliability in Centrifugal Compressors. Dresser-Rand, Olean.
69. Tousi, A. M., and A. Tourani, 2008. "Comparison of turbulence methods in CFD analysis of compressible flows in radial turbomachines." *Aircraft Engineering and Aerospace Technology* 80.6: 657-665.
70. Tøndell, E., 2006. CO2-expansion work recovery by impulse turbine. Doctoral thesis. NTNU
71. Vernon, M. et al., 2010. Pressure Rise & Thrust Modeling of the Supercritical CO2 Hardware by Sandia National Laboratories
72. Versteeg, H. K., and W. Malalasekera, 1995. "An Introduction to Computational Fluid Dynamics: The Finite Volume Approach."
73. Vrancik, J. E., 1968. Prediction of windage power loss in alternators. NASA Technical Note D-4849.

74. Vuksta, T., 1961. Steam turbine governing stage impulse blade vibration investigation. Paper 61-WA-122. ASME Winter Annual Meeting in New York.
75. Wang K., Sun, J., He, Z., Song, P., 2011. Predictions of axial thrust load acting on a cryogenic liquid turbine impeller. Proceedings of ASME Turbo Expo 2011. June 6-11, Vancouver, British Columbia, Canada
76. Whitfield, Arnold, and Nicholas C. Baines, 1990. "Design of radial turbomachines."
77. Wright, S.A., Radel, R.F., Vernon, M.E., Rochau, G.E., Pickard, P.S., 2010. Operation and Analysis of a Supercritical CO2 Brayton Cycle, Sandia Report SAND2010-0171
78. Yang, Jun Lan, et al., 2005 "Exergy analysis of transcritical carbon dioxide refrigeration cycle with an expander." Energy 30.7 (2005): 1162-1175.
79. Yahya, S. M., Transient velocity and mixing losses in axial flow turbines with partial admission, Int. J. Meh. Sci. Pergamon Press. 1968. Vol 10, pp. 65-82
80. Yahya, S. M., 1969. Aerodynamic losses in partial admission turbines, Int. J. Mech. Sci, Pergamon Press. 1969. Vol. 11 ,pp. 417-431

Paper I

INTERNATIONAL JOURNAL OF REFRIGERATION XXX (2013) 1–12

Available online at www.sciencedirect.com

SciVerse ScienceDirect

journal homepage: www.elsevier.com/locate/ijrefrig

Development of one-dimensional model for initial design and evaluation of oil-free Co_2 turbo-compressor

Bartosz Kus, Petter Nekså*

Norwegian University of Science and Technology, 7491 Trondheim, Norway

ARTICLE INFO

Article history:
Received 26 February 2013
Received in revised form
15 May 2013
Accepted 17 May 2013
Available online xxx

Keywords:
Radial turbo-compressor
Carbon dioxide
Compression
Oil-free compressors
Oil-free refrigeration

ABSTRACT

A 1-dimenional tool for preliminary design and performance prediction of oil-free CO_2 compressor is presented. The model describes high speed centrifugal compressor in a hermetic configuration supported on foil gas bearings. To give possibly comprehensive overview of the technology, a wide range of loss mechanisms is considered. The model predicts aerodynamic performance of the compressor as well as losses related to the windage of rotor and bearings and due to the internal cooling. Numerical investigation of different compressor stages was used to validate aerodynamic predictions of the 1D model. Maximal prediction discrepancy amounted 2% for efficiency and 5% for pressure ratio. The prediction of the total compressor efficiency was compared with test data from a 50 kW compressor published Sandia Laboratories. The predicted peak compressor efficiencies are between 66 and 67.5% while experimentally measured values are within 65–70% region.

Développement d'un modèle unidimensionnel pour la conception initiale et l'évaluation d'un turbo-compresseur sans huile au CO_2

Mots clés : turbo-compresseur radial ; dioxyde de carbone ; compression ; compresseurs sans huile ; froid sans huile

1. Introduction

Popularity of carbon dioxide as a working medium has been gaining momentum in the last decade. It is motivated not only by increased environmental awareness of the society but economical factor as well. CO_2 installations can be more compact than its hydrocarbon- or synthetic-counterparts and in many cases more energy efficient (Nekså et al., 2010, NARECO$_2$, 2009, Chen et al., 2006). Recent development in supercritical CO_2 power cycles has brought attention to the new type of machines used in the CO_2 field, namely high speed oil-free turbo-compressors and turbo-expanders. Sandia National Laboratories (SNL) has published a report (Wright et al., 2010) from successful testing of 50 kW radial compressor

* *Corresponding author*. Tel.: +47 735 937 48; fax: + 47 735 953 10.
E-mail addresses: Bartosz.Kus@ntnu.no, kus.bartosz@gmail.com (B. Kus), Petter.Neksa@sintef.no (P. Nekså).
0140-7007/$ – see front matter
http://dx.doi.org/10.1016/j.ijrefrig.2013.05.009

Please cite this article in press as: Kus, B., Nekså, P., Development of one-dimensional model for initial design and evaluation of oil-free Co_2 turbo-compressor, International Journal of Refrigeration (2013), http://dx.doi.org/10.1016/j.ijrefrig.2013.05.009

spinning at up to 75 krpm and producing pressure ratios of up to 1.8. Although rather low efficiencies of the compressor are reported, such a concept can be perceived as an interesting option for other CO_2 based systems, such as air conditioning or refrigeration. Benefits of oil-free operation are multiple and include simplified architecture of the system, broader range of operating conditions (Hafner et al., 2011) and improved heat exchange.

Schiffmann and Favrat (2009, 2010) have designed and successfully tested small oil-free radial compressor for domestic heat pump utilizing R134a as a working fluid. 78% isentropic efficiency is reported for a small 20 mm impeller reaching pressure ratios in excess of 3.3. Mechanical efficiency quantifying windage losses is calculated to be in the range of 92–95%. It is expected that such a high mechanical efficiency will be very difficult to reach for CO_2 systems due to the significantly higher density of the gas.

To gain more understanding about which applications and what operating conditions are particularly interesting for the new type of machine, efficient design tools must be available. The purpose of the present study is to introduce a tool that allows for quick prediction of basic dimensions and performance of CO_2 oil-free compressor based on a set of designer inputs.

The importance of reliable preliminary estimation of compressor parameters should not be underestimated as an early identification of performance potential can save a lot of time and resources in subsequent phases of the system development as well as in its operation. It is expected that the tool could be used as a very first step in the machine design, providing rapid identification of possibly weak points of the technology depending on a particular field of application.

The 1D model consists of two essential parts. The first part predicts aerodynamic performance of a centrifugal compressor stage. The second one models losses resulting from hermetic operation and includes gas bearing friction, rotor windage and internal cooling losses.

One- or two-stage configuration can be simulated. The preliminary validation of the tool is based on CFD analysis and test data presented in the SNL report (Wright et al., 2010). Configuration of the two-stage compressor with brushless permanent magnet motor is shown in Fig. 1.

The presented model is used in Kus and Nekså (2013), where more comprehensive overview of the oil-free CO_2 compression technology is given, to assess feasibility of introducing oil-free turbo-compressors into commercial and industrial CO_2 refrigeration applications.

1.1. Modeling

1.1.1. Tool structure

The design tool has been made with a Microsoft Excel interface where a user has the full control of all important model constants and assumptions. These involve: impeller clearance, axial length of impeller (as a fraction of impeller diameter), inducer diameter ratio, diffuser diameter ratio, mean inducer blade angle, impeller discharge flow angle, magnetic shear stress of the motor, thrust bearing diameter ratio, motor electric efficiency, labyrinth seal dimensions, radial gap in journal bearings, load capacity of the gas bearings and internal cooling ratio (degree of cooling that is performed by fraction of the compressed gas).

The procedure itself takes place in VBA macros activated from the interface sheet. The algorithm contains three main iteration loops; the first two calculating dimensions and aerodynamic performance of the stages and the third one calculating the total machine's performance including additional losses generated by windage, electrical components and the cooling flow (see Fig. 2). The tool also predicts basic dimensions of bearings, rotor and shaft.

1.2. Aerodynamic modeling

It was decided to base the design procedure on 1D (mean line) approach, treating a compressor stage as a set of characteristic parts, each defined by inlet and outlet surfaces. Losses occurring in each of these parts are modeled with empirical correlations developed during the past several decades. The mean line method is regarded as a most practical one and providing acceptable accuracy (Oh et al., 1997, Sungho and Baek, 2001). Furthermore, a tool based on basic thermodynamic equations and pointing out specific loss mechanisms has also significant educational valor. It gives a designer an opportunity to test impact of particular design choices on the final performance of the machine.

Table 1 presents loss models used in the present study.

The basic design procedure is given below.

1.2.1. 1D design procedure

The specific work needed to compress the fluid to required pressure is calculated according to:

$$W_{comp} = (h_{02s} - h_{00})\eta_{s\ total} \quad (1)$$

where both enthalpies are calculated by the REFPROP code based on the designer inputs: the inlet temperature and

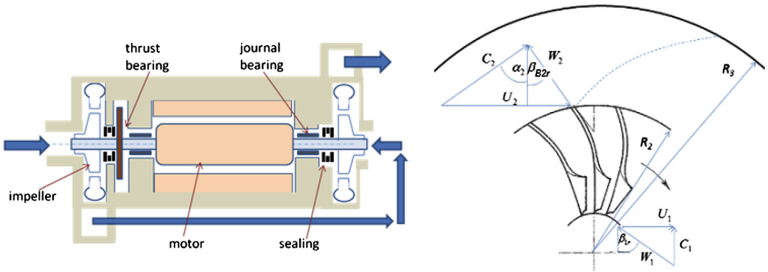

Fig. 1 – 2-stage compressor configuration.

Please cite this article in press as: Kus, B., Nekså, P., Development of one-dimensional model for initial design and evaluation of oil-free Co_2 turbo-compressor, International Journal of Refrigeration (2013), http://dx.doi.org/10.1016/j.ijrefrig.2013.05.009

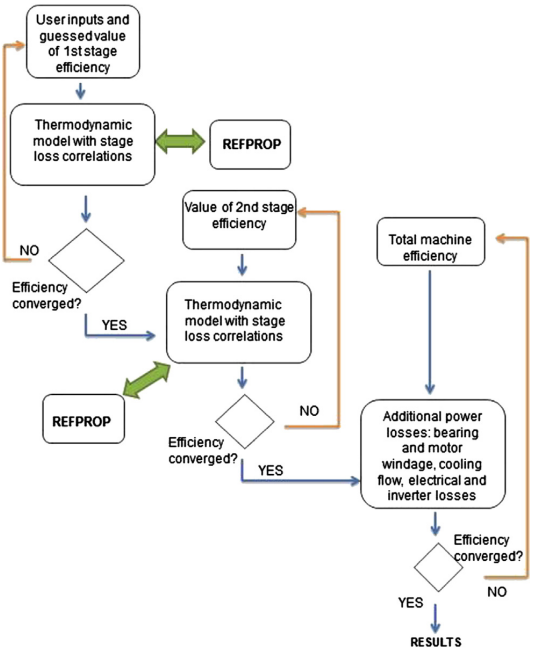

Fig. 2 – The calculation tool structure under Refprop thermodynamic data library.

pressure and discharge pressure. The total isentropic efficiency is assumed to start first main iteration loop.

Total discharge conditions are calculated from the isentropic efficiency definition:

$$\eta_{s\ total} = \frac{(h_{02s} - h_{00})}{(h_{02} - h_{00})} \tag{2}$$

An inlet velocity triangle is established in an iterative procedure so as to satisfy the requirement of the assumed inlet relative flow angle $\beta_{1\ r}$ (mean) and D_{1h}/D_{1t} ratio. The admission of the gas at the impeller inlet is axial.

The discharge velocity triangle is established from Euler equation:

$$\frac{P_{comp}}{\dot{m}} = U_2 C_{\theta 2} \tag{3}$$

and includes reduction of tangential velocity component by backward blade sweep β_{B2} and slip σ, according to equations:

$$C_{\theta 2} = \sigma U_2 + C_r \tan\beta_{B2} \tag{4}$$

$$\sigma = 1 - \frac{0.63\pi}{Z_B} \tag{5}$$

The above procedure aims at providing specified impeller discharge absolute flow angle α_{2r}.

With calculated discharge blade tip speed U_2 and assumed rotational speed one can easily find impeller discharge diameter:

$$D_2 = \frac{U_2}{\pi\omega} \tag{6}$$

To calculate impeller discharge blade height b_2 discharge static gas conditions have to be known. These are found from calculated (based on loss corellations) impeller efficiency. Determination of vaneless diffuser ideal discharge velocity triangle is based on two equations known as mass conservation equation and angular momentum equation.

$$\dot{m} = \rho_2 A_2 C_{r2} = \rho_3 A_3 C_{r3} \tag{7}$$

$$\tau = \dot{m}(r_3 C_{\theta 3} - r_2 C_{\theta 2}) \tag{8}$$

Real diffuser discharge conditions are calculated based on the total compressor discharge temperature and calculated passage losses.

Once the main stage dimensions and properties of the gas in the characteristic sections of the compressor are established, the loss correlations can be employed to predict the stage efficiency.

$$\eta_{s\ total} = \frac{(h_{02s} - h_{00})}{(h_{02} - h_{00})} = \frac{(h_{02s} - h_{00})}{(h_{02s} - h_{00}) + \sum \Delta h_{loss}} \tag{9}$$

Calculated efficiency is then compared with the initially provided value and the iteration loop will be repeated until both values match within the tolerance specified by the user. Analogical procedure is applied to predict efficiency of the second stage and the overall compressor efficiency.

After convergence of the calculation some general performance coefficients can be defined and calculated to judge the design of the compressor stage. These may include:

$$\text{Flow rate coefficient} \quad \phi = \frac{Q}{U_2 d_2^2}\frac{4}{\pi} \tag{10}$$

$$\text{Work coefficient} \quad \psi = \frac{\Delta h_{t-t}}{U_2^2} \tag{11}$$

$$\text{Machine Mach Number} \quad M_U = \frac{U_2}{a_{01}} \tag{12}$$

$$\text{Machine Reynolds Number} \quad Re = \frac{U_2 D_2}{\upsilon_{01}} \tag{13}$$

$$\text{Specific speed} \quad N_s = \frac{\omega\sqrt{Q}}{\Delta h_{0s}^{0.75}} \tag{14}$$

1.3. *Rotor windage modeling*

It is identified that high speed motors operating in high ambient pressure tend to induce windage losses that cannot be neglected in the initial design of the compressor (Briggs et al., 2008, Wright et al., 2010).

While there are many correlations well proven for some specific operating conditions (Raymond et al., 2008, Walton et al., 2012) present study will use correlation (1) developed by Vrancik (1968) and validated for high speed CO_2 compressor (Wright et al., 2010).

$$P_{mw} = \pi C_f \rho R^4 \omega^3 L \tag{15}$$

where:

$$\frac{1}{\sqrt{C_f}} = 2.04 + 1.768\ln\left(Re\sqrt{C_f}\right) \tag{16}$$

Please cite this article in press as: Kus, B., Nekså, P., Development of one-dimensional model for initial design and evaluation of oil-free Co_2 turbo-compressor, International Journal of Refrigeration (2013), http://dx.doi.org/10.1016/j.ijrefrig.2013.05.009

Table 1 – Loss correlations.

Loss mechanism	Loss model	Reference
Blade loading loss: occurs due to the boundary layer growth, separation and secondary flow development	$\Delta h_{bl} = 0.05 D_f^2 U_2^2$ $D_f = 1 - \frac{W_2}{W_{1t}} + \frac{0.75\Delta h_{Euler}/U_2^2}{(W_{1s}/W_2)[(Z/\pi)(1 - D_{1t}/D_2) + 2D_{1t}/D_2]}$ $\Delta h_{Euler} = C_{\theta 2} U_2 - C_{\theta 1} U_1$	Coppage et al. (1956)
Impeller skin friction: is generated by the viscous shear forces in the flow boundary layers. The procedure is equivalent to the pipe flow friction calculation	$\Delta h_{sf} = 2c_{fi}(L_i/D_{ih})W_m^2$ $W_m = \frac{C_{1t} + C_2 + W_{1t} + 2W_{1h} + 3W_2}{8}$ $c_{fi} = 0.3164(Re_i)^{-0.25}$	Jansen (1967)
Vaneless diffuser loss: The procedure is similar to impeller loss calculation, but the velocity is assumed to be the mean value of inlet and outlet diffuser velocities	$\Delta h_{df} = 2c_{fd}(L_d/D_{dh})C_m^2$ $c_{fd} = k\left(\frac{1.8 \cdot 10^5}{Re_d}\right)^{0.2}$ $k = 0.015$	Japikse (1982)
Clearance loss: results from the leakage of the fluid from the pressure to the suction side of the unshrouded impeller blades	$\Delta h_{cl} = 0.6\frac{\varepsilon}{b_2} C_{\theta 2}\left\{\frac{4\pi}{b_2 Z_b}\left[\frac{r_{1s}^2 - r_{1h}^2}{(r_2 - r_{1t})(1 + \rho_2/\rho_1)}\right] C_{\theta 2} C_{r1}\right\}^{1/2}$	Jansen (1967)
Mixing loss: is a result of non-uniform discharge of the flow from the impeller and is calculated based on the jet/wake theory	$\Delta h_{mix} = \frac{1}{1 + \tan^2\alpha_{2r}}\left(\frac{1 - \varepsilon_{wake} - b*}{1 - \varepsilon_{wake}}\right)^2 \frac{C_2^2}{2}$ where: $\varepsilon_{wake} = 0.25$, $b^* = 1$	Johnston and Dean (1966) Oh et al. (1997)
Disc friction loss: Is generated by the shear flow forces acting on the impeller backplate	$\Delta h_{disc} = C_{f\,disc}\frac{\overline{\rho} r_2^2 U_2^3}{4\dot{m}}$ $\begin{cases} \frac{2.67}{Re_{disc}^{0.5}}, & Re_{disc} < 3 \times 10^5 \\ \frac{0.0622}{Re_{disc}^{0.2}}, & Re_{disc} > 3 \times 10^5 \end{cases}$ $Re_{disc} = \frac{U_2 r_2}{\nu_2} \quad \overline{\rho} = \frac{\rho_1 + \rho_2}{2}$	Daily and Nece (1960)
Recirculation loss: results from reversal into the impeller of a portion of the flow that does not have enough momentum to overcome pressure gradients in the diffuser	$\Delta h_{rc} = 0.02 D_f^2 U_2^2 \sqrt{\tan\alpha_{2r}}$	Jansen (1967)
Volute loss: It is assumed that the meridional velocity component of the fluid leaving the diffuser is lost in the volute	$\Delta h_{vol} = C_{3r}^2/2$	

Dimensions of the rotor are determined from the formula found in Hanselman (2006):

$$TRV = \frac{\tau}{\frac{\pi}{4} D_{mot}^2 L_{mot}} \tag{17}$$

where:

$$TRV = 2\sigma_m \tag{18}$$

Required torque is calculated from compressor power and angular speed. Important design parameter is the gap sheer stress which is the tangential force per unit rotor surface area. When expressed in Pa units, low cost brushless permanent magnet motors typically exhibit a shear stress in the range of $3400 < \sigma_m < 13800$ ($0.5 < \sigma_m < 2$ psi), higher cost motors in the range $10300 < \sigma_m < 20600$ ($1.5 < \sigma_m < 3$ psi), very high performance motors are typically in the range $13800 < \sigma_m < 69000$ ($2 < \sigma_m < 10$ psi), and large liquid cooled motors $69000 < \sigma_m < 138000$ ($10 < \sigma_m < 20$ psi). The designer must also decide on L/D ratio of the rotor. To reduce windage losses it is desirable to have long slender rotor. One have to bear in mind however that longer motors are more likely to exhibit rotordynamics issues, especially pronounced in machines with gas foil bearings. For Sandia's CO_2 compressor L/D ratio amounted to 3.7 (Wright et al., 2010). Final size of the motor should always be preceded by rotordynamics analysis.

Rotor tip speed must be also checked. The limiting constraint is to keep the magnets in compression. Depending on the magnets material different peripheral speeds can be allowed. For a high strength, low resistivity and high modulus material such as Inconel 718 maximum rotor peripheral speed of 200 m s-1 is acceptable.

Please cite this article in press as: Kus, B., Nekså, P., Development of one-dimensional model for initial design and evaluation of oil-free Co_2 turbo-compressor, International Journal of Refrigeration (2013), http://dx.doi.org/10.1016/j.ijrefrig.2013.05.009

1.4. Gas bearings modeling

Estimation of gas bearing losses consists of three stages: predicting radial and axial forces acting on the rotor, sizing the bearing based on bearing load capacities and applying an appropriate loss model.

1.4.1. Predicting axial loads

Simple 1D prediction of axial loads in a CO_2 centrifugal compressor is a subject to a significant uncertainty. There can be up to few tens of thousands N of force across the front and back face of the impeller, therefore the model must subtract two very large numbers. It means that not only prediction of thrust magnitude but also its direction could be challenging. Noall and Batton (2011) used a 1D correlation to predict thrust in a radial turbine working in supercritical state for CO_2. Measurements showed that actual thrust was not only a third of the predicted one, but also acted in the opposite direction. It is more difficult to predict static pressures at a radial turbine's intermediate stations than in radial compressors; however it shows that simple mathematical operations with big numbers can give misleading results.

During testing of the SCO_2 (supercritical CO_2) compressor performed by SNL (Wright et al., 2010) the following approach was taken. First, the rotor was installed on typical roller bearings and during the initial tests a load cell was used to measure the thrust. The compressor was equipped with pump out vanes on the back side of the impeller wheel. Gradual trimming of the vane outer radius allowed for balancing of the axial loads. Once the load cell indicated magnitudes of thrust acceptable for gas bearings they were installed instead of ball bearings.

The literature suggests that CFD methods can be reliable sources of information about axial forces acting on centrifugal compressor impeller. Shi et al. (2010) used numerical simulations to predict axial thrust in a deep well pump. Comparison of simulation results with measured values gave error of 0.3–5.9% across the full range of operating conditions.

An attempt to validate the CFD model against experimental data published by Sandia is made in the present study. 3D model (Fig. 3) of compressor stage was generated based on the geometrical description provided in the SNL report. Numerical simulation was conducted with FLUENT 13 code. The turbulence was predicted with the k-ε model and wall boundary layers were solved with wall functions. The second-order discretization scheme was used for simulations. Inlet conditions of the tested compressor were very close to the critical point. It resulted in simulation convergence problem when real gas (REFPROP) equations were used to determine thermodynamic properties of gas. Changing inlet boundary conditions to higher temperature and higher pressure would solve convergence issues as the solver would have more "space" to search for a solution around the assigned boundary conditions without crossing the saturation line. Simulating the compressor with different pressure levels does not however enable direct validation of CFD method against the experimental data. The approach taken was instead to use constant density model and reach simulation convergence maintaining inlet boundary conditions in accordance with test data. Sandia actually used the test data to adjust their 1D model for thrust prediction based on incompressible gas equations. Good agreement was achieved.

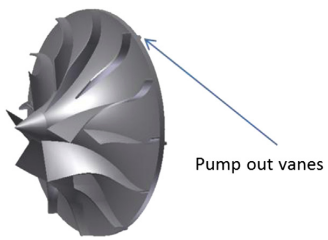

Fig. 3 – 3D model of Sandia's impeller with pump out vanes.

1.4.2. CFD simulation of Sandia's compressor

Simulation parameters are presented in Table 2

To reduce computational effort periodic boundary condition was applied and only 1/6 of the compressor domain was used for simulation.

Fig. 4 presents predicted thrust load acting on the full impeller versus grid size of the simulated domain. It is important to note that that presented results take into account thrust component resulting from cavity pressure acting on the compressor shaft. Shaft diameter and cavity pressure used for calculation are also taken from Sandia's report. It can be observed that direction of the thrust and its magnitude matches quite well with the data presented by Sandia, around 533 N (120 lbs) of force for 40k revolutions per minute. The not exact match can be attributed to the usage of the constant density model instead of real gas equations and the not perfect reproduction of real compressor's blade curvature. The analysis however confirms that CFD can be a reliable tool for prediction of magnitude and direction of axial thrust acting in a centrifugal compressor.

Additional simulations were performed for 3 different impellers in order to get more insight into what magnitude of axial forces can be expected in CO_2 turbo-compressor. Parameters of each simulated stage are presented in more detail in the *Results* section of present paper. Predicted axial thrusts are shown in Fig. 5. Negative values mean that resultant thrust acted toward compressor inlet, positive ones indicate thrust direction toward impeller back plate.

It is shown that axial forces acting in CO_2 turbo-compressors can be of significant value and due to the complex 3-dimensional nature of the gas flow it is difficult to predict them in a quick analytical way. There seems to be a potential however to use CFD results as an input for development of more accurate 1D models in the future. So far, if a quick performance prediction of oil-free CO_2 compressor is needed, the magnitude of thrust should be assumed on some reasonable level, to provide for its future balancing with assistance of CFD or experimental methods.

1.4.3. Sizing a thrust bearing

Widely accepted "rule-of-thumb" for load capacity (expressed in N) that can be supported by a thrust foil bearing is given by (19):

$$W_{LC\,AB} = f_{AB}(\pi w D_{AB\,m}) D_{AB\,m} N \tag{19}$$

Please cite this article in press as: Kus, B., Nekså, P., Development of one-dimensional model for initial design and evaluation of oil-free Co_2 turbo-compressor, International Journal of Refrigeration (2013), http://dx.doi.org/10.1016/j.ijrefrig.2013.05.009

Table 2 – Simulation data for Sandia's impeller.

Parameter	Inlet mass flow, kg s^{-1}	Inlet static pressure, bar	Outlet static pressure, bar	Density, kg m^{-3}	Rotational speed, rpm	Pump out vane clearance, mm
Value	3.96	80	93.85	630	40,000	0.15

where:, w – difference between the inner and outer top foil diameters or radial extent of the top foil (m);N – shaft speed (krpm)

Dykas et al. (2009) cites different load coefficients obtained by various researchers. They vary from 664 to 3460 kg m-3 Krpm-1 (0.024–0.125 lb in-3 Krpm-1) for different rotational speeds. New generation of bearings is reported to achieve load coefficients of around 2770 kg m-3 Krpm-1 (0.1 lb in-3 Krpm-1) and this value is proposed to be used with the present model. The above equation can be used to calculate the size of axial bearing once the axial load is determined.

1.4.4. *Windage of thrust bearing*

Calculation of the power loss generated by the thrust bearing employs the theory of flow around a disc rotating in a housing and is presented in Schlichting (1968). It defines a dimensionless torque coefficient c_M from the laminar "free" rotating disc case (20).

$$c_M = \frac{\tau}{0.5\rho_{cav}\omega^2 r^5} \tag{20}$$

Correlations for turbulent torque coefficient were proposed by various authors.

Recent windage measurements of foil bearing rotating in supercritical state CO_2 was presented by Milone (2010). It shows significant underestimation of the torque coefficient by the often used Schultz-Grunow formula (see Fig. 6). The overview of other correlations developed for free rotating disc case is presented in Miles (2011). It is found that correlations given by von Kármán (1921), Dorfman (1958) and Bayley and Owen (1969) match quite well with test data obtained for free rotating disc in pressurized air. Superimposing all three correlations to supercritical CO_2 conditions also gives a reasonable match (Fig. 6). The Bayley and Owen formula will be used as a default setting in the present tool.

Schultz – Grunow $c_M = 0.0622(Re)^{-1/5}$ (21)

von Kármán $c_M = 0.146(Re)^{-0.2}$ (22)

Dorfman $c_M = 0.982(\log_{10}Re)^{-2.58}$ (23)

Bayley and Owen $c_M = 0.131(Re)^{-0.186}$ (24)

where:

$$Re = \frac{r^2\omega}{\upsilon} \tag{25}$$

Once the torque coefficient is estimated the power loss of the thrust bearing can be calculated:

$$P_{AB} = 0.5c_M\rho\omega^3(r_0^5 - r_{in}^5) \tag{26}$$

1.4.5. *Radial load prediction*

Provided rotor dimensions and its construction material density, one can simply calculate the radial force that is generated on the journal bearings. Radial force resulting from non-uniform pressure distribution across the volute of the compressor is believed to be negligible in the design point operation and thus is not taken into account (Reunanen and Larjola, 2005).

1.4.6. *Sizing a radial bearing*

Load capacity that can be supported by a journal bearing is given by:

$$W_{LC\,JB} = f_{JB}(L_{JB}D_{JB})D_{JB}N \tag{27}$$

Typical advanced journal foil bearing performance coefficient value f_{JB} expressed in kg m-3 krpm-1 is 27680 (1 lb in-3 krpm-1) (Dykas et al., 2009). If calculated dimensions are smaller than the journal foil bearings commercially available on the market, they are scaled up to match commercial

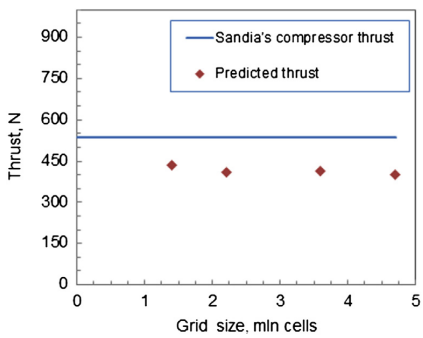

Fig. 4 – Mesh independence study for prediction of axial thrust.

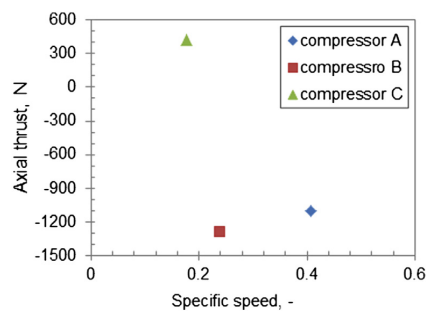

Fig. 5 – Prediction of axial thrust for different CO_2 compressors.

Please cite this article in press as: Kus, B., Nekså, P., Development of one-dimensional model for initial design and evaluation of oil-free Co_2 turbo-compressor, International Journal of Refrigeration (2013), http://dx.doi.org/10.1016/j.ijrefrig.2013.05.009

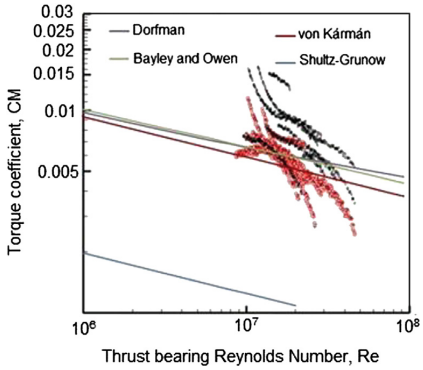

Fig. 6 – Theoretical torque coefficients for free rotating disc versus experimental data for supercritical CO_2 conditions.

bearings sizes. Minimum diameter of a journal bearing is assumed to be 30 mm.

1.4.7. *Windage of radial bearing*

It is proposed that foil journal bearing can be treated as a special case of rotor-stator system where the outer cylinder is at rest and the inner is rotating and modeled with Taylor-Couette flow theory (Schlichting, 1968). The theory predicts three operational regimes which can be described by relating two non-dimensional numbers, the torque coefficient (C_M) and the Taylor number (T_a).

$$T_a = \frac{U_i \varepsilon}{\upsilon}\sqrt{\frac{\varepsilon}{r_i}} \tag{28}$$

$$C_M = \frac{Mi}{0.5\pi\rho U_i^2 r_i^2 \varepsilon} \tag{29}$$

For Taylor numbers higher than 400 the flow becomes turbulent and this is the region where high speed bearings are expected to operate. The validation of the theory for high pressure and high speed CO_2 applications can be found in Bruckner (2009) and Howard et al. (2007). The measured toque coefficients obtained for various CO_2 pressures and rotor shafts fit reasonably well with the theoretical predictions.

To calculate windage of a journal bearing the following formula for turbulent torque coefficient can be used (Sukhomlinov et al., 2003):

$$C_M = 0.02 T_a^{-0.2} \tag{30}$$

Power loss is then simply found from angular speed and torque relationship.

1.5. *Cooling loss modeling*

Hermetic CO_2 compressors require efficient cooling. It is known that friction losses occurring due to the rotor and bearing windage can be significant. Proven practice is to allow some ratio of the compressed gas to leak into the rotor cavity. Throttling of the gas in the clearance of the shaft seal will provide necessary cooling capacity needed to remove friction heat from bearings and the rotor. If labyrinth seals are used the actual mass flow of the cooling stream can be approximated by the "Martin" (17) formula and depends on the geometry of the seal, density of the gas and pressure levels on both sides of the seal.

$$m_l = C_d S_0 \sqrt{p1\rho 1 \left(\frac{\left(1 - \frac{p_2}{p_1}\right)^2}{N - \ln\left(\frac{p_2}{p_1}\right)} \right)} \tag{31}$$

where: S_0 is the leakage area and C_d is dimensionless discharge coefficient

The correlation was found to predict leakage reasonably well for a tested supercritical CO_2 compressor (Wright et al., 2010).

If assumed dimensions of the seal (diameter, number and height of the teeth) results in mass flows and cooling capacity not sufficient to remove friction losses then the geometry is changed iteratively to allow more coolant flow into the cavity.

The tool's default pressure value in the cavity is set to inlet pressure of the compressor. This eliminates the need for booster pump/compressor that would otherwise have to pump the leaked stream back into the compressor inlet pressure. The designer can however specify different pressure levels.

It is assumed that the heat removal process is isobaric. To find the mass flow required for cooling the cavity discharge temperature must be also provided. It is assumed to keep this temperature around 100 °C in order to keep the motor cool enough to perform efficient and safe operation.

The cooling loss is defined as a power needed to compress the stream leaving the cavity to the discharge pressure of the compressor. Efficiency of this process is assumed to be that of the compressor. Cooling demand generated by the windings of the electrical motor is not taken into account here. It is assumed that additional casing cooling will be provided.

2. Results

2.1. *CFD verification of stage performance*

It is believed that CFD can be used as a reliable method to predict turbo-machinery internal flows. This was validated experimentally by Krain and Hah (2003), Roberts and Steed (2004), Swain (2005), Xu and Amano (2009). Therefore, an attempt to verify predictions of the 1D tool with CFD analysis was made.

Three different compressor geometries (Fig. 7) were created based on the output from the 1D tool. Parameters for each compressor stage are collected in Table 3.

Design point operation was simulated. Each CFD model includes clearance between back plate of the impeller and the housing, so disc friction loss is included in both models (1D and numerical). Volute losses are excluded from both models.

Please cite this article in press as: Kus, B., Nekså, P., Development of one-dimensional model for initial design and evaluation of oil-free Co_2 turbo-compressor, International Journal of Refrigeration (2013), http://dx.doi.org/10.1016/j.ijrefrig.2013.05.009

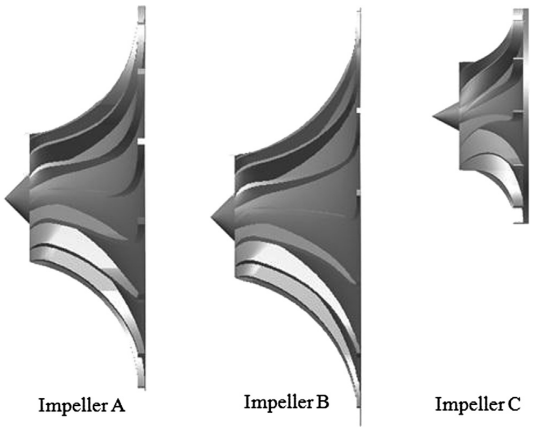

Fig. 7 – Different impellers tested with CFD method.

Table 4 – Mesh independence study for CFD pressure and efficiency predictions.

	Mesh size	$\mu_{is\ (t-t)}$	Average y^+	$P_{out}/P_{in\ (t-t)}$
Compressor A				
Grid 1	1.7 mln	0.806	290	1.59
Grid 2	3.9 mln	0.806	260	1.59
Grid 3	8.5 mln	0.808	108	1.59
Compressor B				
Grid 1	1.3 mln	0.711	270	1.70
Grid 2	3.8 mln	0.710	145	1.70
Grid 3	10 mln	0.710	122	1.70
Compressor C				
Grid 1	0.9 mln	0.908	614	1.66
Grid 2	3.0 mln	0.910	220	1.66
Grid 3	7.8 mln	0.906	143	1.67

2.1.1. *Numerical modeling*

Steady state CFD simulations were executed with FLUENT 13 code. The turbulence was predicted with the k-ε model and wall boundary layers were solved with logarithmic wall functions. The second-order discretization scheme was employed.

An inlet mass flow boundary condition was used with total temperature and static pressure specified (operating pressure was set to zero). Pressure outlet boundary condition with a prescribed static pressure and backflow total temperature was used for stage outlet. The turbulent kinetic energy was assumed to be uniformly distributed with intensity of 10%.

Only one blade passage was modeled and periodic boundary condition applied. Each compressor stage consisted of three volumes: impeller zone, vaneless diffuser zone and back plate clearance. Interfaces between zones adopt a frozen rotor model. This allows inlet distortion to be transferred across the different frames of reference.

Frozen rotor model can be used for turbomachinery applications in which rotor-stator interaction is relatively weak. Centrifugal compressor with vaneless diffuser and without inlet vanes can be treated as such a case (Liu and Hill, 2000, Engeda et al., 2003). For each compressor model mesh independence study was performed (see Table 4).

Results of analytical and numerical prediction are presented in Fig. 8.

Good fit between prediction of pressure ratio and efficiency can be observed for Case A and B. For super-critical compressor (Case C) the 1D model under-predicts the pressure ratio compared to CFD. Without experimental verification it is difficult to conclude which method is more accurate in this case. It can be however expected that some general approximation present in the 1D model tend to reduce accuracy prediction in supercritical region where small under- or over-prediction of one thermodynamic property can result in significant variation of another.

An additional insight into non-dimensional performance coefficients of a machine can be beneficial in assessing efficiency predictions obtained with a given model. Most

Table 3 – Parameters of different compressor stages used in CFD simulations.

Parameter	Unit	Compressor A	Compressor B	Compressor C
Speed	krpm	47.5	47.5	75
Pressure inlet	bar	30	30	120
Temperature inlet	K	305	300	320
Mass flow	Kg s^{-1}	1.5	1.3	6.3
Blade height	m	0.0015	0.0082	0.0017
Discharge blade angle	°	−45	−45	−40
Number of blades	–	15	15	12
Inlet blade angle at tip	°	54	57.6	61
Tip clearance	m	0.00025	0.00035	0.00025
Impeller diameter	m	0.084	0.094	0.0374
Inlet hub diameter	m	0.011	0.0094	0.005
Inlet shroud diameter	m	0.0275	0.027	0.0187
Diffuser diameter	m	0.151	0.188	0.070
Axial length of impeller	m	0.028	0.031	0.0124
Shaft diameter	m	0.025	0.025	0.014
Back plate clearance	m	0.0004	0.0004	0.0004

Please cite this article in press as: Kus, B., Nekså, P., Development of one-dimensional model for initial design and evaluation of oil-free Co_2 turbo-compressor, International Journal of Refrigeration (2013), http://dx.doi.org/10.1016/j.ijrefrig.2013.05.009

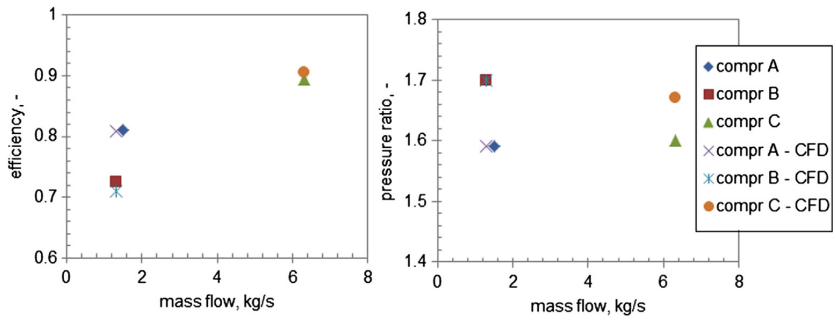

Fig. 8 – Comparison of analytical and numerical predictions of efficiency (t–t) and pressure ratio (t–t).

important performance coefficients for the three simulated compressors are calculated and presented in Table 5.

It can be concluded that the results of the non-dimensional analysis are quite consistent with the analytical and numerical predictions of the compressors' efficiency. The high Reynolds numbers favor reaching high efficiency in all of the presented cases. Both specific speed and flow coefficient of Compressor C are found to be within the optimal range applicable for radial compressors. It is therefore to be expected that this design will achieve the best efficiency among the tested configurations. Still, the 90% prediction of the isentropic efficiency may appear overly optimistic. If however, one takes into account relatively low pressure ratio and high molecular mass of the gas, and that the cited efficiency is calculated based on the total-to-total conditions, the prediction seems more realistic. Accordingly, a compressor with the lowest specific speed and flow coefficient and with the highest Mach numbers is expected to perform least efficiently. The lowest performance among the tested designs is predicted for Compressor B by both the analytical and numerical model.

Based on the numerical results the chart presenting the area averaged absolute Mach numbers along meridional span of the impellers is depicted in Fig. 9. It is shown that for machines operating at similar pressure ratios, Reynolds numbers and work coefficients the performance is dependent on the velocity profile across the stage. Among presented cases, the compressor with the highest maximal Mach number and the steepest Mach number profile across the impeller achieves the worst efficiency.

2.2. *Tool verification with existing experimental results*

SNL test results were used to validate 1D prediction of total compressor efficiency. Performance of the compressor working in its design point (no incidence at the impeller inlet) was predicted for three rotational speeds: 40, 50 and 55 krpm. In order to compare 1D prediction with experimental results the set of parameters were extracted from Sandia's report and

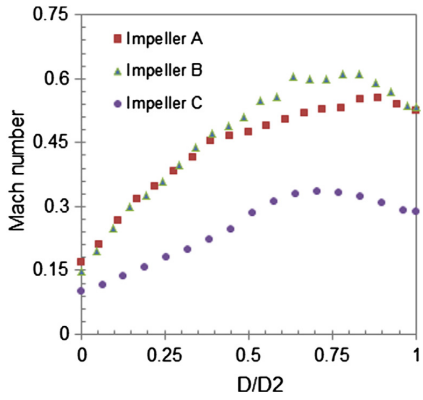

Fig. 9 – Numerical prediction of averaged absolute Mach numbers across the impellers.

Table 5 – Non-dimensional performance coefficients for the simulated compressors.

Parameter	Unit	Compressor A	Compressor B	Compressor C
Machine mach number	–	0.84	0.95	0.49
Flow coefficient	–	0.021	0.012	0.064
Work coefficient	–	0.68	0.68	0.66
Specific speed	–	0.40	0.34	0.66
Machine Reynolds number	–	7 e07	9 e07	7.1 e07

Please cite this article in press as: Kus, B., Nekså, P., Development of one-dimensional model for initial design and evaluation of oil-free Co_2 turbo-compressor, International Journal of Refrigeration (2013), http://dx.doi.org/10.1016/j.ijrefrig.2013.05.009

Table 6 – Parameters of 1D simulation for Sandia's compressor..

Parameter	Unit	Value	
Pressure inlet	bar	77	
Temperature inlet	K	305	
Cavity pressure	bar	13.8	
Cavity temperature	K	320	
Number of blades	-	12	
Mean inlet blade angle	°	51	
Tip clearance	m	0.00025	
Motor length	m	0.168	
Rotor diameter	m	0.044	
Rotor gap	m	0.0031	
Axial load	N	1000	Inputs
Axial bearing load capacity	Kg m-3 krpm-1 (lb in-3 krpm-1)	2767 (0.1)	
Radial bearing load capacity	Kg m-3 krpm-1 (lb in-3 krpm-1)	27670 (1)	
Seal leakage area	m2	1.67E-06	
Dimensionless discharge coefficient	-	2.1	
Number of seal lands	-	4	
Electrical efficiency	-	0.93	
D1h/D1s	-	0.27	
B2b	°	-50	
Inlet shroud radius	m	0.0094	
Inlet hub radius	m	0.0025	Targets
Blade height	m	0.0017	

Table 7 – Results of the 1D simulation of Sandia's compressor.

Parameter	Unit	45 krpm	50 krpm	55 krpm
Pressure ratio (total)	–	1.35	1.43	1.56
Efficiency t–s	–	0.662	0.670	0.675
Efficiency t–t	–	0.698	0.707	0.714
Leakage flow	% (of main mass flow)	0.95	1.09	1.31
Impeller discharge flow angle	°	70.3	71	73
Mass flow	Kg s^{-1}	2.9	3.1	3.25

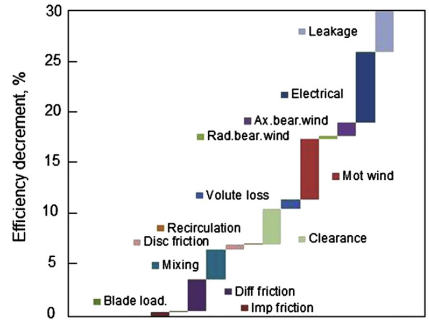

Fig. 10 – Loss breakdown predicted for Sandia's compressor operating at 45 krpm.

used either as an input or a target of the simulations. For example, inlet conditions, rpms, size of the rotor were input constraints. Parameters such as impeller diameter and discharge blade height were results of the simulations obtained by adjusting other input parameters such as mass flow or absolute discharge flow angle. The list of parameters that were common for each simulation is presented in Table 6.

Predicted efficiencies as well as the remaining results of simulations are collected in Table 7. Predicted peak compressor efficiencies agree reasonably well with experimental data where upper range of measured efficiencies (t–s) is found within 65–70% region.

2.3. *Predicted loss breakdown for SNL compressor*

Loss breakdown for 45 krpm machine is shown in Fig. 10. Several loss mechanisms seem to have particularly pronounced impact on compressor efficiency. Small diameter of the impeller results in big relative clearance and therefore significant leakage of the gas from high to low pressure side of the blade (clearance loss). Despite significantly reduced cavity pressure high shaft speed still results in non-negligible rotor windage. Significant seal leakage loss is a result of big pressure difference between rotor cavity and impeller back plate. This leakage is accounted in the model as a cooling. The pumping power needed to compress leaked gas from the lowered cavity pressure to the inlet pressure of the compressor is not included as it was also not included in Sandia's efficiency measurements. Electrical losses are inevitable in every kind of compressor and come from switching circuitry of the inverter and magnetic losses within the stator windings. 93% electrical efficiency was assumed according to the Sandia's report.

3. Conclusions

A 1D model for prediction of performance of CO_2 oil-free radial compressor has been proposed. 1D predictions of aerodynamic performance and pressure ratios of different compressor stages are in satisfactory agreement with results obtained with numerical methods. Efficiency predictions of a

Please cite this article in press as: Kus, B., Nekså, P., Development of one-dimensional model for initial design and evaluation of oil-free Co_2 turbo-compressor, International Journal of Refrigeration (2013), http://dx.doi.org/10.1016/j.ijrefrig.2013.05.009

compressor model based on a 50 kW Sandia's compressor are found to correlate reasonably well with the measurements.

The CO_2-based turbo-machinery can be of very small sizes due to the significant density of the working fluid, especially when it is in the supercritical state. In some cases, the big relative clearance and the high surface roughness can be of a major issue when high stage efficiency is a priority. On the other hand the relatively high molecular weight of carbon dioxide and relatively low pressure ratios present in CO_2 cycles favors reaching reasonably high stage efficiency of the radial compressor. It is the overall efficiency of the hermetic CO_2 machine that may be challenging to achieve, due to the non-stage windage and cooling losses.

Prediction of axial thrust is an important step in the CO_2 compressor development. Due to the complex 3-dimensional nature of the gas flow it is difficult to carry out in a quick analytical way. Various methods of thrust reduction, such as manipulations of number and diameter of impellers, adjusting the size of the labyrinth seal, varying the pressure in the motor cavity or applying pump-out vanes can be applied.

In a present form the tool requires axial thrust to be assumed. To give some preliminary orientation of a thrust magnitude that can be present in relatively small CO_2 compressor, a CFD method was used to analyze three different radial compressor stages with back-plate clearance. More research in the area of quick axial thrust prediction seems however very desirable.

The present model was developed with a view to assess possibility of introducing oil-free compression technology into the area of commercial grade CO_2 refrigeration. Hence, machines in the range of a few tens to a few hundreds of kW of shaft power are subject of interest. Rather low pressure ratios of between 2 and 3combined with at least 2 stages of compression usually result in subsonic operation; hence shock wave effects are not included in the present form of the model. The correlations predicting friction in the passages of the compressor assume smooth surfaces. Their applicability for very small geometries is therefore limited to those with a good surface finish.

Acknowledgments

This publication forms a part of the CREATIV project, performed under the strategic Norwegian research program RENERGI. The authors acknowledge the partners: Sintef Energy Research, Danfoss, FHL, Hydro Aluminium, John Bean Technology, Norske Skog, REMA1000, Systemair, TINE, and the Research Council of Norway (195182/S60) for their support. The authors would like to thank Barber-Nichols Inc. for the valuable comments to the present work.

Nomenclature

b	blade height (m)
b*	ratio of vaneless diffuser inlet width to impeller exit width (–)
C	absolute velocity (m s^{-1})
c_f	skin friction coefficient (–)
c_M	Dimensionless torque coefficient (–)
D	diameter (m)
D_f	diffusion factor (–)
h	specific entalphy (kJ kg^{-1})
L	length (m)
p	pressure (Pa)
P	Power (W)
r	radius (m)
Re	Reynolds number (–)
T	temperature (K)
U	impeller blade tip speed (m s^{-1})
Z_B	number of blades (–)
ε	clearance (m)
α	absolute flow angle (rad)
β_{b2}	discharge blade angle (rad)
ε	clearance (m)
ε_{wake}	wake fraction of blade-to-blade space (–)
ω	angular velocity (rad s-1)
W	relative velocity (m s^{-1})
τ	torque (N m)
μ	viscosity (Pa s)
ρ	density (kg m^{-3})
σ_m	the motor air gap shear stress (Pa)

Subscripts

1	impeller inlet
2	impeller discharge
3	diffuser discharge
AB	axial bearing
bl	blade loading
d	diffuser passage
cav	motor cavity
cl	clearance
df	diffuser friction
h	hub/hydraulic
i	Impeller channel
JB	journal bearing
LS	labirynth seal
m	mean
mix	mixing
mot	motor's rotor
mw	motor windage
r	meridional direction (angle)/meridional component
sf	skin friction
t	shroud
t–s	Total to static
t–t	Total to total
θ	circumferential direction (angle)/circumferential component

REFERENCES

Bayley, F.J., Owen, J.M., 1969. Flow between a rotating and Stationary disc. Aeronaut. Q. 20, 330–354.
Briggs, M.H., Prahl, J.M., Bruckner, R., 2008. High pressure performance of foil journal bearings in various gases. In:

Proceedings of STLE/ASME International Joint Tribology Conference IJTC, Miami, Florida USA.

Bruckner, R.J., 2009. Windage Power Loss in Gas Foil Bearings and the Rotor-stator Clearance of High Speed Generators Operating in High Pressure Environments. NASA/TM—2009–215826.

Chen, Y., Lundqvist, P., Johansson, A., Platell, P., 2006. A comparative study of the carbon dioxide transcritical power cycle compared with an organic rankine cycle with R123 as working fluid in waste heat recovery. Appl. Therm. Eng. 26, 2142–2147.

Coppage, J.E., Dallenbach, F., Eichenberger, H.P., Hlavaka, G.E., Knoernschild, E.M., Van Lee, N., 1956. Study of supersonic radial compressors for refrigeration and pressurization systems. WADC Rep., 55–257.

Daily, J.W., Nece, R.E., 1960. Chamber dimension effects on induced flow and frictional resistance of enclosed rotating disks. Trans. ASME, J. Basic Eng. 82, 217–232.

Dorfman, L.A., 1958. Hydrodynamic Resistance and the Heat Loss of Rotating Solids, first ed. Oliver and Boyd.

Dykas, B., Bruckner, R., DellaCorte, C., Edmonds, B., Prahl, J., 2009. Design, fabrication, and performance of foil gas thrust bearings for Microturbomachinery applications. J. Eng. Gas. Turb. Power 131, 012301–012307.

Engeda, A., Kim, Y., Aungier, R., Direnzi, G., 2003. The inlet flow structure of a centrifugal compressor stage and its influence on the compressor performance. J. Fluid Eng. 125/779.

Hafner, A., Nekså, P., Ladam, Y., Eikevik, T.M., 2011. Oil-free R744 Systems for Industrial/commercial Applications. ICR, Prague, Czech Republic.

Hanselman, D., 2006. Brushless Permanent Magnet Motor Design Second Edition. Magna Physics Publishing.

Howard, S.A., Bruckner, R.J., DellaCorte, C., Radil, K.C., 2007. Gas foil bearing technology advancements for closed Brayton cycle turbines. AIP Conf. Proc. 880, 668.

Japikse, D., 1982. Advanced diffusion levels in turbocharger compressors and component matching. In: IME Conference on Turbocharging and Turbochargers, p. 143. paper C45/82.

Jansen, W.A., 1967. Method for calculating the flow in a centrifugal impeller when entropy gradients are present. In: Royal Society Conference on Internal Aerodynamics (Turbomachinery). IME.

Johnston, J., Dean, R., 1966. Losses in vaneless diffusers of centrifugal compressors and pumps. Analysis, experiment and design. Trans. ASME, J. Eng. Power 88, 49–62.

Krain, H., Hah, C., 2003. Numerical and experimental investigation of the unsteady flow field in a Transonic centrifugal compressor. In: Proc. Int. Gas Turb. Congress, Tokyo.

Kus, B., Nekså, P., 2013. Oil-free turbo-compressors for CO_2 refrigeration applications. Int. J. Refrigeration.

Liu, Z., Hill, D.L., 2000. Issues surrounding multiple frames of reference models for turbo compressor applications. In: International Compressor Engineering Conference. Paper 1369.

Miles, A., 2011. An experimental study of windage due to rotating and static bolts in an enclosed rotor-stator system. In: Thermo-fluid Mechanics Research Centre. University of Sussex.

Milone, D., 2010. Windage and gas foil bearing losses in a supercritical carbon dioxide turbine Generator. In: Supercritical CO_2 Power Cycle Symposium May 24–25, 2011 Boulder, Colorado.

Natural refrigerant CO, 2009. Leonardo Project "NARECO$_2$". KHLim.

Nekså, P., Walnum, H.T., Hafner, A., 2010. CO_2 – a refrigerant from the past with prospects of being one of the main refrigerants in the future. In: 9th IIR Gustav Lorentzen Conference, Sydney. ISSN: 0151-1637, ISBN 978-2-913149-74-8.

Noall, J., Batton, W., 2011. Correlation of reaction to isentropic velocity ratio for a subsonic radial Inflow turbine. In: Supercritical CO_2 Power Cycle Symposium, Boulder, Colorado.

Oh, H., Yoon, E., Chung, M., 1997. An optimum set of loss models for performance prediction of centrifugal compressors. Proc. Inst. Mech. Eng. Part A: J. Power Energy 211, 331–338.

Raymond, M.S., Kasarda, M.E.F., Allaire, P.E., 2008. Windage power loss modeling of a smooth rotor supported by Homopolar Active magnetic bearings. J. Tribol. 130, 1–8.

Roberts, D.A., Steed, R., 2004. A comparison of steady-state centrifugal stage CFD analysis to experimental Rig data. In: ANSYS/CFX Canada Int ANSYS Conf.

Reunanen, A., Larjola, J., 2005. Radial forces in a centrifugal compressor; Experimental investigation by using magnetic bearing and static pressure distribution. J. Therm. Sci. 14 (No.1), 1–8.

Schiffmann, J., Favrat, D., 2009. Experimental investigation of a direct driven radial compressor for domestic heat pumps. Int. J. Refrigeration 32, 1918–1928.

Schiffmann, J., Favrat, D., 2010. Design, experimental investigation and multi-objective optimization of a small-scale radial compressor for heat pump applications. Energy 35/8, 436–450.

Schlichting, H., 1968. Boundary-layer Theory. McGraw-Hill, New York.

Shi, W., Wang, H., Zhou, L., Zou, P., Wang, C., 2010. The estimation and experiment of axial force in deep well pump basing on numerical simulation. IJMECS 2, 53–61.

Sukhomlinov, I. Ya, Golovin, M.V., Tagantsev, O.M., Ravikovich, Yu. A., Ermilov, Yu. I., Kholobtsev, D.P., 2003. Power loss in a built-in high-frequency electric drive for a centrifugal refrigeration compressor. Chem. Petrol. Eng. 39 (Nos), 7–8.

Sungho, Y., Baek, J.H., 2001. A sensitivity analysis of centrifugal compressors' empirical models. KSME Int. J. 15 (No.9), 1291–1301.

Swain, E., 2005. Improving a one-dimensional centrifugal compressor performance prediction method. Proc. Inst. Mech. Eng., Part A: J. Pow. Ene 219, 653.

von Kármán, T., 1921. Technical Memorandum on Laminar and Turbulent Friction. National advisory committee for aeronautics. Report No. 1092.

Vrancik, J.E., 1968. Prediction of Windage Power Loss in Alternators. NASA Technical Note D-4849.

Walton, J.F., Heshat, H., Tomaszewski, M., 2012. Power loss in high-speed micro-machinery – an experimental study. Proc. of ASME Turbo Expo.

Wright, S.A., Radel, R.F., Vernon, M.E., Rochau, G.E., Pickard, P.S., 2010. Operation and Analysis of a Supercritical CO_2 Brayton Cycle. Sandia Report SAND2010–0171.

Xu, C., Amano, R.S., 2009. Development of a low flow coefficient single stage centrifugal compressor. Int. J. Comput. Methods Eng. Sci. Mech. 10, 282–289.

Please cite this article in press as: Kus, B., Nekså, P., Development of one-dimensional model for initial design and evaluation of oil-free Co_2 turbo-compressor, International Journal of Refrigeration (2013), http://dx.doi.org/10.1016/j.ijrefrig.2013.05.009

Paper II

INTERNATIONAL JOURNAL OF REFRIGERATION XXX (2013) 1–8

Available online at www.sciencedirect.com

SciVerse ScienceDirect

journal homepage: www.elsevier.com/locate/ijrefrig

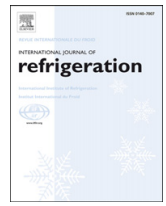

Oil free turbo-compressors for CO_2 refrigeration applications

Bartosz Kus, Petter Nekså*

Norwegian University of Science and Technology, 7491 Trondheim, Norway

ARTICLE INFO

Article history:
Received 17 August 2012
Received in revised form
26 February 2013
Accepted 4 March 2013
Available online xxx

Keywords:
Radial turbo-compressor
Carbon dioxide
Compression
Oil-free compressors
Oil-free refrigeration

ABSTRACT

Feasibility of replacing oil-lubricated compressing equipment in CO_2 based refrigeration systems with oil-free turbo-machinery is assessed. Presented concept enables efficient compression for systems ranging from 0.1 to 5 MW of cooling capacity, provided that the operating pressures are low, i.e. 30/10 bar. Performance of the systems with higher operating pressures, i.e. 77/30 bar is penalized in wide range of capacities due to the excessive windage losses, especially pronounced in the systems with cooling capacities lower than 1 MW. In some cases, possibility of using longer motor should be analyzed. This may require special strategies for rotordynamic issues or driving each impeller with separately mounted motor. It is observed that optimal specific speed of the compressor stage does not always result in optimal overall performance. The trade-off between aerodynamic efficiency and non-stage losses must be found.

Turbo-compresseurs sans huile pour les applications frigorifiques au CO_2

Mots clés : turbo-compresseur radial ; dioxyde de carbone ; compression ; compresseurs sans huile ; froid sans huile

1. Introduction

Small vending machines, residential heat pump water heaters, commercial and industrial refrigeration, ventilation and air conditioning, small to medium scale power production from waste heat - these are only some of the areas where CO_2 is used as a working fluid (Nekså et al. (2010), "NARECO2" (2009), Chen et al. (2006), Zhang et al. (2006)). Environmentally benign characteristics, low cost and good thermophysical properties of carbon dioxide account for its increasing popularity. Depending on the type of application, designers of the system must cope with different type of often antagonizing requirements such as: energy efficiency, size and manufacturing limitations, maintenance costs and safety aspects.

Regardless of the application, oil-free operation is almost always a desired characteristic as it usually results in simplified architecture of the system due to the elimination of oil separation and distributing components, reduced investment and maintenance cost and improved heat exchange conditions. For refrigeration systems, oil-free operation additionally means increased maximum discharge temperature (no risk of decomposition of lubricant) allowing for higher pressure ratios per compressor stage, and thus limiting number of

* *Corresponding author*. Tel.: +47 735 937 48; fax: + 47 735 953 10.
E-mail addresses: Bartosz.Kus@ntnu.no, kus.bartosz@gmail.com (B. Kus), Petter.Neksa@sintef.no (P. Nekså).
0140-7007/$ – see front matter
http://dx.doi.org/10.1016/j.ijrefrig.2013.03.002

Please cite this article in press as: Kus, B., Nekså, P., Oil free turbo-compressors for CO_2 refrigeration applications, International Journal of Refrigeration (2013), http://dx.doi.org/10.1016/j.ijrefrig.2013.03.002

Table 1 – Assumptions for the 1D model.

Assumption	Comment/Reference
Impeller is open	Closed impellers are more typical for large process compressors, were casing protects blades from the damage. They are also more expensive to manufacture.
Work split between stages is based on equal pressure ratios	To maintain similar stage efficiency the preceding stage has usually higher pressure ratio. It is expected however that similar pressure gradients acting on both impellers will contribute to better axial thrust balancing
Radial gap in journal bearings = 20 μm	Values of 12–75 μm are reported (Agrawal (1997), Müller and Fréchette (2002), Bruckner (2009)). As choosing too big clearance would result in underestimation of the bearing windage the value from the lower bound of the range was assumed.
Journal foil bearing load capacity coefficient = 27700 kg m^{-3} $krpm^{-1}$ (1 lb in^{-3} $krpm^{-1}$)	Typically achievable for journal foil-bearings (Dykas et al. (2009)).
Axial foil bearing load capacity coefficient = 2770 kg m^{-3} $Krpm^{-1}$ (0.1 lb in^{-3} $Krpm^{-1}$)	Typically achievable for new generation of axial foil-bearings Dykas et al. (2009) Wright et al. (2010)
Motor electrical efficiency = 0.97	New generation of electric motors with efficiencies exceeding 96% is reported by Tokai University (2009)
Driver electrical efficiency = 0.97	Typically cited by the vendors
Gas superheat at compressor inlet = 5 K	A few degrees of superheat is typically advised to protect impeller blades from droplets of liquid
Inner to outer diameter ratio of thrust bearing = 0.35	Various values are reported: 0.42, 0.5 (Dykas et al. (2009)) Lower diameter ratio will result in smaller overall size of the bearing and therefore in smaller windage.
Axial length of impeller = $0.3D_2$	Came and Robinson (1999) suggest using 0.32–0.37 for high inlet Mach numbers of 0.9–1.2. For simulated compressors inlet Mach numbers were usually below this range.
σ_m = 20.7 kPa (3 psi)	Shear stress in the gap of the motor. Hanselman (2006)
D_{1h}/D_{1t} = 0.265	Inducer hub/shroud ratio. Following values are reported: 0.2–0.3 (Witkowski (2004)) 0.265 (Wright et al. (2010))
α_{2r} = 75°	High values of the absolute discharge angle result in good diffusion rates across impeller but may result in excessive length of the flow path across diffuser. Angles higher than 75° are not recommended (Whitfield and Baines (1990))
β_{1r} (mean) = 45°	It is proven that the minimum relative Mach numbers occurs at the relative flow angle between 56 and 64 at the shroud of the inducer (Whitfield and Baines (1990)). Such flow angles at the shroud will result in approximately 45° mean relative flow angle.
β_{2r} = 45°	Application of backward swept blades reduces impeller discharge absolute Mach numbers, broadens operating range of the compressor and reduces secondary flow losses (Came et al. (1979)). While there is no optimum back swept angle values between 40 and 60° are often found in literature [Whitfield and Baines (1990)].
Z_B = 15	The number of blades at the discharge of impeller. For small impellers number of blades at the inducer could be smaller. Optimal number of blades (with or without splitter blades) depends on the particular case and requires more detailed analysis (CFD)
Clearance = 0.3% of D_2	Came and Robinson (1999)
L_{rot}/D_{rot} = 3.8	Relative length of the rotor. In order to reduce windage losses one aims at possibly long slender rotor. Too long rotor can result in rotordynamic issues and final choice must be always preceded by rotordynamic analysis. CO_2 compressor tested at Sandia National Lab compressor has relative rotor length of 3.8 (Wright et al. (2010)).
D_3/D_2 = 1.8	The larger the diffuser radius ratio, the greater the pressure recovery attainable under ideal conditions. In practice, too long diffuser flow path leads to excessive friction losses. It was been shown that increasing diffuser ratio above 1.8 does not improve overall efficiency ((Brown and Bradshaw (1947))
L_{JB}/D_{JB} = 1	Relative length of the journal bearing (DellaCorte and Bruckner (2011)).
Axial thrust = 1500 N	Example thrust values for CO_2 radial compressor stages are presented in Kus and Nekså (submitted for publication)

Please cite this article in press as: Kus, B., Nekså, P., Oil free turbo-compressors for CO_2 refrigeration applications, International Journal of Refrigeration (2013), http://dx.doi.org/10.1016/j.ijrefrig.2013.03.002

necessary components. It also allows entering new areas, enabling ultra-low temperature refrigeration technology, at temperatures below −40 °C or even −62 °C (Hafner et al. (2011), Niu et al. (2011)).

In typical closed circuit processes an oil or lubricant is used to provide lubrication of mechanical moving parts in the compressor. Due to the imperfect containment of the lubricant, its fraction is transported with the working fluid into the system and contaminates inner surfaces of tubes, expansion devices and heat exchangers. This oil has to be captured using different types of oil separation and management systems which are usually costly and add complexity to the system. It is therefore desirable to enable an oil free system.

We can distinguish between three main types of compressors: reciprocating, rotary (screw, scroll, swing) and turbo-compressors. Oil-free reciprocating piston compressors are typically of the labyrinth seal type. These are slow running costly compressors with relatively low efficiency. Oil free screw compressors are also costly and the efficiency is relatively low due to excessive leakage losses. Radial oil-free turbo-compressors were proven to work successfully in a wide range of applications (DellaCorte and Bruckner (2011), Walton and Heshmat (1994)).

The selection of the appropriate bearing technology is crucial for proper design of an oil-free compressor. According to Molyneaux and Zanelli (1996), replacing oil or grease in the rolling element of the bearing with refrigerant in liquid phase is possible, however at the expense of the additional losses due to the constant delivery of a bypass refrigerant stream. The life span of such bearing operating at high speeds was not reported. Magnetic bearings are an option. The technology is commercially proven, but adds complexity to the system (auxiliary feedback control, touchdown bearings) and increased investment cost.

Fluid film bearings are the most common candidate for oil-free machinery as they are relatively simple in construction and exhibit successful track record from various fields of application and over a wide range of rotating speeds. Schiffmann (2008) gives an overview of different types of gas lubricated bearings pointing out two especially interesting alternatives, namely foil bearings and herringbone grooved bearings. Both technologies have been successfully applied in many systems and both have their pros and cons. While herringbone groove bearings are easier to manufacture, they display lower misalignment tolerance and load capacities than foil bearings.

Foil bearings, on the other hand, with its greater misalignment tolerance, can affect impeller efficiency due to the higher impeller tip clearances required, and they are more difficult to model. The literature on foil bearings seems richer and covers a wide range of applications, from micro-turbines producing barely 100 W to a few hundred kW compressors. The foil bearing air cycle machine on the Boeing 747 aircraft has demonstrated an MTBF (mean time between failures) in excess of 100,000 h. Air cycle machines with foil bearings has served on many other passenger and military aircrafts and their application is a common practice today (Agrawal (1997)).

While substantial amount of information can be found on air oil-free turbo-machinery, the literature on CO_2 oil-free applications is rather scanty. Wright et al. (2010) performed testing and analysis of a supercritical CO_2 Brayton loop with a 50 kW shaft power compressor supported on foil bearings. The study confirms feasibility and performance potential of such cycles and takes notice of significant motor windage losses in high density gas at high shaft speeds. Performance test of foil journal bearing in various gases conducted by Briggs et al. (2008) confirm power loss sensitivity to gas density and rotational speeds.

The purpose of this work is to assess the feasibility of replacement of standard oil-lubricated compressors operating in various industrial and commercial applications utilizing CO_2 as a working fluid with a new generation of oil-free turbo-machinery.

Due to the closed loop nature of a predominant number of these systems, the study will consider hermetic type of compressors with internal recirculation of gas leaked to the motor cavity through the seals. Foil bearings are selected for this study as a proven technology with high development potential in the future.

2. Theory and modeling

The intension of this study is to include all possible inefficiencies constituting the final performance of the machine. Not only the aerodynamic performance is predicted, but bearings and motor windage, electrical losses of driver and motor and cooling flow loss are also taken into account. Full assessment of the total contribution of various loss

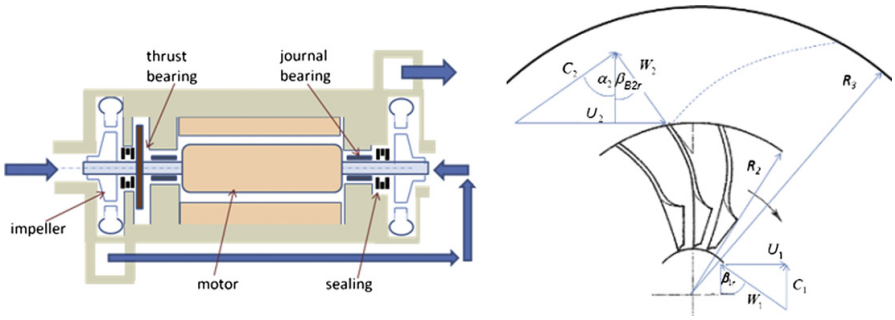

Fig. 1 – Simulated compressor configuration.

Please cite this article in press as: Kus, B., Nekså, P., Oil free turbo-compressors for CO_2 refrigeration applications, International Journal of Refrigeration (2013), http://dx.doi.org/10.1016/j.ijrefrig.2013.03.002

mechanisms is necessary to compare a new type of compressor with existing commercial solutions.

The performance predictions presented in the study are based on the 1D model presented and validated in Kus and Nekså (submitted for publication). In order to run each simulation a user must provide a set of inputs including operational conditions, mass flow, various geometrical relations of the compressor stage, the rotor and the bearings, electrical efficiencies, etc.

These relations are assumed and kept constant for different machine applications to provide consistent point of reference in assessing different applications' feasibility. It should be acknowledged that each machine's design is not optimized, but rather based on good engineering practice. The most important assumptions together with commentary or reference are presented in Table 1. If it is unclear how some assumption were made, a reader is advised to refer to Kus and Nekså (submitted for publication) were more detailed description of the tool's default settings is given. The configuration simulated in this study is a two-stage compressor with a brushless DC motor placed between two impellers oriented in opposite direction, so as to balance axial forces generated on each impeller due to the pressure gradients (see Fig. 1). The presented efficiencies are calculated based on total–total conditions.

3. Results and discussion

3.1. Design issues with the test case compressor

A lower stage loop in a cascade refrigeration system was chosen as an example case for the design of the turbo-compressor. Evaporation and condensation pressures are assumed to amount 1 and 3 MPa respectively. Mass flow is set to 2 kg s^{-1}.

Very often, the first step in the design process is the determination of the specific speed (1) of the new machine, and its comparison with the existing machines operating under similar specific speeds. If the designer has the freedom

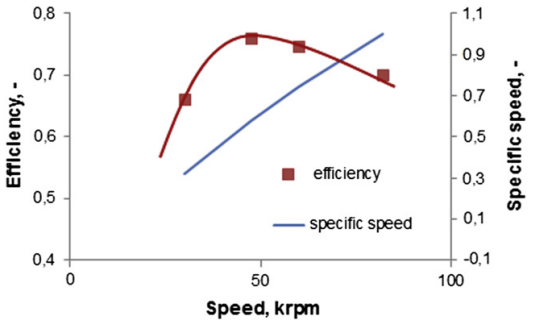

Fig. 3 – Estimated efficiency and specific speed of a CO_2 compressor with varying motor speed.

to adjust the speed of the compressor then specific speed can be varied to provide optimal efficiency.

$$n_s = \frac{\omega\sqrt{Q}}{\Delta h_{0s}^{3/4}}, \quad (1)$$

An example of the graph depicting peak stage efficiencies of existing geometrically similar machines correlated against specific speed is presented in Fig. 2.

Specific speed approach has however a few drawbacks. Firstly, efficiency/specific speed graphs are created for a single fluid and the data available in literature concerns mainly air or water (when it comes to pumps). Secondly, it does not take into account additional losses occurring due to the hermetic design. Prediction of the efficiency of the test case compressor designed for different operational speeds proves that pursuing optimal stage efficiency (optimal specific speed) does not always result in maximum overall compressor efficiency, see Fig. 3.

Typically, it could be expected that peak efficiency would occur for the compressor designed for specific speeds between 0.8 and 0.9, according to Fig. 2. It is shown, however, that peak performance of the machine occurs at lower specific speed than the one optimal from aerodynamic point of view.

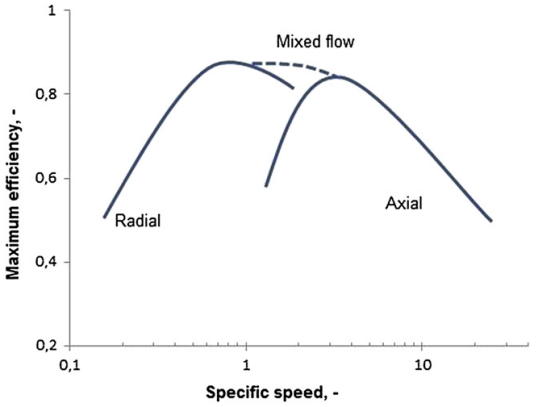

Fig. 2 – Selection of machine type with specific speed Adapted from Whitfield and Baines (1990).

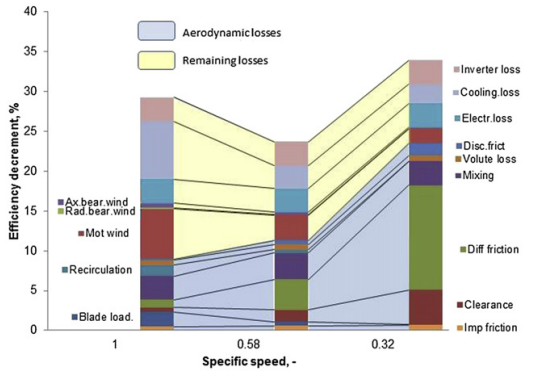

Fig. 4 – Loss breakdown for selected compressors designed for different specific speeds.

Please cite this article in press as: Kus, B., Nekså, P., Oil free turbo-compressors for CO_2 refrigeration applications, International Journal of Refrigeration (2013), http://dx.doi.org/10.1016/j.ijrefrig.2013.03.002

To better understand this relation the loss breakdown for three compressors designed for different operating speeds is presented in Fig. 4. Compressor designed to achieve high stage efficiency (specific speed = 1) will suffer from pronounced windage losses triggered by higher speeds of the shaft. This automatically results in increased leakage flow required to remove friction heat generated in the cavity of the motor and in the gas bearings. Too big reduction of rotational speed (specific speed = 0.32) will contribute to reduction of non-stage losses but will also significantly deteriorate aerodynamic efficiency. The aim of the designer is therefore to find the tradeoff between the stage performance and the losses stemming from hermetic type of operation.

3.2. *Overall results*

The purpose of this study is to investigate whether a new class of oil-free turbo-machinery could provide efficient compression for CO_2 based refrigeration systems. To give a possibly comprehensive overview of where new turbo-compressor might be reasonable choice, a wide range of compressors with different operating conditions, rotational speeds and capacities were simulated. In Figs. 5–7 it is shown how total efficiency of the compressor varies for fixed operating conditions and fixed rotational speeds. The parameter varied is the mass flow. For each mass flow a new design of the compressor is simulated. It can be seen that if one of the design constraints is the shaft speed, only a certain range of compressor capacities can be considered for the proposed concept.

If one connects points of peak efficiency for each compressor speed, curves depicting maximal efficiencies for given operating conditions and compressor capacities can be created. Such curves for are presented in Figs. 8–10.

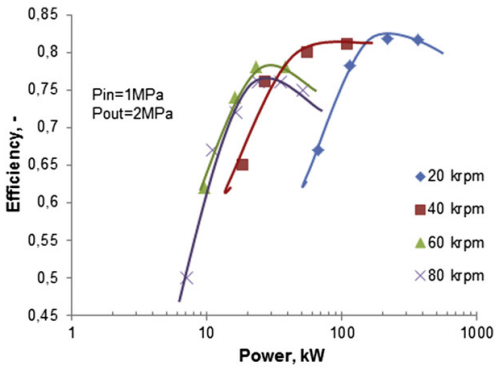

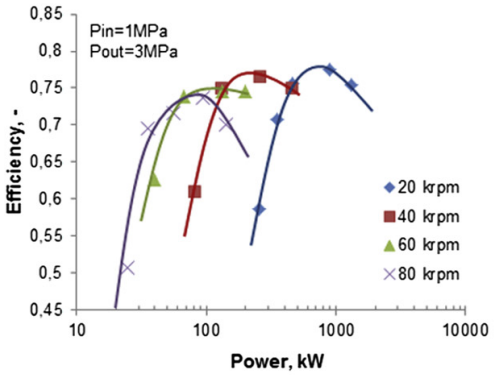

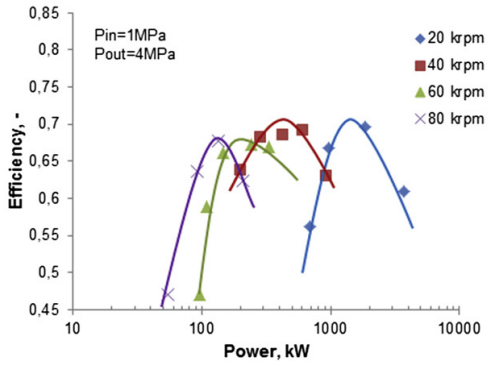

Fig. 5 – Predicted efficiency for compression from Pin = 1 Mpa for different compressor speeds as function of shaft power.

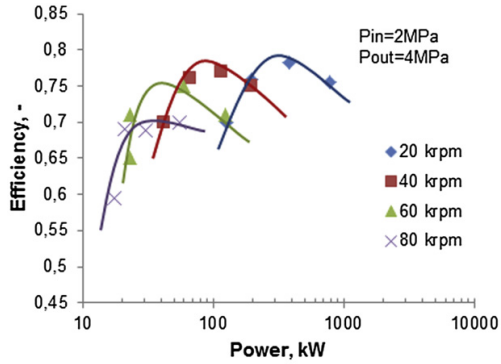

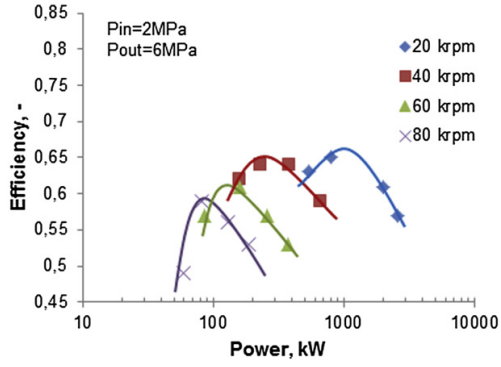

Fig. 6 – Predicted efficiency for compression from Pin = 2 Mpa for different compressor speeds as function of shaft power.

Please cite this article in press as: Kus, B., Nekså, P., Oil free turbo-compressors for CO_2 refrigeration applications, International Journal of Refrigeration (2013), http://dx.doi.org/10.1016/j.ijrefrig.2013.03.002

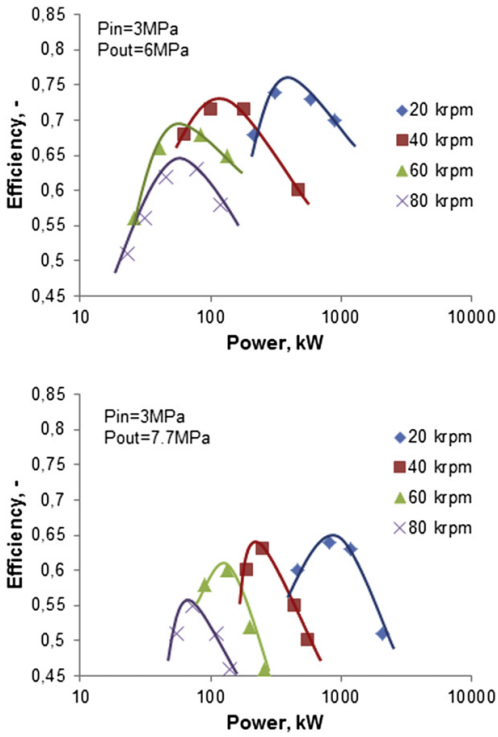

Fig. 7 – Predicted efficiency for compression from Pin = 3 Mpa for different compressor speeds as function of shaft power.

It is observed that with increased inlet pressure the attainable compressor efficiency is reduced. It is mainly a result of pronounced windage losses caused by the rotor spinning in higher density gas, but also at the higher rotational speeds required by reduced volumetric flow (according

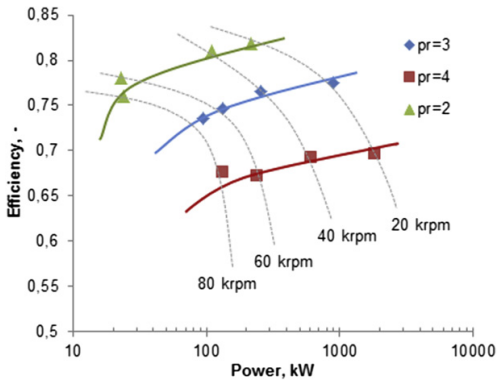

Fig. 8 – Predicted peak efficiencies for compression from 1 MPa as function of compressor shaft power for different compression pressure ratios.

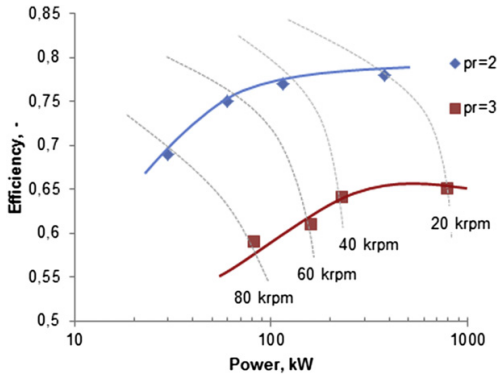

Fig. 9 – Predicted peak efficiencies for compression from 2.3 MPa as function of compressor shaft power for different compression pressure ratios.

to Eq. (1)). It can therefore be expected, that for a given mass flow compression efficiency of an oil-free compressor will tend to reduce significantly towards higher stages of compression. There is no easy solution to this challenge. One approach is suggested in the SNL report (Wright et al. (2010)) where a pump reducing the cavity pressure is applied. In the proof-of-concept compressor operating in the supercritical CO_2 region, relative pumping power is however significant and overall compression efficiency low. The authors of the report believe that for large scale commercial application, the fractional pumping power will be much smaller, largely because conventional sealing technologies could be used. For smaller applications however, use of the pump will result in excessive leakage losses leading to high pumping powers. The next drawback of such an approach will be higher complexity and introduction of some amount of oil into the system, which itself contradicts the oil-free concept. Another approach to

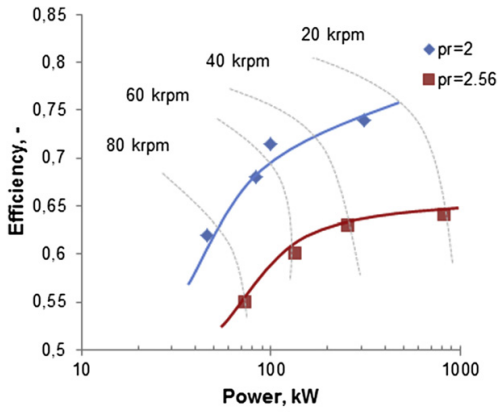

Fig. 10 – Predicted peak efficiencies for compression from 3 MPa as function of compressor shaft power for different compression pressure ratios.

Please cite this article in press as: Kus, B., Nekså, P., Oil free turbo-compressors for CO_2 refrigeration applications, International Journal of Refrigeration (2013), http://dx.doi.org/10.1016/j.ijrefrig.2013.03.002

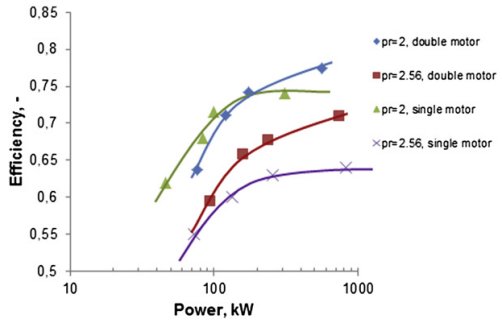

Fig. 11 – Impact of incorporation of double motor on compressor efficiency.

reduce the excessive windage losses may be to incorporate a longer more slender motor. Due to the rotordynamic issues that are likely to occur with a longer motor, the present study proposes to drive each impeller with separate motors supported independently. The change in the efficiency due to the application of a double motor for the compressor with inlet pressure of 3 MPa is presented in Fig. 11. It was assumed that the total axial load increased from 1500 to 2500 N due to the lack of the balancing-force from the second impeller. Improvement of efficiency is noticeable in higher capacity range, especially for the higher pressure ratio case (pr = 2.56). At a lower range of capacities (50–100 kW) not balanced axial trust becomes significant source of windage and overall efficiencies are still not expected to reach 70% level. Further improvement of efficiency, especially at lower capacities, could be achieved by increasing number of stages, i.e. arranging two two-stage compressors in series. Such an approach based on the previous version of the present 1D tool was presented in Kus and Nekså (2012). The increased cost of such solution may however outweigh potential performance improvement. For applications where axial thrust becomes an issue, a magnetic bearing option should be also considered.

4. Conclusions

Performance of oil-free CO_2 compressors that might be applicable for commercial and industrial HVAC/refrigeration systems is assessed based on 1D modeling. Proposed model of the compressor employs two centrifugal stages placed on opposite sides of the motor and orientated in the opposite direction to reduce axial thrust. The study takes into account possibly comprehensive set of loss mechanisms that may occur in an oil-free hermetic compressor concept. Predicted compression efficiencies vary depending on the operational conditions and capacity. For low inlet pressures and low to moderate pressure ratios (Pin = 1 Mpa, Put = 2 or 3) the compressor is expected to achieve good efficiency (>70%) in a wide range of capacities. Potential for good efficiency deteriorates with increasing operational pressures. It is caused by the reduced volumetric flow requiring higher shaft speeds to maintain reasonable aerodynamic performance. High speeds and high density of the gas are, in turn, factors contributing to significant windage of the motor operating in a hermetic configuration. The aim of the designer is therefore to find the trade-off between aerodynamic performance and the remaining parasitic losses. Depending on the case, it may occur that optimal specific speed of the compressor is different than the one providing the best aerodynamic performance of the stages. In cases where the level of windage losses in unacceptable, application of double motor (each impeller driven by separate motor) can be of advantage in terms of overall performance, but at the cost of increased system complexity. It should be stressed that present study is based on a 1D model (Kus and Nekså (submitted for publication)) and its aim is to give preliminary design and performance estimation rather than a final optimized solution.

Acknowledgment

This publication forms a part of the CREATIV project, performed under the strategic Norwegian research program RENERGI. The authors acknowledge the partners: Danfoss, FHL, Hydro Aluminium, John Bean Technology, Norske Skog, REMA1000, Systemair, TINE, and the Research Council of Norway (195182/S60) for their support.

Nomenclature

D	diameter (m)
L	length (m)
Q	volumetric flow rate ($m^3\ s^{-1}$)
h_{0s}	total enthalpy increase ($kJ\ kg^{-1}$)
ω	angular velocity ($rad\ s^{-1}$)

Subscripts

1	impeller inlet
2	impeller discharge
3	diffuser discharge
h	hub/hydraulic
JB	Journal bearing
r	meridional direction/component

REFERENCES

Agrawal, G.L., 1997. Foil Air/gas Bearing Technology – an Overview. Publication 97-GT-347. ASME.

Briggs, M.H., Prahl, J.M., Bruckner R., 2008. High pressure performance of foil journal bearings in various gases. In: Proceedings of STLE/ASME International Joint Tribology Conference IJTC, Miami, Florida USA.

Brown, W.B., Bradshaw, Guy R., 1947. Method of Designing Vaneless Diffusers and Experimental Investigation of Certain Undetermined Parameters. NASA TN 1426.

Bruckner, R.J., 2009. Windage Power Loss in Gas Foil Bearings and the Rotor-stator Clearance of High Speed Generators

Operating in High Pressure Environments. NASA/TM-2009-215826.

Came, P.M., McKenzie, I.R.I., Dadson, C., 1979. The Performance of a 6.5 Pressure Ratio Compressor Having an Impeller with Swept-back Blades. NGTE Memorandum 79013. Pyestock, Hants, UK.

Came, P.M., Robinson, C.J., 1999. Centrifugal compressor design. Proc. Instn Mech. Engrs. 213. Part C.

Chen, Y., Lundqvist, P., Johansson, A., Platell, P., 2006. A comparative study of the carbon dioxide transcritical power cycle compared with an organic rankine cycle with R123 as working fluid in waste heat recovery. Appl. Therm. Eng. 26, 2142–2147.

DellaCorte, C., Bruckner, R.J., 2011. Remaining technical challenges and future plans for oil-free turbomachinery. J. Eng. Gas. Turb. Power 133, 042502–042507.

Dykas, B., Bruckner, R., DellaCorte, C., Edmonds, B., Prahl, J., 2009. Design, fabrication, and performance of foil gas thrust bearings for microturbomachinery applications. J. Eng. Gas. Turb. Power 131, 012301–012307.

Hafner, A., Nekså, P., Ladam, Y., Eikevik, T.M., 2011. Oil-free R744 Systems for Industrial/commercial Applications. ICR, Prague, Czech Republic.

Hanselman, D., 2006. Brushless Permanent Magnet Motor Design, second ed. Magna Physics Publishing.

Kus, B., Nekså, P., 2012. Oil free turbo-compressors for refrigeration applications. In: Proceedings of 10th IIR Gustav Lorentzen Conference, June 25–27 Delft, the Netherlands. International Institute of Refrigeration, ISBN 978-2-913149-90-8.

Kus, B., Nekså, P. Development of one-dimensional model for initial design and evaluation of oil-free CO_2 turbo-compressor. Int J Refrig., Submitted for publication.

Molyneaux, A., Zanelli, R., 1996. Externally Pressurized and Hybrid bearings lubricated with R134A for oil-free compressors. International Compressor Engineering Conference at Purdue, vol. II, pp. 419–424.

Müller, N., Fréchette, L.G., 2002. Performance analysis of Brayton and Rankine cycle microsystems for portable power generation. Proc. IMECE, ASME International Mechanical Engineering Congress & Exposition, New Orleans, Louisiana.

Natural refrigerant CO, 2009. Leonardo Project "NARECO2". KHLim.

Nekså, P., Walnum, H.T., Hafner, A., 2010. CO_2 – a refrigerant from the past with prospects of being one of the main refrigerants in the future. 9th IIR Gustav Lorentzen Conference, Sydney, ISBN 978-2-913149-74-8, ISSN 0151-1637.

Niu, X.-D., Yamaguchi, H., Iwamoto, Y., Nekså, P., 2011. Experimental study on a CO_2 solid–gas-flow-based ultra-low temperature cascade refrigeration system. Int. J. Low-carbon Tech. 6, 93–99.

Schiffmann, J., 2008. Integrated design, optimization and experimental investigation of direct driven turbocompressor for domestic heat pumps. Thesis.

Tokai University, 2009. Tokai University Unveils 100W DC Motor with 96% Efficiency. http://techon.nikkeibp.co.jp/english/NEWS_EN/20090403/168295/.

Walton, J.F., Heshmat, H., 1994. Compliant Foil Bearings for Use in Cryogenic Turbopumps, vol. 1. NASA, pp. 372–381. Report No. CP 3282.

Whitfield, A., Baines, N.C., 1990. Design of Radial Turbomachines. Longman Scientific & Technical.

Witkowski, A., 2004. Sprężarki wirnikowe. Teoria, konstrukcja, eksploatacja. Wydawnictwo Politechniki Śląskiej, wydawnictwo, ISBN 83-7335-217-1.

Wright, S.A., Radel, R.F., Vernon, M.E., Rochau, G.E., Pickard, P.S., 2010. Operation and Analysis of a Supercritical CO_2 Brayton Cycle. Sandia Report SAND2010-0171.

Zhang, X.R., Yamaguchi, H., Uneno, D., Fujima, K., Enomoto, M., Sawada, N., 2006. Analysis of a novel solar energy-powered Rankine cycle for combined power and heat generation using supercritical carbon dioxide. Renew. Energy 31, 1839–1854.

Please cite this article in press as: Kus, B., Nekså, P., Oil free turbo-compressors for CO_2 refrigeration applications, International Journal of Refrigeration (2013), http://dx.doi.org/10.1016/j.ijrefrig.2013.03.002

Paper III

INTERNATIONAL JOURNAL OF REFRIGERATION XXX (2013) 1–14

Available online at www.sciencedirect.com

SciVerse ScienceDirect

journal homepage: www.elsevier.com/locate/ijrefrig

Novel partial admission radial compressor for CO_2 applications

Bartosz Kus, Petter Nekså*

Norwegian University of Science and Technology, 7491 Trondheim, Norway

ARTICLE INFO

Article history:
Received 14 May 2013
Received in revised form
12 July 2013
Accepted 17 July 2013
Available online xxx

Keywords:
Novel partial admission compressor
Oil-free compressors
Oil-free refrigeration
CO_2 turbo-compressor

ABSTRACT

A novel partial admission turbo compressor concept is proposed as an alternative to a conventional radial oil-free CO_2 compressor. The concept aims at the improvement of the overall performance through the reduction of the non-stage windage and cooling losses enabled by compression at significantly reduced shaft speeds. Transient CFD analysis gives fairly optimistic prediction of more than 80% of base stage efficiency at around 1.4 total pressure ratio. The study shows potential for efficiency improvement by optimization of the shape and number of blades. The conceptual compressor may be an interesting alternative for commercial CO_2 applications operating at close to critical pressures, provided that the deceleration of the gas in the diffuser is efficient.

Nouveau compresseur radial à admission radiale pour applications au dioxyde de carbone

Mots clés : Nouveau compresseur centrifuge ; Compresseurs secs ; Dioxyde de carbone ; Turbine

1. Introduction

According to Kus and Nekså (2013a and b) the performance of high pressure oil-free hermetic CO_2 turbo-compressors suffers from high windage and cooling losses triggered by operation under high shaft speeds and in a dense gas area. This concerns compressors particularly from lower capacity range (below 100 kW of shaft power) typically found in various commercial refrigeration applications. Refrigeration market consumes around 15% (IIR, 2010) of global electricity production. Since employment of CO_2 as a working fluid often becomes an obvious choice for many of the refrigeration cycles, the matter of increased machinery efficiencies deserves more focus.

Although oil-free operation of refrigeration systems, including those using CO_2 is highly desirable, this issue is not widely addressed in the literature. Schiffmann and Favrat (2009, 2010) successfully tested small oil-free radial compressor for domestic heat pump utilizing R134a as a working fluid and spinning at up to 210,000 rpm. Although

* *Corresponding author*. Tel.: +47 735 937 48; fax: +47 735 953 10.
E-mail addresses: kus.bartosz@gmail.com, Bartosz.Kus@ntnu.no (B. Kus), Petter.Neksa@sintef.no (P. Nekså).
0140-7007/$ – see front matter
http://dx.doi.org/10.1016/j.ijrefrig.2013.07.015

Please cite this article in press as: Kus, B., Nekså, P., Novel partial admission radial compressor for CO_2 applications, International Journal of Refrigeration (2013), http://dx.doi.org/10.1016/j.ijrefrig.2013.07.015

good efficiency of the compressor is reported, significantly higher density of the natural refrigerant CO_2 does not promise achieving similar efficiencies in case of a CO_2 compressor. This is due to the nature of the losses induced by the relative motion between the rotor and the stator of the electric motor. These losses according to Vrancik (1968) are directly proportional to the density of the ambient and increase with third power of rotational speed. An additional loss mechanism that is directly linked to the windage is the cooling loss, calculated based on a work input required to recompress the fraction of the gas that has to be throttled into the cavity to remove the friction heat generated by the rotor.

Previous studies on the subject of oil-free CO_2 compression (Kus and Nekså (2013b), Wright et al. (2010)) suggest that pursuing high efficiencies is not an easy task and more research is needed. There seem to be two main approaches to reducing significant windage losses, namely introducing smaller motors with improved cooling or reducing rotational speeds. None of these approaches is straightforward. Development of new customized motors with better cooling strategies is expensive and involves extensive testing. Furthermore, additional cooling infrastructure will likely result in added cost and complexity to the compression systems. Significant reduction of shaft speeds is not the obvious solution either. In a typical radial compressor it will reduce specific speed of the impeller and therefore limit its aerodynamic efficiency.

Where small flow rates and low rotational speeds are design targets, partial admission machines could be considered. It is a commonly adopted practice to use partial admission machines in high pressure stages of small axial steam turbines. Such a configuration allows using relatively high blades and avoiding significant blade losses that would occur due to friction if the flow was admitted in the full arc. It is generally known that the efficiency of a partial admission stage is lower than that of a full admission one. This is caused by the rotor blades periodically passing through admitted arcs as well as the not admitted ones. Non-uniform velocity profile across the admitted arc can be also expected to result in impaired conditions of the diffusion process.

Sakai et al. (2006) validated 3D numerical analysis of a one-nozzle partial admission steam turbine with experimental data. The numerical grid for a one-stage turbine used in the CFD experiments of Sakai is presented in Fig. 1.

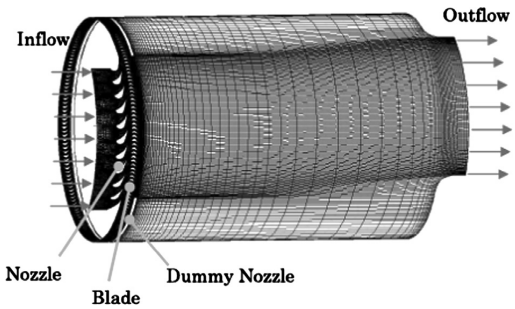

Fig. 1 – Numerical grid for simulation of partial admission axial steam turbine. Source: Sakai et al. (2006).

According to Yahya (1969) the principal losses in partial admission turbines are due to the rotor blades pumping the gas in the inactive sector, mixing of the active and inactive gas, leakage of the active gas into the inactive sector, and sudden expansion of the active gas into a rotor blade passages either entering or leaving the active admission sector. It is stated that the mixing, leakage and sudden expansion losses are the main contributors to the lowered efficiency of a partially admitted machine. The theory for prediction of these losses is also formulated by the author and validated experimentally. While the authors of the present paper are not aware of studies implementing similar partial admission concept to the axial compressor, it is supposed that analogical loss mechanisms will be present.

The partial flow principle is also known in centrifugal machines, when the typical full emission impeller designed for very low specific speeds is characterized by very narrow passages leading to significant friction losses. This can be modified by using a conventional rotor but with higher blades and blocking a part of the diffuser. Such concept is schematically shown in Fig. 2.

Test data reported by Van Lee (1961) shows that the static pressure in the inactive area of the partial emission centrifugal compressor is considerably higher than in the “live” flow area. According to Balje (1981), this implies strong recirculatory flow tendencies coupled with sudden flow deceleration of the blocked flow after leaving the impeller. The author gives a procedure to calculate the losses associated to the high pressure fluid leaking into the active flow path and the losses caused by the increased windage in the unemitting arc. The rather scanty amount of attention devoted to this concept in more recent literature may indicate that its performance was not satisfactory.

Another example of a partially admitted machine is the cross-flow blower, depicted in Fig. 3. This type of machine is nowadays used extensively in the HVAC industry. Usually it consists of forward curved blades with inner-to-outer diameter ratio of approximately 0.75 (Dang and Bushnell (2009)). Various casing designs exist, but most of them are intended

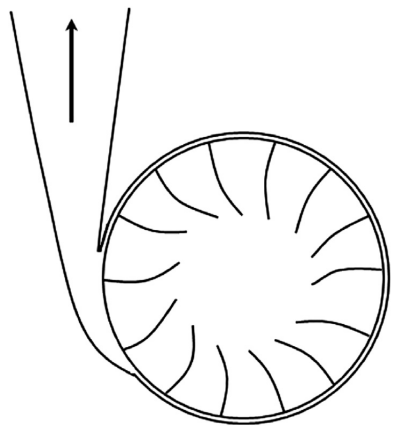

Fig. 2 – Partial emission configuration of a centrifugal compressor.

Please cite this article in press as: Kus, B., Nekså, P., Novel partial admission radial compressor for CO_2 applications, International Journal of Refrigeration (2013), http://dx.doi.org/10.1016/j.ijrefrig.2013.07.015

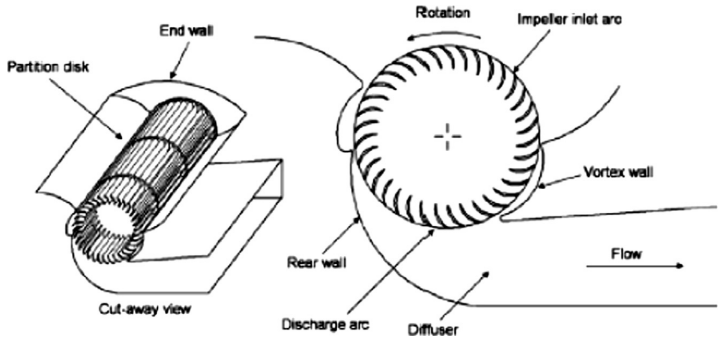

Fig. 3 – Typical cross-flow blower layout. Source: Dang and Bushnell (2009).

for approximately 90° flow turning from inlet to outlet. The cross-flow blower is two-stage machine where the flow is admitted on a certain part of the wheel arc and discharged through the opposite arc. Such a design creates characteristic fluid flow zones that limit the machine's efficiency.

Three main zones can be distinguished, as indicated in Fig. 3. In the zone designated with A, the main part of useful work is done. Due to the partial admission, zone B is formed, which behavior resembles that of a paddling wheel. The energy transfer in this region is regarded insignificant. Nevertheless, it contributes to the inefficiency of the compression process. In early 1950s, research by Eck (1962) and then Laing led to the discovery that the flow within the impeller was characterized by the formation of a vortex eccentric to the axis of the fan's rotation. This vortex (zone C in Fig. 4) affects the shape of the through flow region, causing its contraction in the middle of the wheel. This contraction is an undesirable phenomenon as one would aim at proper diffusion process before the next compression stage. Additional reduction of the efficiency comes from energy dissipation in the vortex. On the other hand, in a properly designed machine the vortex is used as an aerodynamic seal preventing the return of the outflow.

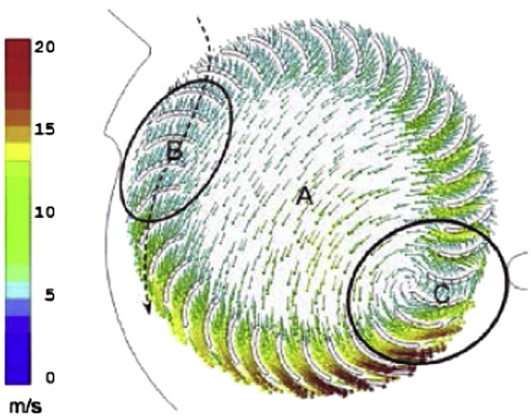

Fig. 4 – Three characteristic flow zones in cross flow blower. Source: Dang and Bushnell (2009).

Overall efficiency of the cross flow blower is however known to be low, as well as achieved pressure ratios.

The present paper attempts to utilize chosen features of both partial admission and cross-flow concepts and merge them into a novel concept with proposed name of "partial admission radial compressor". This study will try to answer whether the partial admission hermetic CO_2 compressor can be superior in terms of the overall efficiency compared to a state-of-the-art centrifugal concept. To be able to compare the novel compressor concept with a state-of-the-art machine the term "reference compressor" is introduced. For the sake of simplicity one-stage compressors will be compared.

2. The reference compressor concept

The reference one-stage high-speed hermetic radial compressor concept is depicted in Fig. 5.

For the preliminary design and performance estimation of the reference compressor the 1D tool presented and validated in Kus and Nekså (2013a) will be used. The design assumptions used in the present study are analogical to those presented and explained in detail in Table 1 in Kus and Nekså (2013b). In the present comparison an optimistic value of 1000 N is assumed for the axial thrust generated by the centrifugal impeller, which somewhat favors the standard compressor concept. Overall efficiency predictions presented in the present study do not include power loss in the electric driver.

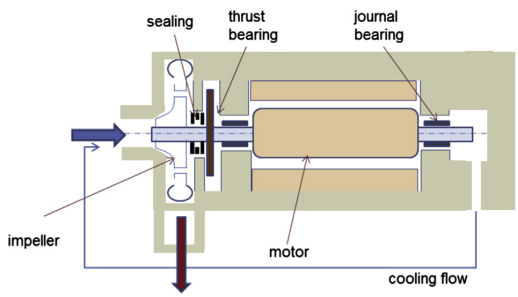

Fig. 5 – The reference compressor concept.

Please cite this article in press as: Kus, B., Nekså, P., Novel partial admission radial compressor for CO_2 applications, International Journal of Refrigeration (2013), http://dx.doi.org/10.1016/j.ijrefrig.2013.07.015

Table 1 – Important design parameters for centrifugal compressor stage.

Parameter	Unit	Value
Blade height	mm	1.81
Discharge blade angle	°	−45
Number of blades	–	15
Inlet blade angle at tip	°	62.3
Inlet blade angle at hub	°	26.7
Tip clearance	mm	0.25
Impeller diameter	mm	71.9
Inlet hub diameter	mm	7.3
Inlet shroud diameter	mm	27.5
Diffuser diameter	mm	129.5
Axial length of impeller	mm	38.8

An expected loss breakdown for a reference compressor designed for high operating pressure (80/113 bar), mass flow of 3.5 kg s^{-1} and inlet temperature of 320 K is depicted in Fig. 6.

The machine is expected to operate at the shaft speed of 40,000 rpm, being a trade-off between good aerodynamic efficiency and low non-stage losses. The issue of optimal specific speed for hermetic CO_2 compressor is commented in Kus and Nekså (2013b). The most important results of the design procedure are collected in Table 1.

The design can be compared against typical non-dimensional performance coefficients defined and calculated for the reference compressor in Table 2.

It can be concluded that the results of the non-dimensional analysis are rather consistent with the analytical prediction of stage efficiency. High Reynolds number, relatively low pressure ratio, moderate machine Mach number and not optimal but good values of specific speed and flow rate coefficient applicable for radial compressor allow expecting good performance of the stage.

It must be stated that while the expected stage efficiency is maintained at a rather high level, the overall efficiency of the machine is not satisfactory, especially when compared to state-of-the-art piston compressors used in CO_2 commercial refrigeration (Hafner et al. (2012)).

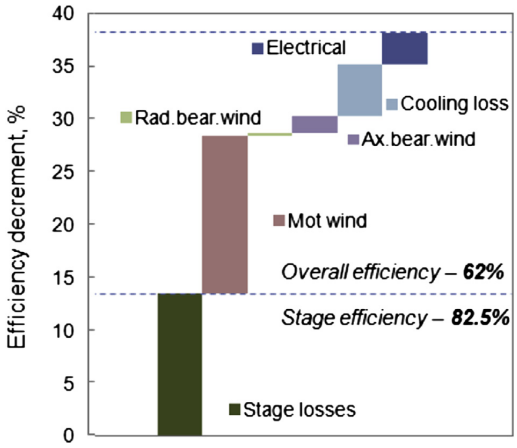

Fig. 6 – Predicted loss break-down for a state-of-the-art reference compressor designed for 80/113 operating pressure.

Table 2 – Non-dimensional coefficients characterizing centrifugal stage performance.

Coefficient	Formula	Value
Flow rate coefficient	$\varphi = \frac{Q}{U_2 d_2^2} \frac{4}{\pi} o$	0.025
Work coefficient	$\psi = \frac{\Delta h_{t-t}}{U_2^2}$	0.74
Machine Mach Number	$M_U = \frac{U_2}{a_{01}}$	0.68
Machine Reynolds Number	$\mathrm{Re} = \frac{U_2 D_2}{\nu_{01}}$	1.2e8
Specific speed	$N_s = \frac{\omega\sqrt{Q}}{\Delta h_{0ts}^{0.75}}$	0.4

The main loss source in the considered machine is the motor windage. It is to be expected as the high density of the gas (around 215 kg m^{-3} in the motor cavity) and high rotational speeds are the main contributors to high friction losses of a rotating cylinder, according to the Formula (1) developed by Vrancik (1968) and validated for a high speed CO_2 compressor (Wright et al., 2010).

$$P_{mw} = \pi C_f \rho R^4 \omega^3 L \tag{1}$$

where:

$$\frac{1}{\sqrt{C_f}} = 2.04 + 1.768 \ln\left(\mathrm{Re}\sqrt{C_f}\right) \tag{2}$$

To visualize impact of the shaft speed on the motor windage several motors where sized for the power required by the reference compressor and windage was calculated. Dimensions of the motors are calculated based on formula presented in Hanselman (2006).

$$2\sigma_m = \frac{\tau}{\frac{\pi}{4} D_{\mathrm{mot}}^2 L_{\mathrm{mot}}} \tag{3}$$

Assumptions about motor length/diameter ratio and gap sheer stress incorporated in this study (L/D = 3.7 and σ_m = 20.7 kPa) are made based on Hanselman (2006) and Wright et al. (2010).

Fig. 7 shows the windage exerted by the motors sized for the same rated power (73.7 kW) but different design speeds. It can be seen that the 4-fold reduction of rotational speed

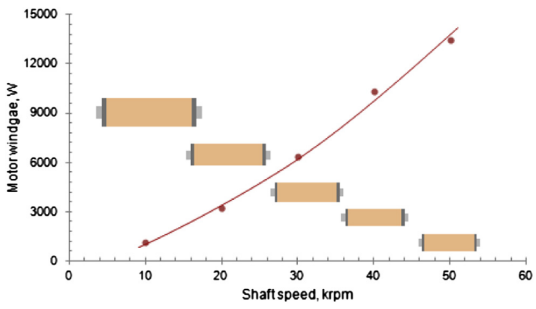

Fig. 7 – Windage losses and proportions of electric motors sized for the same rated power but different operating speeds.

Please cite this article in press as: Kus, B., Nekså, P., Novel partial admission radial compressor for CO_2 applications, International Journal of Refrigeration (2013), http://dx.doi.org/10.1016/j.ijrefrig.2013.07.015

results in around 90% reduction of the windage, despite 60% bigger dimensions of the motor.

It is therefore reasoned that if one was be able to maintain a reasonably high aerodynamic efficiency of the machine while significantly reducing operational speed then the overall performance of the CO_2 compressor could be improved. The partial admission radial compressor concept is introduced in an attempt to find out whether it could be possible.

3. The "partial admission radial compressor" concept

In Table 3 a summary of the challenges occurring with hermetic CO_2 oil-free compression are presented and two possible ways of tackling them are proposed. The two alternatives include a partial admission concept and application of a smaller, more slender motor. As mentioned, designing smaller motors with higher gap shear stress and therefore increased cooling demand involves necessary experimental work. Another approach could be to employ special rotordynamic strategies for longer more slender motors. Applicability of such a strategy will also have limited impact (Kus and Nekså (2013b)). Pursuing both approaches at once could give desirable effects. A detailed study of such an approach is however beyond limitations of the present work.

Instead, a strategy for development of a partial admission stage is pursued by performing a 2D CFD analysis, which could be made relatively rapid and inexpensive. The main question that the authors will try to answer in the present and the following papers is whether it is possible to maintain reasonable aerodynamic efficiency of a machine operating at significantly lower shaft speeds without significant increase in applicable flow rates.

The concept of a partially admitted radial compressor is shown in Fig. 8. In the presented version of the concept the flow is admitted through a 33° arc. The impeller has an outer diameter of 16 cm and consists of 200 blades of which 18 are active. The wheel rotates at 13000 revolutions per minute. The diffuser is not shown in the figure. The 3D design of the wheel is created by a simple extrusion of a 2D profile, hence initial modeling and optimization can be performed with help of 2D simulations. The flow is admitted in the radial direction. There is no turning of the flow from axial to radial direction across the impeller as it happens in centrifugal compressors. The static head created in the impeller is very low, as will be shown in a later section of this publication. Furthermore, the blades are much shorter than those in the centrifugal machine. It is therefore expected that axial loads generated by the wheel will be negligible, resulting in reduced windage and wear of the thrust bearing.

4. Numerical modeling

For all CFD calculations the finite volume method code ANSYS FLUENT 14.0 was used. Averaged Navier Stokes equations were solved, and turbulence was modeled using the k-ε model. As the standard k-ε ceases to be valid in the vicinity of walls the wall boundary layers were calculated using wall functions. A second-order discretization scheme was used for all simulations. Peng–Robinson equations are used to simulate thermodynamic properties of CO_2.

The calculation domain consisted of three zones: stationary inlet zone, rotating impeller zone and stationary outlet zone. The diffuser is not simulated in the present work.

4.1. *Boundary conditions*

There is one flow inlet and one flow outlet. For the inlet, a mass flow boundary condition was used with total temperature and static pressure specified. A pressure outlet boundary condition with a prescribed static pressure and backflow total temperature was used for the stage outlet. The turbulence intensity at the boundaries is expected to be high in fast rotating turbo-machinery. A value of 10% was assumed for the simulations.

5. Results and discussion

The whole analysis consisted of several steps. First, steady-state simulation of a 2-dimensional model fully bladed with 200 blades and 8 guiding vanes in the inlet section was conducted. Frozen rotor model was employed to preserve any circumferential non-uniformities occurring at the inlet and the

Table 3 – Comparison of a partial admission concept with a standard radial compressor. ● = Advantageous, ◐ = Moderate, ○ = Disadvantageous.

	Partial admission		Smaller/more slender motor	
Axial bearing windage	●	No or near zero axial thrust – axial bearing dimensions significantly reduced	○	Balancing significant axial forces remains a challenge
Motor windage	●	Greatly reduced	○	Moderate reduction
Aerodynamic efficiency/pressure ratio	○	Inherently lower efficiencies and pressure ratios	●	High stage efficiencies/pressure ratios
Bearing/seal technology	●	Lift-off seal more likely to be applied (non-hermetic work). Gas bearings still remain an option	○	Small and fast rotating shafts require hermetic operation and gas or magnetic bearings
Rapidity/Cost of initial development	●	Initial design and analysis possible with fairly rapid and inexpensive 2D CFD methods	◐	Rotordynamic strategies possible to analyze with theoretical methods. Cooling strategies involve 3D modeling/testing

Please cite this article in press as: Kus, B., Nekså, P., Novel partial admission radial compressor for CO_2 applications, International Journal of Refrigeration (2013), http://dx.doi.org/10.1016/j.ijrefrig.2013.07.015

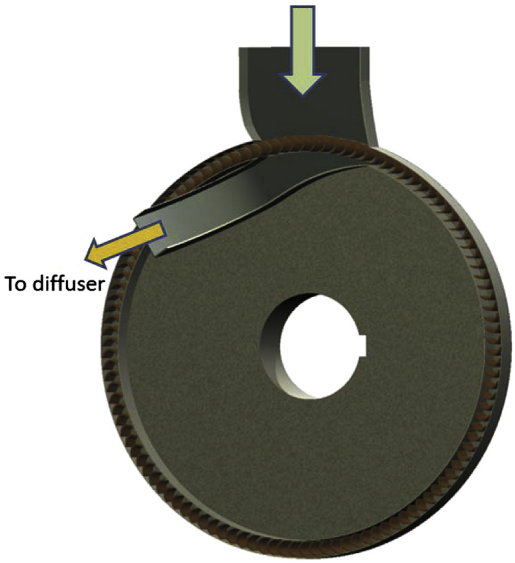

Fig. 8 – The concept of the partial admission CO_2 turbo-compressor.

outlet of the impeller wheel. The mesh developed in the first step was then used in a 2D transient simulation. Due to the time consuming nature of transient simulations only a single run was performed. To give the initial impression whether the performance of the compressor obtained from transient simulation could be maintained for other operating conditions, additional steady-state simulations were performed.

5.1. *Mesh development*

The mesh was developed for the boundary conditions summarized in Table 4. The same boundary conditions were used for the transient run.

The development of the mesh is presented in Table 5.

Steady state simulations were considered converged when solution residuals reached at least default values of absolute convergence criterion, amounting to 10e-6 for energy residual and 10e-3 for the remaining residuals and when further iterations did not bring visible changes to the monitored quantities. The history of residuals and important solution monitors for simulation of Mesh 6 are presented in Fig. 9.

Based on the mesh independence study Mesh nr 6 was accepted as one providing sufficient resolution and was used for the further simulations. Snapshots of the geometry and final mesh are depicted in Fig. 10.

Table 5 – Mesh independence study based on steady-state simulations.

	Mesh size, mln cells,	$\eta_{is\ (t\text{-}t)}$	Average y^+	P_{ratio}
Mesh 1	0.68	0.824	250	1.42
Mesh 2	0.76	0.825	136	1.42
Mesh 3	0.90	0.829	80	1.42
Mesh 4	0.85	0.826	200	1.42
Mesh 5	0.95	0.826	114	1.42
Mesh 6	1.22	0.830	115	1.42
Mesh 7	1.4	0.833	66	1.42

The standard k-ε model was used for the simulations as an industrial standard for turbulent flows. There are no visible flow disturbances in form of separation or recirculation at the discharge of the impeller, as shown in Fig. 12. On the other hand, the downstream region where the blades are entering the inactive sector can be viewed as rapidly straining the flow. Even if some degree of separation occurs here, the main part of the through flows appears to be unaffected. It is nevertheless important to know if the applied turbulence model overestimates the efficiency levels. To check this, three additional turbulence models that could be superior in terms of predicting complex phenomena present in turbomachinery were tested for the developed mesh. The additional models used are:

- k-ε Realizable model: recommended for problems characterized by boundary layers under strong adverse pressure gradients, separation, rotation, recirculation and strong streamline curvature
- k-ε RNG model: advised for cases with high streamline curvature and strain rate and transitional flows
- k-ω SST model: considered to effectively combine the ability to solve inner parts of the boundary layer as well predict the behavior in the free-stream. Often advised for the problems were adverse pressure gradients and separating flows are present

The performance predictions obtained using different turbulence models are presented in Table 6. All of the three models predict a few percent higher efficiency of the base part of the compressor than the standard k-ε model. Without experimental work it is difficult to give a definitive judgment about applicability of the models for the current case. Furthermore, the level of the solution residuals obtained for the k-ε RNG and k-ω SST are low compared to the k-ε Realizable and Standard k-ε models. This may indicate that to obtain more realistic results based on these models, further improvement of the mesh is required. For the current study the standard k-ε model will be used as the one giving the most

Table 4 – Simulation set-up used for mesh development.

Parameter	Inlet mass flow, kg s-1	Reference thickness of 2D profile, m	Outlet static pressure, bar	Inlet total temperature, K	Rotational speed, rpm
Value	180	1	40	330	13,000

Please cite this article in press as: Kus, B., Nekså, P., Novel partial admission radial compressor for CO_2 applications, International Journal of Refrigeration (2013), http://dx.doi.org/10.1016/j.ijrefrig.2013.07.015

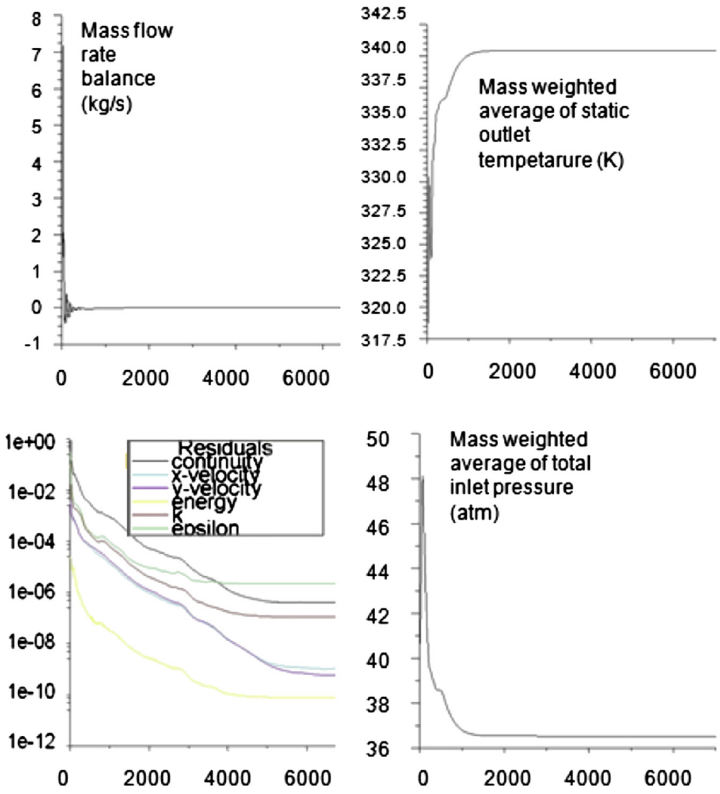

Fig. 9 – Convergence history of steady-state simulation for Mesh 6.

conservative prediction of the efficiency. It should be noted however, that turbulence modeling, in this special case, deserves more insight in future research.

5.2. *Steady state performance predictions*

The developed mesh was used to perform several more steady-state simulations for slightly different rotational speeds and various operating pressures. The predicted peak efficiencies together with corresponding pressure ratios and absolute discharge Mach numbers are presented in Table 7.

Based on the results presented in Table 7 one can expect that for optimized flow rates the proposed concept can achieve similar performance for different operating conditions and that pressure ratios higher than 1.4 could be achieved with reasonable efficiencies.

5.3. *Transient operation performance prediction*

Due to the inherently transient nature of the processes present in a partially admitted machine, dynamic simulation with a sliding mesh was run. The simulation run for 19,000 times steps representing twelve full revolutions of the wheel. The time step of 3e-6 s resulted in the 10 time steps passing period for one blade. For each time step a maximal of 20 iterations were performed, according to the recommendations of the software provider. After around 15 iterations all the residuals were reaching default absolute convergence criterion, amounting to 10e-6 for energy residual and 10e-3 for the remaining residuals. Hence, it was judged that the selected time step does not require further reduction. Typically, it is advised to reduce the time step instead of performing too much iteration during a single time step. Otherwise, one risks obtaining non-realistic transient behavior.

The history of important solution monitors is presented in Fig. 11.

The comparison of the velocity field obtained by steady state and transient simulations are presented in Fig. 12.

It can be observed that steady state simulation has limited ability to capture two important phenomena depicted in Fig. 12 within Zone A and Zone B. Zone A covers a region where the discharge of the fluid passing the blades is restricted by the collector wall. This restriction results in reduced fluid velocity compared to the main through flow (Zone C) and therefore reduced velocity at the inlet of the blades. The result is increased incidence losses but also dissipation of part of the energy transferred to the fluid into the cavity (marked with an arrow). In this region a combination of clearance and sudden expansion loss occurs. The

Please cite this article in press as: Kus, B., Nekså, P., Novel partial admission radial compressor for CO_2 applications, International Journal of Refrigeration (2013), http://dx.doi.org/10.1016/j.ijrefrig.2013.07.015

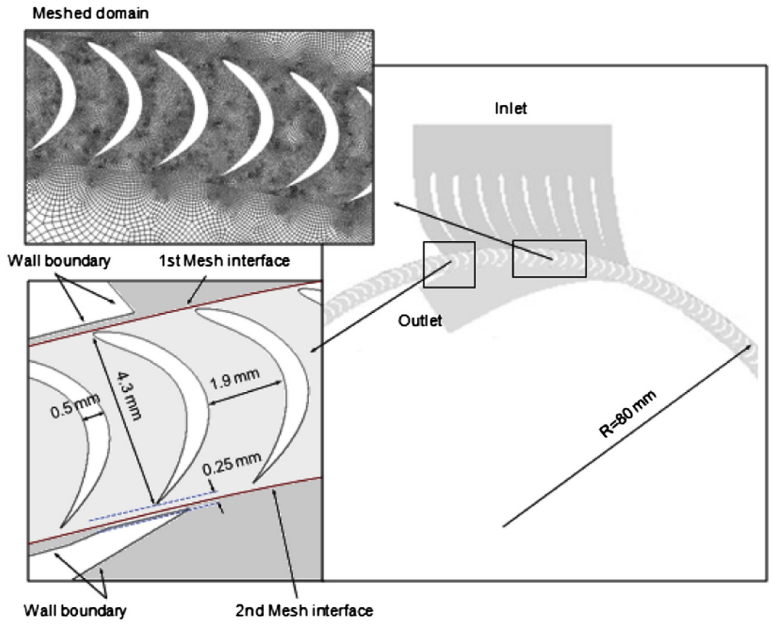

Fig. 10 – Two-dimensional geometry and mesh developed for steady-state and transient simulations.

increased incidence loss is also present in the Zone B where the impeller blades only starts transferring usable work to the incoming fluid. The mixing of the active and inactive gas results in the mixing losses. The impact of a sudden expansion and mixing losses can theoretically be limited by increasing admission ratio of the compressor or by applying shorter blades. The optimal size of the blade will likely depend on a necessary curvature that must be achieved across the blade relatively smoothly and mechanical and manufacturability limitations.

Increased admission rate must also be analyzed carefully for each case. Firstly, because the particles leaving each particular blade, due to the inward flow configuration, have conflicting flow paths. Hence, for a given impeller diameter increased admission will result in worse flow uniformity in the collector channel. In such a case, application of discharge vanes does not guarantee improved performance due to the additional friction and incidence losses resulting from high velocity discharge conditions. Secondly, for a given design flow rate increased admission arc must be followed by a lower extrusion of the 2D profile (blade height) and therefore higher impact of radial clearance and wall effects.

In the presently analyzed case, due to the already very short blades and reasonably high admission ratio the impact of transient effects resulted in a total efficiency reduction from 83 to 82.5% for steady state and transient run respectively. Accordingly, the total pressure ratio dropped from 1.42 to 1.38.

The more pronounced difference between steady state and dynamic simulation is visible in the prediction of the discharge velocity profile. Non uniform velocity profile presented in Fig. 10b is very undesirable phenomenon with regard to the efficient deceleration of the gas during the diffusion process. Furthermore, the diffuser channel must include a bent section required to direct the gas outside of the wheel. It is therefore anticipated that the proper design of the diffuser will be of critical importance to the high overall stage efficiency of the presented concept. The static pressure field presented for the transient simulation in Fig. 13 visualizes the importance of the diffusion process. The static head produced

Table 6 – Steady-state performance prediction employing different turbulence models.

Turbulence model	$\eta_{is\ (t\text{-}t)}$	P_{ratio}	Continuity residual
k-ε Realizable	0.857	1.43	8e-08
k-ε RNG	0.875	1.44	1e-03
k-ω SST	0.863	1.44	3e-03

Table 7 – 2D Steady-state simulations. No diffuser included.

Inlet conditions				Results		
P_{in}, bar	T_{in}, K	rpm	Mass flow, kg s^{-1}	P_{ratio}, –	$\eta_{is(t\text{-}t)}$, %	M_{02}, –
38.6	330	13,000	210	1.44	83.3	0.73
38.6	330	15,000	242	1.61	82.7	0.85
76.6	340	13,000	458	1.50	83.9	0.67
73.7	340	14,000	458	1.58	83.5	0.69

Please cite this article in press as: Kus, B., Nekså, P., Novel partial admission radial compressor for CO_2 applications, International Journal of Refrigeration (2013), http://dx.doi.org/10.1016/j.ijrefrig.2013.07.015

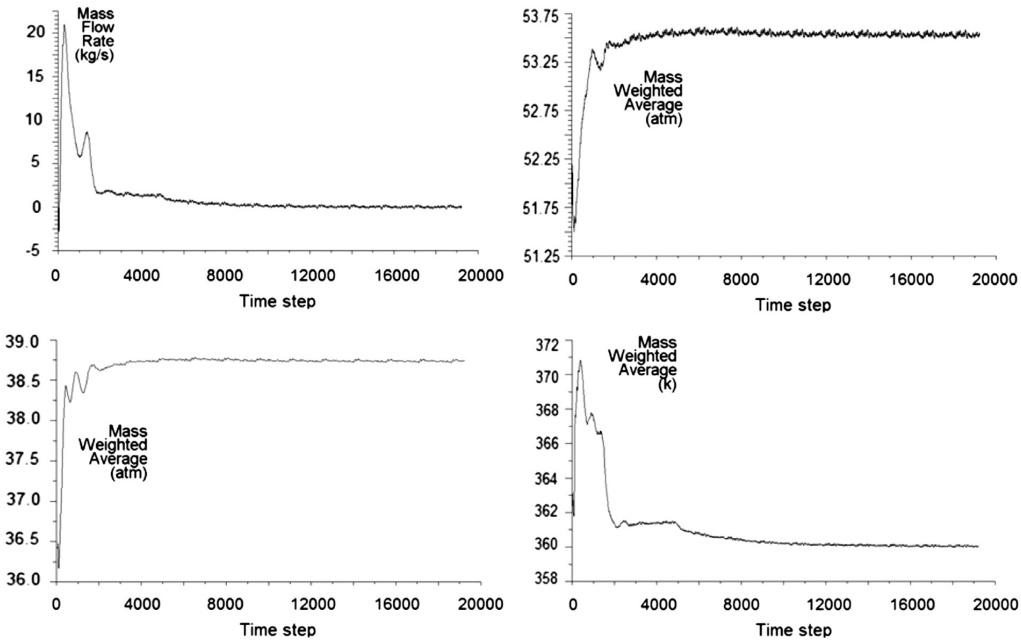

Fig. 11 – Main monitors' history of the transient simulation.

across impeller is minimal; it is in the diffuser where the main part of the kinetic energy must be converted to static pressure.

5.4. *Impact of a blade shape*

The presented transient simulation was run for a particular number and shape of the blades. A further study has shown that efficiency of the blade and therefore efficiency of the machine could be improved. Due to the time consuming nature of transient simulations for a complete geometry, a few additional blade configurations were examined with respect to their maximum performance at the rotational speed of 13,000 rpm. Steady-state simulations of the fully admitted wheel were performed. A frozen rotor approach with periodic boundary of 7.2° was utilized in order to reduce computational effort. An example of a meshed domain depicting the reference blades (used in transient simulation run) is presented in Fig. 14.

In Table 8 the impact of the shape and number of blades on the maximum wheel efficiency is presented. Alternative blade shapes with velocity triangles are depicted in Fig. 15. The direction of the flow, inlet and discharge angles and the radial span of analyzed blades remain the same as in the base geometry used for transient simulation. It is shown that increasing number of the reference blades from 200 to 250 will improve the wheel efficiency by around 1%. Application of droplet-like blade (Blade B) will reduce the wheel efficiency but also the flow rate for which the wheel achieves optimal performance. The reduced peak efficiency can be attributed to the increased blockage at the leading edge of the blade and less smooth through flow compared to the reference blade. The best peak performance among analyzed blades was achieved for the Blade C. It achieves 2.3% higher efficiency than the reference blade, both in 200 blades configuration. It can likely be attributed to the lowest curvature of the though flow for this blade and sharp leading edge resulting in low blockage. Furthermore, Blade C due to its thickness is expected to achieve higher stiffness that could prove to be critical in a further mechanical design process.

5.5. *Initial structural analysis of the blade*

The presented shapes of the blades have very small dimensions. This can lead to challenges both in terms of manufacturability and ability to withstand the loads. The present paper aims primarily at the introducing of the novel concept. The full scope of structural analysis deserves proper amount of space in a separate publication. Nevertheless, it is important to give the first impression about possible challenges. A simple static analysis of the safety factor of a blade mounted on a rotating disc was conducted with the help of Ansys Structural 13 software. Blade C was chosen for the simulation. The height of the blade is set to 7 mm. The disc has 16 cm diameter and rotates at 14,000 rpm. Pressure loads of 0.5 and 1 MPa were applied to the pressure side of the blade to simulate the pressure difference generated on both sides of the blade during compressor operation. Judging from Fig. 13 such pressure loads are maximal for the analyzed blades and during flow conditions occur only locally along the blade span. It is therefore expected that assumptions made for the structural

Please cite this article in press as: Kus, B., Nekså, P., Novel partial admission radial compressor for CO_2 applications, International Journal of Refrigeration (2013), http://dx.doi.org/10.1016/j.ijrefrig.2013.07.015

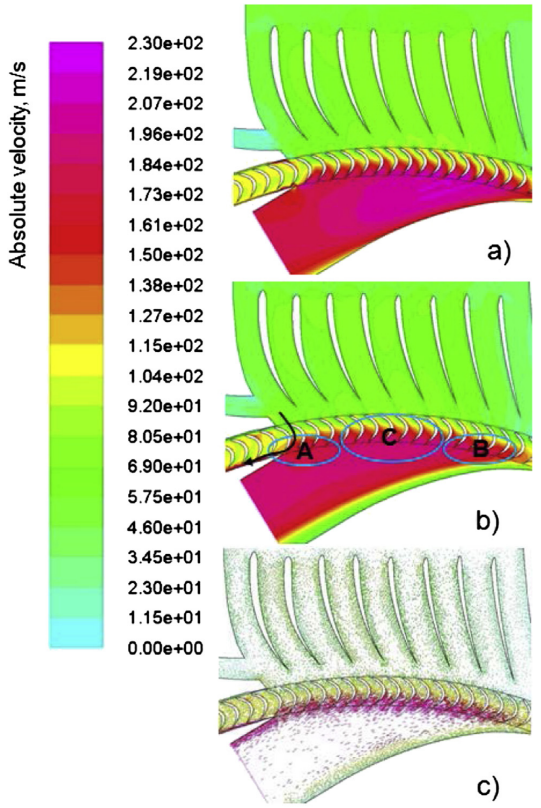

Fig. 12 – Steady state (a) and transient (b, c) prediction of velocity field and velocity vectors.

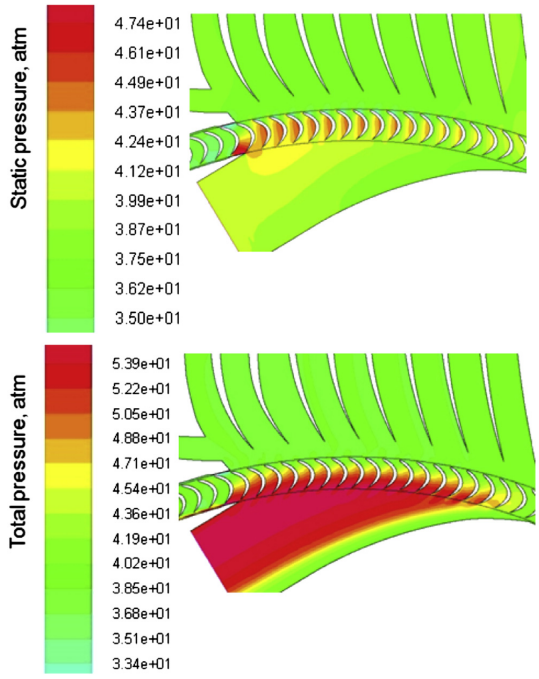

Fig. 13 – Pressure fields obtained by transient CFD analysis.

analysis pose more demanding conditions for the blade than would occur during compressor operation. The prediction of safety factors for the analyzed blade is shown in Figs. 16 and 17. In Fig. 17 the 7 mm blade is set on a 3 mm slightly thicker base that is expected to partially relieve the pumping part of the blade. It is further assumed that the base part of the blade could be covered by attaching an additional plate to the disc while exposing only active parts of the blade. The analysis of safety factors indicate that the proposed size of the blade may require using very strong and more expensive materials. Depending on factual loads acting on a blade and taking into account other factors such as vibration and potential fatigue resulting from cyclic operation, some further blade modifications may be necessary, and one should realize that aerodynamic performance may also be affected. It is also expected that the small size of the blades and the small distances between them may require electrochemical machining, especially when difficult-to-machine alloys will be used.

5.6. *Stage efficiency estimation*

To specify the overall stage performance the total pressure loss coefficient of the diffuser must be known. The initial study of the diffuser/return channel that may be applicable for current design was conducted and will be presented in Kus and Nekså (2013c). According to the study, the diffuser/return channel assembly achieving the best performance for the inlet conditions approximating those at the discharge of the

Fig. 14 – The meshed domain of 1/50 of the full wheel depicting the reference blade shape.

Please cite this article in press as: Kus, B., Nekså, P., Novel partial admission radial compressor for CO_2 applications, International Journal of Refrigeration (2013), http://dx.doi.org/10.1016/j.ijrefrig.2013.07.015

Table 8 – Impact of the shape and number of blades on the attainable wheel efficiency.

Blade shape/nr of blades	$\eta_{t\text{-}t}$	P_{ratio}	Q/Q_{ref}
Blade A, 200 bl	89.0	1.45	1
Blade A, 150 bl	84.6	1.41	1
Blade A, 250 bl	90.0	1.41	0.78
Blade B, 200 bl	82.6	1.36	0.75
Blade C, 200 bl	91.3	1.47	1

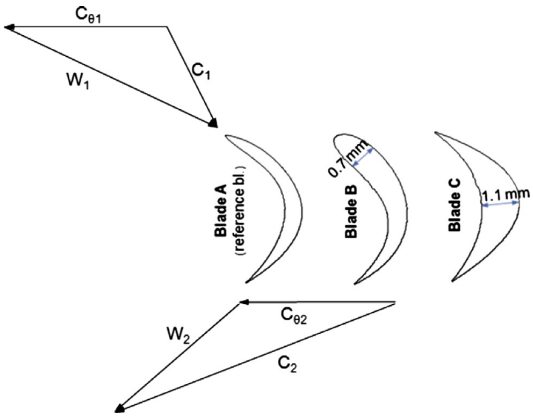

Fig. 15 – Alternative blade shapes and velocity triangles.

presently analyzed transient case is characterized by pressure recovery coefficient of 0.82 and a total pressure loss coefficient of 0.13. The authors believe that there is a potential for further improvement of the diffuser performance provided that the discharge of the gas from the wheel is more radial. Fig. 18 is showing what final stage efficiency can be expected when the base stage efficiency and total pressure loss coefficient of the diffusers are known. When, for example, 82.5% base efficiency is combined with 0.13 total pressure loss coefficients of the diffuser/return channel, then around 74% stage efficiency can be expected. In reality, further reduction of this value may occur due to the 3D effects in the base part of the machine. These may include: wall effects, radial clearance leakage and interaction of the diffuser with the blade through flow.

5.7. *Overall efficiency prediction*

An attempt to predict the overall efficiency of the novel compressor and compare it with a centrifugal machine is made. It must be emphasized that to give more accurate prediction of partial admission stage efficiency, at least 3D dynamic CFD simulations of a full wheel with the radial clearance and the diffuser and preferably prototype testing should be made. Such scope of the work unfortunately exceeds limitations of the present project.

Despite the limitations of the present study, predicting the non-stage losses of the novel compressor and comparing overall loss breakdown of both concepts is believed to be of interest.

For estimation of both concepts' overall performance the tool presented in detail and validated in Kus and Nekså (2013a) is used. The 1D tool developed for radial compressor concept must be provided with a stage efficiency of the novel compressor in order to predict its overall efficiency. The non-stage losses for both concepts can be calculated in the same manner.

To commence a 1D overall performance prediction of the new concept a new value of 75% total stage efficiency is now assumed. This efficiency is further expected to drop for compressors designed for reduced flow rates. At this stage of

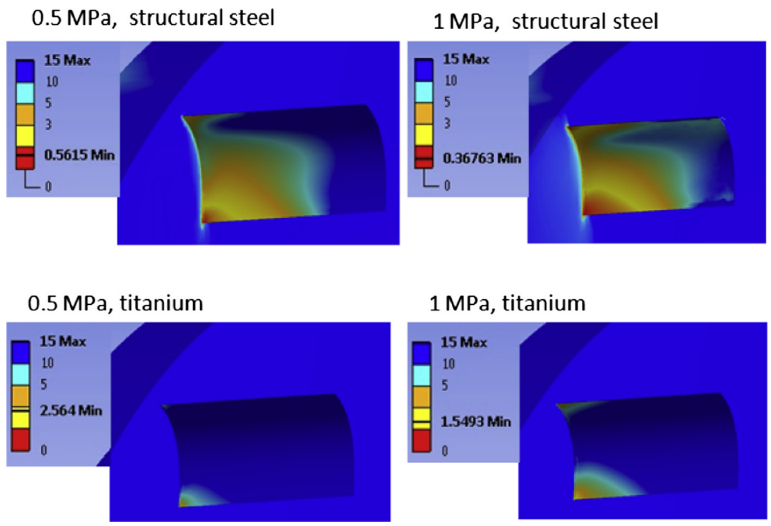

Fig. 16 – Structural analysis of the 7 mm blade mounted on a rotating disc under different pressure loads applied to the suction side of the blade.

Please cite this article in press as: Kus, B., Nekså, P., Novel partial admission radial compressor for CO_2 applications, International Journal of Refrigeration (2013), http://dx.doi.org/10.1016/j.ijrefrig.2013.07.015

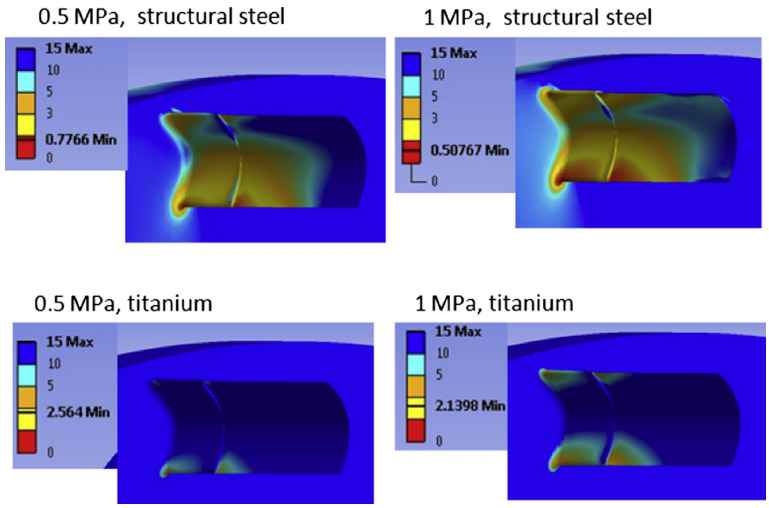

Fig. 17 – Structural analysis of the 7 mm blade with 3 mm base mounted on a rotating disc under different pressure loads applied to the suction side of the blade.

the analysis radial clearance is not taken into account, but this issue deserves future considerations. 3D CFD steady state simulations were performed for different geometries created by simple extrusion of 2D profile to roughly assess impact of the wall friction on the compressor efficiency. To reduce the computational effort a periodic boundary was applied and only 1/6 of the wheel was simulated.

From Fig. 19 it can be seen that for a given 2D design the basic stage efficiency starts to drop significantly for the design flow rates lower than 0.02 $m^3 s^{-1}$. Such a flow rate corresponds to around 30 kW of the stage compression power for the compression conditions used in the transient simulation run. The impact of wall effects must be incorporated into the 1D model in order to evaluate performance of the partial admission compressor for various flow rates. Also the disc friction which is not accounted for in the CFD prediction is taken into account. The remaining losses common for both concepts are included as well:

- Electrical loss in the motor
- Cooling loss
- Motor windage
- Bearing windage

The calculation of the above losses incorporates default settings of the 1D tool presented in Kus and Neksa (2013a and b). The assumed axial loads amount to 200 N and 1000 N for a novel and reference compressor respectively. 1D predictions

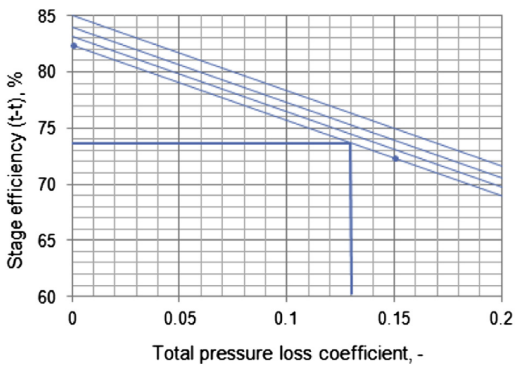

Fig. 18 – Stage efficiency vs total pressure loss coefficient in the diffuser.

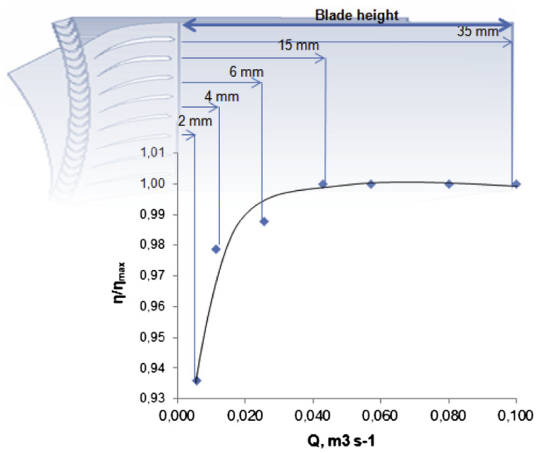

Fig. 19 – Predicted impact of wall effects on the performance of a partial admission compressor depending on a blade height.

Please cite this article in press as: Kus, B., Nekså, P., Novel partial admission radial compressor for CO_2 applications, International Journal of Refrigeration (2013), http://dx.doi.org/10.1016/j.ijrefrig.2013.07.015

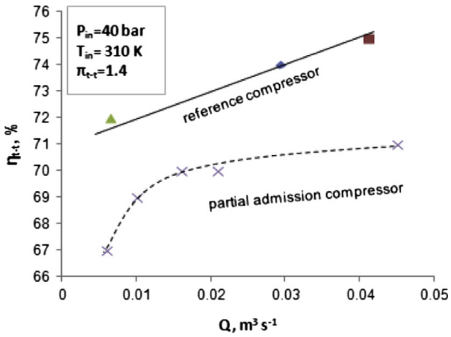

Fig. 20 – Prediction of overall peak efficiencies for two compressor concepts designed for different flow rates.

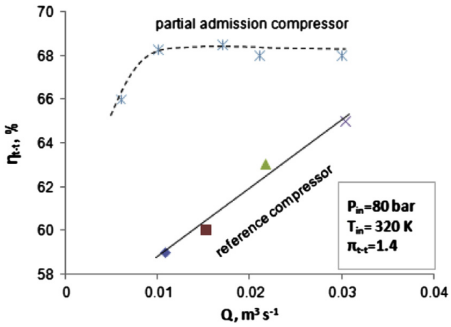

Fig. 21 – Prediction of overall peak efficiencies for two compressor concepts designed for different flow rates.

of overall efficiencies for both compressor concepts are presented for different operating conditions in Figs. 20 and 21. Estimation of loss break-down for the partial admission compressor operating at conditions equivalent to those of the reference compressor is presented in Fig. 22 for different stage efficiencies.

The overall performance predictions allow presuming that the partial admission concept can be an interesting option especially for the applications where operating pressure is high and flow rates moderate, i.e. supercritical CO_2 commercial applications. In such cases lower stage efficiency of the partial admission concept can be accepted due to the significantly reduced non-stage losses, such as windage and internal cooling. In cases where operating pressures are low to moderate, high aerodynamic performance of a traditional radial compressor and moderate non-stage losses will favor a conventional radial compressor concept over a partially admitted machine.

6. Conclusions

A novel partial admission concept of an oil-free turbocompressor for CO_2 applications is presented as an alternative to high speed centrifugal machines. The main advantage over state-of-the-art centrifugal compressor is significant reduction of the non-stage losses typically triggered by the elements of the compressor rotating at high speeds in a dense gas. Greatly reduced shaft speeds enable the designer to consider more typical variants of bearings, namely oil or grease lubricated bearings in conjunction with shaft sealed with dry gas seals.

It is generally known that partial admission machines are aerodynamically less efficient then their fully admitted counterparts. However results of CFD simulations of the proposed concept are reasonably optimistic when it comes to the stage efficiency. The transient 2D simulation performed for the base geometry showed around 82.5% isentropic efficiency for a stage achieving 1.38 total pressure ratio. This efficiency is predicted for the main part of the compressor including an inlet vanes row, the impeller wheel and the outlet collector. Depending on the 3D depth the profile (blade height), a drop in the base efficiency caused by the wall effects and other 3D effects can be expected. These aspects should be analyzed more extensively in future research. It is predicted that a more pronounced drop in efficiency occurs for blade heights of less than 5 mm. It accounts for volumetric flow rates of less than

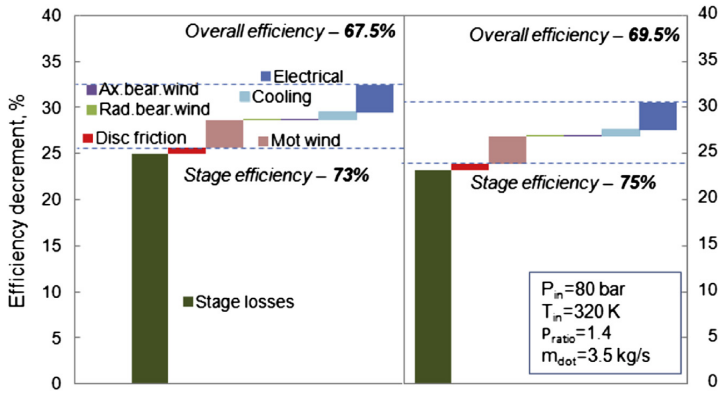

Fig. 22 – Predicted loss breakdown for partial admission compressor with different stage efficiencies.

Please cite this article in press as: Kus, B., Nekså, P., Novel partial admission radial compressor for CO_2 applications, International Journal of Refrigeration (2013), http://dx.doi.org/10.1016/j.ijrefrig.2013.07.015

0.02 $m^3\ s^{-1}$ corresponding to cooling capacity of around 500 kW at 60 bar. Applicability of the proposed concept may also be limited for significantly higher flow rates where stiffness of the long blades can become an issue. Further reduction of the base efficiency will also occur in the diffuser. The diffuser design will be covered in later publications.

Achieved efficiencies cannot be regarded as what optimally can be achievable for the partial admission concept, but hopefully they give a first reasonable approximation. Presented geometry cannot be regarded as the optimal one either. It is shown that optimization of the blade shape and number of blades should improve the base efficiency of the concept.

It is viewed that achieved CFD results and estimates of total efficiency are reasonably optimistic and will be used as a starting point for the design of the diffuser. The diffuser will have deciding impact on the final stage efficiency, and therefore more attention will be devoted to its design in a separate publication. It should also be noted that presented work does not take into account radial leakage that will be present in the partial admission compressor. This leakage however may be of particular significance especially at lower flow rates. To gain more confidence in the presented CFD and in 1D predictions study an experimental work will be necessary.

Acknowledgments

This publication forms a part of the CREATIV project, performed under the strategic Norwegian research program RENERGI. The authors acknowledge the partners: SINTEF Energy Research, Danfoss, FHL, Hydro Aluminium, John Bean Technology, Norske Skog, REMA1000, Systemair, TINE, and the Research Council of Norway (195182/S60) for their support. The authors would like to thank Barber-Nichols Inc. for the valuable comments to the present work.

Nomenclature

a (m s^{-1})	speed of sound
C_f (–)	skin friction coefficient
d (m)	diameter
Δh (J)	enthalpy difference
L (m)	length
M (–)	Mach number
m_{dot} (kg s^{-1})	mass flow
P_{ratio} (–)	pressure ratio
Q ($m^3\ s^{-1}$)	volumetric flow rate
R (m)	radius
U (m s^{-1})	blade tip speed
Y^+ (–)	dimensionless wall distance
η (–)	efficiency
ω (rad s^{-1})	rotational speed
ν ($m^2\ s^{-1}$)	kinematic viscosity
σ_m (Pa)	the motor air gap shear stress
τ (N m)	torque

Subscripts

01	absolute discharge conditions at the inlet
2	impeller discharge
02	absolute discharge conditions at the discharge
is	isentropic
t–t	total/total

REFERENCES

Balje, O.E., 1981. Turbomachines. A Guide to Design, Selection and Theory. John Wiley & Sons.

Dang, T.Q., Bushnell, P.R., 2009. Aerodynamics of cross flow fans and their application to aircraft propulsion and flow control. Prog. Aerospace Sci. 45, 1–29.

Eck, B., 1962. Ventilatoren. Springer–Verlag.

Hafner, A., Nekså, P., Rekstad, H., 2012. High efficient 100kW shaft power R744 compressor. In: 10th IIR Gustav Lorentzen Conference on Natural Refrigerants (June 2012) in Delft, the Netherlands.

Hanselman, 2006. Brushless Permanent Magnet Motor Design, second ed. Magna Physics Publishing.

IIR, 2010. Statement given by Didier Coulomb, Director of the International Institute of refrigeration. In: United Nations Climate Change Conference, Cancun, Mexico, November 29–December 10, 2010.

Kus, B., Nekså, P., 2013a. Development of one-dimensional model for initial design and evaluation of oil-free CO_2 turbo-compressor. Int. J. Refrigeration, (in press).

Kus, B., Nekså, P., 2013b. Oil-free turbo-compressors for CO_2 refrigeration applications. Int. J. Refrigeration 36 (5), 1576–1583.

Kus, B., Nekså, P., 2013c. Numerical study of diffuser systems for a novel partial admission compressor using CO_2 as refrigerant. Int. J. Refrigeration (Submitted to).

Sakai, N., Harada, T., Imai, Y., 2006. Numerical study of partial admission stages in steam turbine. JSME Int. Journal. Ser. B 49 (2).

Schiffmann, J., Favrat, D., 2009. Experimental investigation of a direct driven radial compressor for domestic heat pumps. Int. J. Refrigeration 32, 1918–1928.

Schiffmann, J., Favrat, D., 2010. Design, experimental investigation and multi-objective optimization of a small-scale radial compressor for heat pump applications. Energy 35 (8), 436–450.

Van Lee, N., 1961. Partial Flow Centrifugal Compressors. ASME Paper No. 61-WA-135.

Vrancik, J.E., 1968. Prediction of Windage Power Loss in Alternators. NASA Technical Note D-4849.

Wright, S.A., Radel, R.F., Vernon, M.E., Rochau, G.E., Pickard, P.S., 2010. Operation and Analysis of a Supercritical CO_2 Brayton Cycle. Sandia Report SAND2010-0171.

Yahya, S.M., 1969. Aerodynamic losses in partial admission turbines. Int. J. Mech. Sci. 11, 417–431. Pergamon Press 1969.

Please cite this article in press as: Kus, B., Nekså, P., Novel partial admission radial compressor for CO_2 applications, International Journal of Refrigeration (2013), http://dx.doi.org/10.1016/j.ijrefrig.2013.07.015

Paper IV

Corresponding author: Tel.: +47 735 937 48; fax: + 47 735 953 10.

Numerical study of diffuser systems for a novel partial admission compressor using CO_2 as refrigerant

Bartosz Kus(a) and Petter Nekså(b)

(a) Norwegian University of Science and Technology

7491 Trondheim, Norway

Bartosz.Kus@ntnu.no

(b) Norwegian University of Science and Technology

7491 Trondheim, Norway

Petter.Neksa@sintef.no

Abstract

A numerical study of a diffuser system for a novel turbo-compressor for commercial CO_2 applications is presented. Geometries with the bent section have been analyzed for a dense high velocity gas with regard to pressure recovery and total pressure loss coefficients.

The best performance was achieved for a circular 3.9 area ratio system achieving total pressure loss and pressure recovery coefficients of 0.13 and 0.82 respectively. Redesign of the impeller discharge should improve this number quite significantly. Application of a 3% pinch reduced the performance of the rectangular assembly. Poorer performance is attributed to the higher friction losses in the initial section of the diffuser channel.

Modifications to the concept design might include: more radial gas discharge from the impeller followed by a smoother curvature of the diffuser and a combination of rectangular type of the diffuser with a square or circular cross section of the return channel.

Keywords

Novel partial admission compressor, Curved diffuser, Oil-free compressors, carbon dioxide

Introduction

In Kus and Nekså (2013c) a novel partial admission radial compressor concept was proposed as a potential solution to tackle an issue of high non-stage losses typically expected in high speed hermetic type radial compressor for commercial CO_2 applications [Kus and Nekså (2013a, b), Wright et. al. (2010)]. The reduction of non-stage losses is expected to be achieved through operation at significantly lower shaft speeds. To ensure high overall efficiency of the new compressor, a reasonable aerodynamic performance of the partial admission stage must be obtained. Numerical investigation of the new compressor wheel with only partial admission provided quite optimistic results. According to the previous studies, a properly designed diffuser will be of critical importance for the overall stage efficiency. In the proposed design, the factors impeding optimal diffusion process include non-uniform impeller discharge velocity profile, close to sonic velocities and a curved shape of the diffuser channel.

It is known that that the velocity profile at the exit of a curved diffuser is non-uniform. This combined with the non-uniform inlet velocity profile makes it reasonable to expect strong pressure fluctuation along the diffuser channel resulting in asymmetric flow separation and significant losses.

The work of Simonsen and Krogstad (2004) describes the flow in an axial to radial bend-diffuser configuration that can be used as a pressure recovery device behind axial compressors when axial space is limited. The analyzed gas is air at 3.3e4 – 8e4 Reynolds numbers. The numerical procedure employs different standard turbulence models and is carried out with the FLUENT code. Predictions of static pressure, time-mean velocity and skin friction are compared against experimental data. It is observed that k–e_{RNG} and k–e_{REALZ} models are in better agreement with the experimental data than the other models. The turbulence k–e_{STD} model delivered erroneous profiles indicating that the peak of the velocity profile was located at the opposite side of the channel compared to the experimental results. The discrepancy between predictions of the pressure recovery coefficients and test data were within 5% for the simulated cases, while the realizable k–e_{REAL} model predicted the mean velocity best among the models. Despite the relatively simple geometry, the complex flow physics due to the combination of the flow curvature and adverse pressure gradients, are emphasized.

El-Askary and Nasr (2009) conducted numerical and experimental investigation of a combined bend-diffuser configuration with a rectangular cross section. The analyzed fluid is air at Reynolds number between 8.8e4 – 1.94e5. The simulation is performed using the high-Reynolds number k–e turbulence model improved by the low-Reynolds number k–e turbulence model near the walls, to improve prediction of the flow with strong adverse pressure gradient. The authors report that the numerical method provides satisfying reproduction of the essential features of upstream curved flow effect on the diffuser performance. The results indicate that there is an optimum diffuser angle that produces a minimum pressure loss in the diffuser system which depends on the inflow Reynolds number. In El-Askary and Balabel (2007) it is also reported that the standard k–e model fails to predict the near-wall flow behavior when strong pressure gradients are present.

A common example of a curved diffuser is the S-shaped diffuser typically found in aircraft applications where a small machinery footprint is an important design requirement. Gopaliya et al. (2007) numerically investigated the effect of offset on an S-shaped diffuser of 90°/90° turn with rectangular inlet and semicircular outlet. The results obtained with a numerical procedure employing standard k–e turbulence model have not been verified against experimental data, however the authors claim that the model has been validated for similar geometry with the measurements presented in Anand et al. (2001).

The technique known to improve efficiency of a centrifugal compressor is application of a converging (pinched) wall at the initial section of the diffuser. The pinch aims at smoothing the flow field non-uniformities transferred from the impeller and therefore improving deceleration process in the diffuser. Turunen-Saaresti et al. (2006) compared numerical simulations with experimental data obtained for radial compressor equipped with six different diffusers (pinch of up to 10% of original height). Both measurements and numerical simulations showed that the pinched diffuser improved the efficiency of

the centrifugal compressor. It is also reported that the pressure ratio was fairly well predicted by the model, whereas the isentropic efficiency was over-predicted. The numerical model failed to provide close match with the test data in terms of span-wise distribution of the total pressure and flow angle at the diffuser inlet. Ludtke (1983) reported that application of pinch ratios higher than 10% becomes ineffective.

The efficiency and the proper functioning of a curved diffuser system depend on many factors. These include the diffuser angle, area ratio, degree of curvature, spacer length between the bend and the diffuser and Reynolds number. The present study undertakes numerical procedure to give initial estimation of the performance and flow behavior in the diffuser and return channel of a novel partial admission CO_2 compressor.

Numerical modeling

Geometrical parameters

The simulated cases can be divided into two main groups: systems with rectangular outlet and systems with circular outlet, see Fig 1. For the sake of convenience they will be further referred to as rectangular and circular systems respectively. All the diffusers have the same curvature resulting from an attempt to provide minimum degree of turning for the gas leaving the compressor wheel. All the diffusers are preceded by the 64 mm straight segment equipped in two mass flow inlets. Its purpose is to provide a non-uniform velocity profile at the inlet (In) of the diffuser. Creating such a profile is necessary to approximate the flow field present at the discharge of the partial admission compressor wheel. In order to compare the geometries, the inlet area and the inlet conditions are fixed. In case of a rectangular diffuser the geometries are created by two sweeps of the inlet geometry. The 1st sweep is identical and provides maximal area ratio for a given geometry of the wheel and discharge collector [see Kus and Nekså (2013c) for reference]. The second segment of the diffuser (outside the wheel) is varied with respect to length and area ratio (A_{Out}/A_{In}). The expansion of the rectangular diffuser area is carried out only in the vertical direction in an attempt to minimize negative impact of curvature on the diffusion process. Thanks to the smoother area expansion in the circular diffuser, the creation sweep was conducted in one step, without conflicting with the wheel geometry, see also Fig 2. Non-dimensional length is introduced to describe the length of the diffusers. It is defined as:

$$LWR = L / h \tag{1}$$

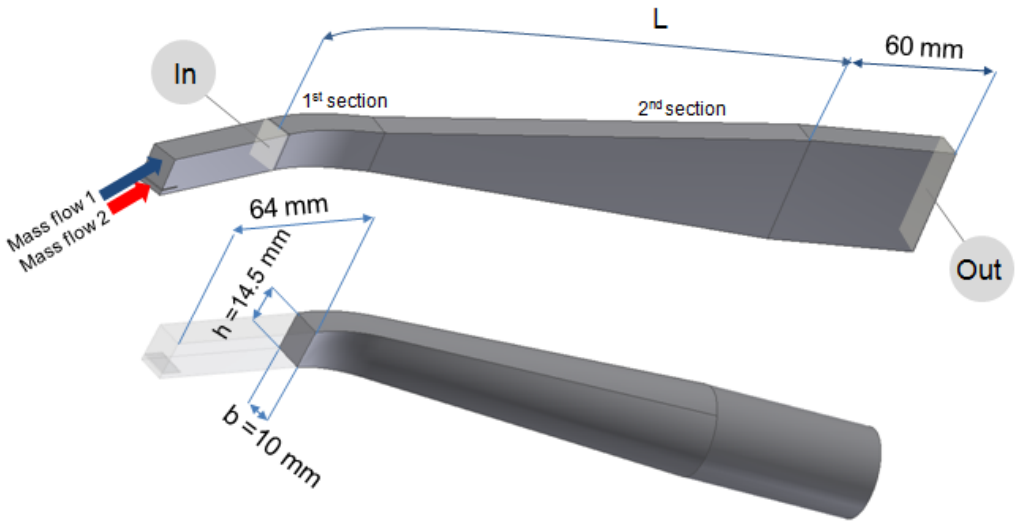

Figure 1. Two diffuser types (with rectangular and circular outlet) simulated in the study

Performance parameters

The overall performance of the diffusers is evaluated using the static pressure recovery coefficient and the total pressure loss coefficient. The static pressure recovery coefficient defined as

$$C_p = \frac{p_{out} - p_{in}}{p_{in\_t} - p_{in}} \tag{2}$$

describes how efficiently the kinetic energy captured in moving fluid is transformed into a static pressure increment. This non-dimensional parameter can be especially useful when single stage compressors are compared and when highest possible static pressure at the outlet is the design target.

During design of the multistage compressor the total pressure loss coefficient or simply total pressure loss between stages describe how well the diffuser/return channel system is designed. The total pressure loss coefficient is defined as follows.

$$K_p = \frac{p_{in\_t} - p_{out\_t}}{p_{in\_t} - p_{in}} \tag{3}$$

In the present study the main emphasize is put on the design of an efficient connection between two compression stages. This is why the simulations are repeated with return channels included for the best diffusers with their respective specific shape and area ratios. How to connect two or more stages of the novel compressor is in itself a rather complex issue, involving a rotorydnamics analysis. The present study does not attempt to analyze all possible solutions, but rather tries to give an initial estimation of the pressure drop that we may face in the novel concept diffuser. Knowing the expected total pressure loss coefficient in the diffuser/return channel one may estimate total efficiency of the novel

compressor stage based on the data presented in Kus and Nekså (2013c). Figure 2 illustrate how the diffuser proceeded with an axial mixing section relates to the original compressor geometry.

Figure 2. Novel partial admission compressor configuration

Computational method

For all the calculations the finite volume method code ANSYS FLUENT 13.0 was used. Averaged Navier Stokes equations were solved, and turbulence was modeled using the k-ε_{REALZ} model. As the model ceases to be valid in the vicinity of walls the wall boundary layers were solved using wall functions. A second-order discretization scheme was used for all simulations. The Peng-Robinson equation of state was used to calculate thermodynamic properties of CO_2.

As mentioned there are two mass flow inlets and one pressure outlet for each of the geometries. The static pressure outlet boundary was adjusted for in each case to obtain a mean inlet velocity of 188 m/s (+/- 7%).The approximate velocity distribution at the diffuser inlet is shown in Fig 3. The total pressure at the inlet of the diffuser was approximately 51 bar.

The mesh generation was conducted with the default Ansys meshing tool to produce structured elements with inflation at the walls to fulfill y^+ requirement of the turbulence model by utilizing standard wall functions. The mean y^+ for all simulations ranged from 60 to 134.

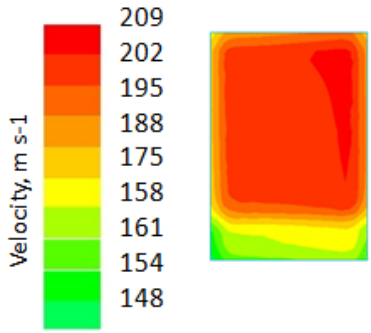

Figure 3. Approximate velocity distribution at the inlet of the diffusers

Results and discussion

Mesh dependency check

It is known that numerical results depend of the resolution of the domain mesh. The solution can be accepted as grid-independent when further refinements of the grid do not bring further variations of the solution. By further variations one should understand changes exceeding some reasonable tolerance assumed by the designer. The mesh dependency check was conducted only for a single geometry, the one with highest area expansion in vertical direction, due to the significant number of geometries tested. The variations of the most important parameters showing the performance of the diffuser depending on the resolution of the mesh are presented in the Fig 4. The sizing variants used for meshing the geometry are collected in the Table 1.

Table 1. Sizing controls used for meshing the geometry.

Sizing variant	Face sizing, mm	Sweep element size, mm	Mesh size, mln cells
A	0.7	0.9	0.31
B	0.5	0.8	0.53
C	0.4	0.8	0.62
D	0.3	0.8	1.06
E	0.2	0.8	1.77
F	0.2	0.6	2.34

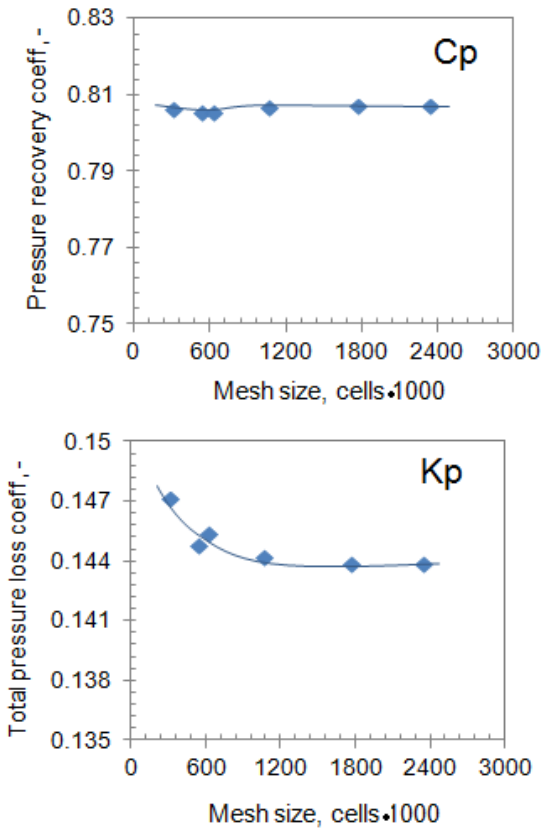

Figure 4. Total pressure loss- and pressure recovery coefficient variation with number of mesh cells

Based on the mesh independence study it was decided that sizing variant D provides sufficient mesh resolution and will be used for sizing of the remaining geometries.

Diffuser comparison

The simulation campaign consisted of several steps. Firstly, two types of diffusers, with rectangular and circular outlet, with varying lengths and area ratios have been simulated. In this step, 18 geometries have been simulated. As mentioned, the boundary conditions at the inlet of the diffuser were obtained by mixing two streams moving at different speeds. As a result, a non-uniform inlet profile was induced. In the second step, for each diffuser area ratio the geometries with the best total pressure loss coefficients were supplemented with the return channel to simulate performance of the system when a multistage compressor is considered. Finally, the third step of the analysis considers application of 3% of pinch to the one selected geometry of the rectangular diffuser. The predictions of pressure recovery and total pressure loss coefficients of diffusers tested in the first part of the campaign are presented in Fig 5.

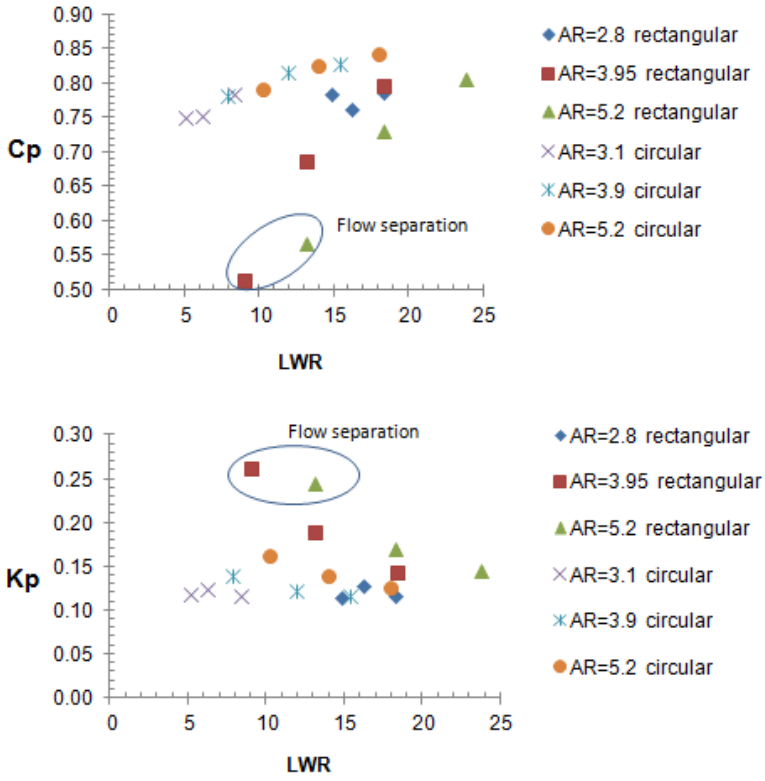

Figure 5. Pressure recovery and total pressure loss coefficients obtained for simulated diffusers

Efficiency of the diffuser channel is characterized by a high degree of pressure recovery and low total pressure loss coefficient. The design that seems to meet both of these requirements best in the above study is a circular diffuser with an area ratio of 5.2 and non-dimensional length of 18. It indicates that if the last stage of the compressor is considered, the diffuser with relatively high area ratio, low angle and circular shape is advisable.

It can be expected that to minimize undesirable effects of horizontal and vertical pressure gradients along the channel caused by curved shape and non-uniform velocity profile, a smooth area expansion is required.

The idea behind analyzing a rectangular shaped diffuser with an area expansion only in the vertical direction was to avoid negative impact of pressure gradients caused by curvature of the diffuser. This aim is met only partially. In terms of pressure losses, rectangular diffuser with a small area ratio (2.8) achieves similar performance as circular diffuser with comparable area ratio (3.1). It is therefore expected, that rectangular design can serve as an efficient connection between compressor stages. In terms of pressure recovery, very low diffuser angles and significant lengths are needed to provide decent pressure lifts and to avoid recirculation zones across the rectangular diffuser. Thus, it can be expected that a rectangular channel serving in the last stage of the compressor will require a significant non-dimensional length and therefore introducing higher friction losses, which again is resulting in poorer performance compared to the circular diffuser.

The general trend in case of low area ratio diffusers can be observed. At low non-dimensional lengths (high diffuser angles) the performance of the diffusion is reduced. This can be attributed to high adverse pressure gradients occurring across shorter distances. Such rapid deceleration linked with general flow non-uniformities reflects in the tendency of the flow to detachment from guiding walls, swirling and recirculation. Reducing the diffuser angle will provide smoother conversion of the kinetic energy into static pressure energy, but at the cost of increased friction losses. The designer must therefore try to find a balance between these two mechanisms. The same trend can also be expected for diffusers with higher area ratios. This behavior is not necessarily captured in the present study due to the limited number of geometries tested.

Diffuser/return channel

In case of a multistage machine, which naturally is a subject of the current deliberations, additional parts of the system will have to be considered. The flow discharged from the diffuser must be directed efficiently to the next stage of the compressor. To achieve a high performance of the diffuser/return channel the following, often antagonizing, goals have to be met: a low total pressure loss coefficient across the diffuser, uniform velocity profile at the discharge of the diffuser, preferably a low velocity at the inlet to the return channel and possibly low wetted perimeter of the channel to reduce friction losses. Additionally, curvature and length of the channel will affect the final performance.

At this stage of the compressor development it is difficult to foresee which configuration of the multistage machine could be optimal. The subsequent stages could be placed on the opposite sides of the motor or only at one side. These considerations must involve rotordynamics analysis which will be a part of the rotating machinery development. It should be noted that in terms of rotordynamics, the novel concept may differ significantly from its centrifugal counterpart. The speeds at which the new impellers will rotate are significantly lower, distribution of radial loads acting on the rotor is different, and the diameter and mass of the new impellers and motor will be higher.

The diffusers achieving the best performance in the diffuser comparison study were supplemented with the return channels to give some preliminary estimation of the performance of the diffuser/return channel system. It was assumed that that the next stage of the compressor will be placed at the same side of the motor, close to the preceding stage. An example configuration of rectangular and circular diffuser/return channel systems is depicted in Fig 6.

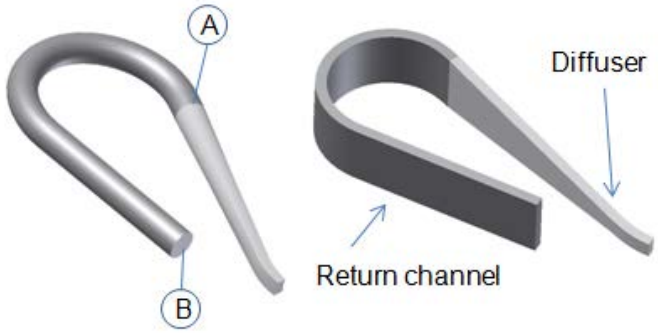

Figure 6. An examples of the diffuser/return channel configurations

Geometrical description and simulation results for the diffuser/return channel systems are summarized in Table 2.

The total pressure loss is extracted for the whole system and for the diffuser alone to compare the impact of the particular parts of the system on the assembly performance. Additionally, velocity fields in the characteristic cross-sections of the system (discharge of the diffuser and discharge of the return channel) are captured for all 6 cases (Fig 7).

Table 2. Geometrical description and results of the performance prediction of diffuser/return channel systems

	LWR, -	L_return, mm	dp_diff, bar	dp_total, bar	Cp, -	Kp, -	mesh size, cells x 1000
Rectangular outlet							
AR=2.8	14.8	321	1.55	2	0.76	0.14	2339
AR=3.95	18.2	411	2.2	2.55	0.79	0.16	3972
AR=5.2	23.7	609	1.92	2.18	0.81	0.15	2599
Circular outlet							
AR=3.1	5.0	249	1.8	2.55	0.73	0.18	1444
AR=3.9	15.3	445	1.55	1.88	0.82	0.13	2652
AR=5.2	18.0	461	1.8	2.01	0.83	0.14	3466

The lowest pressure loss amongst simulated cases is generated in the circular diffuser with area ratio of 3.9. It achieves similar performance in terms of pressure loss in the diffuser section as rectangular diffuser with AR=2.8 but has more favorable flow conditions (more uniform flow field, lower mean velocity) across the return channel. In terms of flow uniformity at the discharge of the return channels, both rectangular and circular concept are able to produce relatively mixed-out velocity fields.

Producing uniform velocity profile before inlet to the next stage of the compression is important to maximize the next stage efficiency. It can be seen that circular discharge produced slightly better conditions for the next stage inlet. It is also apparent that it is not necessary to increase area ratio too much to achieve a uniform discharge. Middle range of area ratio seems satisfactory.

An aim to avoid negative impact of pressure gradients caused by curvature of the diffuser by adopting only vertically expanded rectangular diffuser is met only partially. While relatively low pressure losses can be provided for the diffuser section of the system, the pressure loss across the rectangular return channel is increased compared to the pipe following the circular diffuser. It is expected that decisive factor here is an increased wetted perimeter of the rectangular channel resulting in increased friction losses for the flow with similar velocity. Perhaps, a combination of rectangular shape diffuser and more square-shaped (or circular) cross-section of the return channel could further reduce total pressure losses in the system.

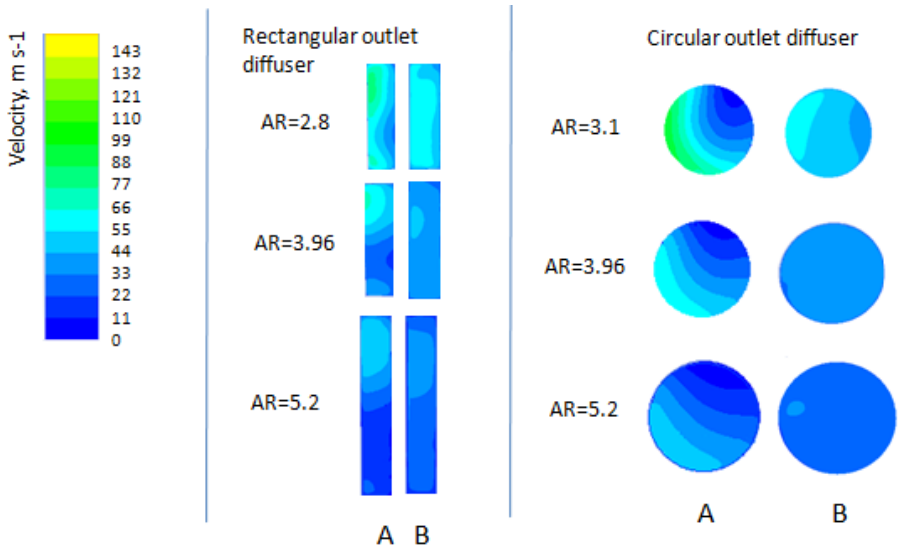

Figure 7. Velocity profiles in characteristic cross-sections of the diffuser/return channel systems

It must be emphasized that the efficiency of both proposed designs can be visibly improved if a more radial discharge from the compressor wheel was provided. In the current impeller discharge configuration, the performance of both types of the diffusers is reduced due to the rather significant curvature of flow path. The rectangular design suffers additional losses due to heightened friction losses in the initial high speed segment of the diffuser, directing the gas outside the wheel. In this critically important segment almost no deceleration is achieved. It is logical to assume that if the geometry of rectangular diffuser was created in one sweep step further improvement of the diffuser performance could be obtained. The resulting geometry will be shorter, thus allowing for a reduction of friction losses not only in the initial segment of the channel, but for the overall geometry as well. This accompanied with the further redesign of the return channel gives a potential for further reduction of the total pressure loss coefficient.

Pinch

One way of improving the performance of the diffusers operating with the non-uniform flow is to introduce the pinch. In this study 3% pinch was applied to the rectangular 2.8 area ratio diffuser presented in Table 2. It was expected that a pinch will improve uniformity of the flow across the diffuser and therefore improve its performance. It turned out that while the uniformity of the flow actually improved, see Fig 8, the total performance dropped. The total pressure loss increased from 1.66 to 1.9 bar for a diffuser simulated without a return channel. Such a result can be attributed to the increase of the already high velocity flow in the initial segment of the rectangular diffuser. Increased friction losses at this section of the channel outweighed the potential gain in the latter parts of the system.

The simulation of higher degrees of pinch was discarded as even higher losses were expected to occur. Presumably due to the speeds being close to sonic at the throat of the diffuser application of pinch can be of limited benefit to the partial admission concept compressor. This aspect should however be further researched in connection with a redesign of the impeller discharge angles. This should result in a proper diffusion process to be commenced just after trailing edges of the rotating blades.

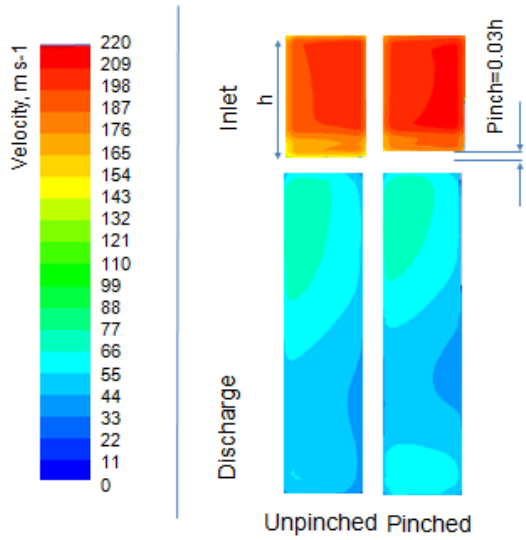

Figure 8. Velocity flow field improvement of 2.8 area ratio rectangular diffuser (no return channel included) after applying 3% pinch

Conclusions

A numerical study of diffuser systems that may be applicable for a novel partial admission radial compressor for commercial CO_2 applications was presented. In total 18 geometries have been tested with regard to attainable pressure recovery coefficients and total pressure losses. They are divided into two main groups: circular and rectangular outlets.

For the best geometries within the given area ratio, return channels were supplemented and performance of the whole system analyzed with regard to its total pressure loss. For the current compressor wheel configuration a target 1.5 bar pressure loss in the diffuser/return channel system was not achieved. The best system with circular cross-section and area ratio of 3.9 generated a total pressure loss of 1.88 bar. It is expected that a redesign of the impeller discharge angles and further modifications to the diffuser channel can improve this number quite significantly.

A rectangular design with area expansion only in vertical direction was introduced in an attempt to reduce the impact of the flow non-uniformity caused by the curved shape of the diffuser channel. This aim was met only partially as the losses generated in the return channel were increased due to the higher friction losses compared to the circular design. Also application of 3% pinch to the rectangular diffuser turned out to worsen the performance of the full system. Here additional losses are attributed to the pronounced friction losses in the initial section of the diffuser channel.

A high efficiency of the partial admission compressor diffuser is critical to achieving a reasonably high total stage efficiency of the compressor. Further improvements of the concept design should include:

- A more radial discharge of the gas from the impeller wheel followed by a smoother curvature of the diffuser channel and probably a combination of rectangular type of the diffuser with a square or circular cross section of the return channel.
- Further analysis of the pinch should be also undertaken for the rectangular diffusers with higher degree of deceleration in the initial segment of the diffuser.

ACKNOWLEDGMENTS

This publication forms a part of the CREATIV project, performed under the strategic Norwegian research program RENERGI. The authors acknowledge the partners: SINTEF Energy Research, Danfoss, FHL, Hydro Aluminium, John Bean Technology, Norske Skog, REMA1000, Systemair, TINE, and the Research Council of Norway (195182/S60) for their support. The authors would like to thank Barber-Nichols Inc. for the valuable comments to the present work.

NOMENCLATURE

AR (-)	Area ratio
dp (bar)	Pressure drop
L (mm)	Length/sweep rate
Subscripts	
diff	diffuser
t	Total conditions
return	Return channel

REFERENCES

1. Anand, R. B., Rai, L., Singh, S. N., Sharma, O. P., 2001. Flow characteristics of a low aspect ratio 90°/90° S-shaped diffuser, Journal of Aeronautical Society of India 53
2. El-Askary, W. A., Balabel, A., 2007. Predictions of reattaching turbulent shear flow in asymmetric divergent channel using linear and non-linear turbulence models. Eng Res Bull 30(4):535–50

3. El-Askary, W. A., Nasr, M., 2009. Performance of a bend–diffuser system: Experimental and numerical studies. Computers & Fluids 38, 160–170
4. Gopaliya, M. K., Kumar, M., Kumar, S., Gopaliya, S. M., 2007. Analysis of performance characteristics of S-shaped diffuser with offset. Aerospace Science and Technology 11, 130–135
5. Kus, B. and Nekså, P., 2013a. Development of one-dimensional model for initial design and evaluation of oil-free CO_2 turbo-compressor. Submitted to Int J Refrig
6. Kus, B. and Nekså, P., 2013b. Oil-free turbo-compressors for CO2 refrigeration applications. Int J Refrig, 2013
7. Kus, B. and Nekså, P., 2013c. Novel partial admission radial compressor for CO2 applications. Submitted to Int J Refrig, 2013
8. Ludtke, K., 1983. Aerodynamic tests on centrifugal process compressors – the influence of the vaneless diffuser shape. Journal of Engineering for Power, vol 105, pp. 902―909
9. Simonsen, A. J., Krogstand, P. A., 2004. Experimental–numerical investigation of a bend–diffuser configuration. In: 15th Australian fluid mechanics conference, University of Sydney, Australia; 13–17 December
10. Turunen-Saaresti, T., Reunanen, A., Larjola, J., 2006. Computational and Experimental Study of Pinch on the Performance of a Vaneless Diffuser in a Centrifugal Compressor. Journal of Thermal Science Vol.15, No.4 306―313
11. Wright, S.A., Radel, R.F., Vernon, M.E., Rochau, G.E., Pickard, P.S., 2010. Operation and Analysis of a Supercritical CO_2 Brayton Cycle, Sandia Report SAND2010-0171